# Coherent electrons and collective modes in quantum-transport through nanostructures


Im Fachbereich Physik der
Freien Universität Berlin
eingereichte

Dissertation

von

Niels Bode

Berlin, im Mai 2012

**1. Gutachter:** Prof. Felix von Oppen, PhD
**2. Gutachter:** Prof. Dr. Piet W. Brouwer

Tag der Einreichung: 22. Mai 2012
Tag der Disputation: 29. Juni 2012

# Kurzfassung

In der vorliegenden Arbeit wird das Wechselspiel von kohärenten Elektronen und kollektiven Freiheitsgraden, wie z.B. Vibrationsmoden oder lokalen Spins, untersucht. Diese Kopplung definiert nanoelektromechanische Systeme (NEMS) oder beeinflusst Transportmessungen durch einzelne Moleküle. Dies ist sowohl für die Grundlagenforschung als auch für Anwendungen in der Miniaturisierung elektronischer Bauelemente von Bedeutung.

Die wichtige Annahme dieser theoretischen Arbeit ist, dass sich die kollektiven Freiheitsgrade auf den typischen elektronischen Zeitskalen nur langsam verändern, so dass sich die Leitungselektronen in einer näherungsweise statischen Konfiguration bewegen. Dies ermöglicht die Beschreibung im Rahmen einer Nichtgleichgewichts-Born-Oppenheimer-[engl.: non-equilbrium Born-Oppenheimer (NEBO)] Näherung. Dadurch können sowohl die vom Strom auf die kollektiven Freiheitsgrade ausgeübten Kräfte als auch *vice versa* die Auswirkungen dieser Kräfte auf den Strom beschrieben werden. Hierbei wird der Landauer-Büttiker Formalismus, in dem kohärenter Transport als ein Streuproblem aufgefasst wird, auf die Theorie strominduzierter Kräfte erweitert, so dass diese Kräfte in allgemeinen Nichtgleichgewichtssituationen durch die Streumatrix des Systems ausgedrückt werden können.

Die in dieser Arbeit hergeleiteten strominduzierten Kräfte beinhalten eine möglicherweise nichtkonservative mittlere Kraft, eine geschwindigkeitsabhängige Reibungskraft, eine Pseudo-Lorentz- sowie eine fluktuierende Langevin-Kraft. Die gewählte NEBO-Näherung erlaubt es Nichtlinearitäten in der Kopplung und die Abhängigkeit von Bias- und Gate-Spannung zu berücksichtigen. Mit diesem Ansatz werden einige für NEMS exemplarische Modell-Systeme untersucht. Die dargelegte Theorie wird auf die Wechselwirkung zwischen Elektronen und einem anisotropen magnetischen Molekül erweitert und es wird die Schaltdynamik der Spinorientierung beschrieben.

Die Kopplung zwischen kohärenten Elektronen und kollektiven Freiheitsgraden bietet faszinierende Möglichkeiten für Anwendungen auf nanoskopischen Größenskalen. Als ein Beispiel für diese Art der Anwendung wird betrachtet, dass den kollektiven Freiheitsgraden durch die Wechselwirkung mit kohärenten Elektronen Energie kontrolliert entzogen wird. Es wird diskutiert wie ein Oszillator bis auf den quantenmechanischen Grundzustand herunter gekühlt werden kann. Als weiteres Beispiel wird mit molekularen Schaltern funktionalisiertes Graphen untersucht. Wie sich dessen elektronische Transporteigenschaften, insbesondere der Leitwert, in Abhängigkeit des Schaltzustandes verändern wird diskutiert wobei gezeigt wird, dass im Bereich kohärenten Transports Interferenzeffekte die Empfindlichkeit erhöhen. Weitere mögliche Anwendungen der hier dargelegten Betrachtung beinhalten z.B. den Einsatz von NEMS als Schalter und Sensoren für Ladung oder Masse, als auch den Betrieb molekularer Motoren.

# Abstract

In this thesis we investigate the interplay between quantum transport of coherent electrons and collective modes. We consider both vibrational modes in nanoelectromechanical systems and localized spin degrees of freedom in single-molecule junctions. This field has attracted considerable interest for reasons of basic research and for possible applications in nanoelectronics.

This thesis focuses on the regime in which the collective modes are slowly varying on the typical time scale of the electrons. While the latter observe a quasistatic configuration, justifying the use of a non-equilibrium Born-Oppenheimer approximation (NEBO), they can affect the collective modes significantly through current induced forces. Within this approach we study these forces and the associated backaction on the current. Most prominently, we generalize the Landauer-Büttiker approach, in which coherent electronic transport is treated as a scattering problem, to the study of current-induced forces expressing the latter in terms of the scattering matrix of the phase coherent conductor.

These current-induced forces include a, possibly non-conservative, mean force, a velocity-dependent frictional force, and a Lorentz-like force, as well as a fluctuating Langevin force. Starting from a microscopic description we derive these forces in terms of the scattering matrix in general out-of-equilibrium situations. The NEBO approximation allows us to include non-linearities of the coupling between collective modes and electrons and to study the dependence of the forces on bias and gate voltages. We apply our approach to a number of illustrative models of nanoelectromechanical systems, focusing on generic situations and interesting dynamical behavior, such as limit-cycles. We generalize our approach to a localized magnetic moment coupled to a coherent conductor and study how its spin orientation can be switched electronically.

Coupling coherent electrons and collective degrees of freedom opens new roads towards fascinating functional devices. We explore this possibility in two projects. First, we consider graphene decorated with photochromic molecular switches. Due to this functionalization the switching state affects the conductance of graphene which can be used for the electronic read-out, being particularly sensitive in the presence of interference effects. Second, we study how the possibility of exchanging energy between vibrational modes and electrons can be utilized for the design of a refrigerator on the nanoscale. We investigate how one can cool an oscillator by these means to the quantum mechanical ground state. Furthermore, our general theory can be useful for the understanding and optimization of sensors of charge or mass, molecular switches operated in an all-electronical fashion, and machines, such as molecular motors, at the nanoscale.

# Contents

# 1. Introduction

The ongoing miniaturization of electronic devices, which can be operated at low temperatures, allows for the study of coherent electronic transport through nanostructures. Quantum mechanical interference effects manifest themselves in a number of transport phenomena which are accessible by today's experimental techniques.

The quantization of conductance in a quantum point contact, or measurements of the magnetoresistance, which probe the Aharonov-Bohm effect are hallmarks of coherent transport. Similarly, an increased resistivity due to partial interference of scattered electron waves, known as weak localization, or universal and reproducible variations of the conductance as a function of external parameters, such as the chemical potential or an applied magnetic field, show the influence of coherence on transport properties. In the presence of interactions additional phenomena such as the Coulomb blockade or the Kondo effect have to be considered. For the theoretical description of coherent transport the approach by Landauer and Büttiker has been particularly fruitful, which describes electronic transport through nanostructures as a scattering problem.

In recent years the interplay between coherent electrons and collective degrees of freedom has attracted considerable interest. Systems under study include nanoelectromechanical systems (NEMS), or molecular junctions in which electrons can couple to vibrational modes or to localized spin degrees of freedom, as in single-molecule magnets. Fabrication of these nanoscale devices proceeds, for instance, by etching down larger structures, or by producing hybrid structures, or by confining regions by electrostatic means. In contrast to these top-down approaches, single molecules have been incorporated into transport junctions, cp. Fig. 1.2, and have been extensively studied. In typical setups, the system (a molecule, a quantum dot, or a nanomechanical resonator) is attached to electrodes and heat baths which set the temperature of the environment. The chemical potentials of the leads can be controlled by an applied bias voltage, while gate voltages are conventionally used in order to control the energy levels of the system, turning the device into a transistor. Measuring the current through such a device can then be viewed as a spectroscopic study of the microscopic properties of the system.

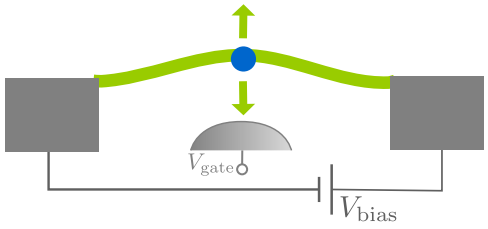


Figure 1.1. Illustration of a typical setup under study. A suspended NEMS can be controlled by means of applied voltages.

The coupling between coherent electrons and collective degrees of freedom in these systems is conceptually interesting. It gives rise to qualitatively new dynamics and

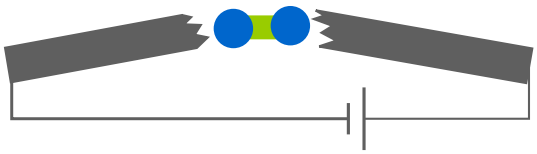

Figure 1.2. Illustration of the breakjunction as considered in the work by Smit *et al.* [2002]. A Pt-wire is bent until it breaks so that surrounding $H_2$ molecules can enter the gap. Transport measurements can reveal that indeed a single molecule has been adsorbed.

mechanisms of exchanging energy between electrons and collective modes, directly affects the current through the device, and may add new functionalities to devices, with potential applications. Transferring energy from the electronic to the collective degrees of freedom, enables one to maintain stable mechanical motion by compensating for dissipation mechanisms. This is the foundation for the fabrication of nanoscale machines, such as nano-cars and molecular motors. The reduced size and high sensitivity of NEMS, accompanied with strong non-linear behavior, make them also attractive for the usage as very accurate sensors of displacement, force, mass, and charge. While heat production can even destroy the device, the opposite process of this energy transfer between electronic and collective degrees of freedom, namely the possibility of energy-harvesting, might also be utilized for cooling the system via backaction. This might allow one to study quantum phenomena at the mesoscopic level, maybe even allowing one to cool a mechanical oscillator to the quantum ground state. For possible applications it is also important to control electronically transitions between distinct configurations of the system and to read out these states through the current, constituting the operation of switches at the nanoscale.

In this thesis we focus on the interplay between coherent electrons and the collective modes. We provide a general theoretical description of the action of the current on the collective modes and the backaction on the current, and we illustrate these concepts within a number of model systems.

## 1.1. Electronic transport and collective degrees of freedom

There has been much recent research interest in the effects of vibrations in molecules and NEMS, and local magnetic moments (molecular spintronics). In order to cope with the plethora of phenomena in the context of current-induced forces, it is instructive to treat the relevant limits individually. Independent of the coupling strength between electrons and the collective modes, two well defined limits can be identified, for which electronic and vibrational or precessional time scales decouple and which give rise to different experimental phenomena.

### 1.1.1. Slow electrons

The limit of slow electronic time scales and weak coupling to the leads is often realized in molecular junctions which are the building blocks of molecular electronics. When the electrons reside on the mesoscopic system for times large compared to typical vibrational or precessional periods, the system can be described in the exact eigenstate basis of the collective degrees of freedom. For instance the Fock states of the vibrational modes provide an appropriate basis, which is altered by the presence of electrons depending on the coupling strength between electrons and phonons.

Due to this interaction, the electronic transport is accompanied by the emission and absorption of phonons affecting the transport properties. For instance, when the electron-phonon coupling is weak, vibrational side bands due to phonon assisted tunneling can be observed in the current-voltage characteristics [Park *et al.*, 2000; Yu *et al.*, 2004]. When electron-phonon coupling is strong, the current can be strongly suppressed by means of the Frank-Condon blockade. Leturcq *et al.* [2009] have measured and analyzed the electronic transport through a quantum dot on a suspended carbon nanotube, in which the strong coupling between a longitudinal stretching mode and the electrons in a sample of high quality allowed them to observe this suppression of the low-bias current.

In this limit of slow collective degrees of freedom the system can be appropriately described theoretically within a rate- or Master equation, allowing one to study these phenomena both for fast vibron relaxations and for slow vibron relaxation with the ensuing non-equilibrium effects. For instance, in the limit of strong electron-phonon coupling, this can be used for the description of the Franck-Condon blockade physics, ascribing the pronounced suppression of the low-bias sequential tunneling to an exponentially small overlap between harmonic oscillator wave functions before and after tunneling, also explaining vibrational sidebands in the current-voltage characteristics and self-similar avalanches of electrons which affect the current-noise significantly [Koch and von Oppen, 2005; Koch *et al.*, 2006].

### 1.1.2. Fast electrons

In the context of nanoelectromechanics, there has recently been much interest in the opposite regime of adiabatic vibrational dynamics, in which the electronic processes are fast compared to the vibrational degrees of freedom. Here, electrons propagate through the nanostructure rapidly, observing a quasistatic configuration of the vibrational modes, but affecting their dynamics profoundly at the same time. It is this regime of slow collective modes that the present thesis focuses on.

Seminal experiments on current-induced forces have been performed by Steele *et al.* [2009] and Lassagne *et al.* [2009] who have investigated suspended carbon nanotubes hosting a quantum dot. These experiments have focused on the flexural mode of the carbon nanotube, which is considerably slower than the longitudinal ones which we have mentioned above. The nanomechanical resonator has been excited externally by a nearby antenna [Steele *et al.*, 2009] or an alternating gate voltage [Lassagne *et al.*, 2009]. The experiments have been performed at cryogenic temperatures and the vibrations have

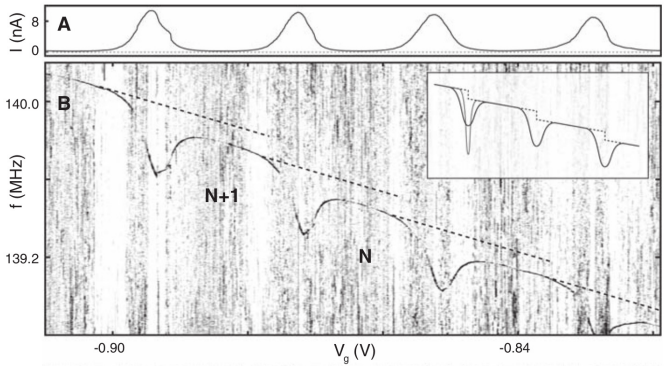


Figure 1.3. (A) Current as a function of the gate voltage demonstrating the regime of the Coulomb blockade, cp. also Fig. 1.4. (B) Resonance signal as function of resonance frequency and gate voltage. Due to the electrostatic coupling the frequency increases with the number of electrons $N$ on the dot. When current flows through the device current-induced forces are excited, as indicated by the dips, in agreement with expectations (inset). *Figure taken from [Steele* et al.*, 2009].*

been monitored by measuring the current through the device. Since the vibrations couple to the density of the electrons on the quantum dot, the rigidity of the oscillator can be tuned by a gate voltage, in analogy with a guitar string, affecting the resonance frequency, see Fig. 1.3. When current flows through these devices, the electrons move rapidly on the timescale of the vibrational frequency of the flexural mode. Then a significant backaction of the single-electron tunneling on the resonator can be observed. Importantly, the current itself can also excite the oscillator in the absence of an external driving force. These current-induced forces generally contain non-linear effects and provide damping mechanisms of the vibrational mode.

In both regimes of fast and slow vibrational degrees of freedom, the electronic transport through the device can be accompanied by substantial energy transfer between electrons and phonons. This opens perspectives for cooling nanomechanical systems [Clerk, 2012].

## 1.2. Outline of the thesis

In this thesis we study the interaction between charge transport and collective degrees of freedom in electronic nanostructures, focusing on the regime of fast electrons. This central issue is addressed in the context of several specific projects which we outline in the remainder of this introduction.

### 1.2.1. Current-induced forces in NEMS

We study NEMS in which the electrons couple to slowly varying vibrational degrees of freedom. In the strictly adiabatic limit and in the absence of interactions, the Landauer-

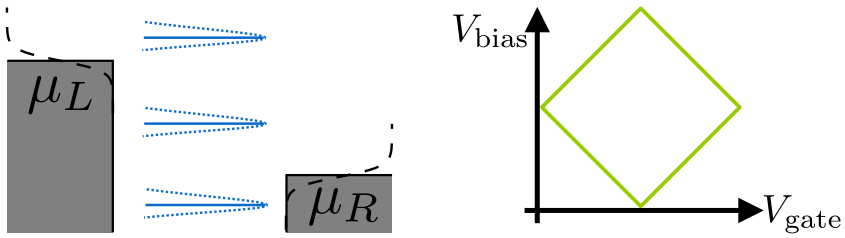


Figure 1.4. Energy levels and current-voltage characteristics. (left) The electronic levels of the system are broadened due to the coupling to the leads (blue, dotted line). Inside the latter the electrons are described by the Fermi-Dirac distribution which are smeared out at finite temperatures (indicated by the dashed lines). The chemical potentials are controlled externally such that a bias voltage $eV_{\text{bias}} = \mu_L - \mu_R$ drives electronic transport. (right) Typical plot of the differential conductance $\mathrm{d}I/\mathrm{d}V$ as a function of $V_{\text{bias}}$ and a gate voltage which controls the position of the electronic levels. Current flows when electronic levels are inside the transport window and the differential conductance is peaked (indicated by the green lines) when the number of them changes.

Büttiker approach conventionally provides a powerful description of phase coherent conductors. The success of this formalism raises the question whether it can be also applied when the slow dynamics of the collective mode affects the conductor. In particular it would be useful to extend the formalism to the study of current-induced forces in order to connect with the existing literature and to obtain a general description of these forces.

In fact, this is what we do in Chapter 3. We give a microscopic description of a nanomechanical system coupled to electronic reservoirs, and derive and study the resulting forces as well as the backaction of the oscillator on the electronic current in terms of the scattering matrix. Our main assumption is that the vibrational modes are slow, justifying to work in a non-equilibrium Born-Oppenheimer (NEBO) approximation. This allows us to retain the non-linearities of the mechanical motion and the full dependencies on external parameters, such as the coupling to the environment and the applied voltages.

Our approach delivers an alternative viewpoints compared to previous studies of NEMS. The case of one electronic level coupled to a single vibrational mode has been studied with a Green's function approach in [Mozyrsky *et al.*, 2006; Pistolesi *et al.*, 2008], where the authors showed that the current-induced forces can lead to a bistable effective potential and consequently to switching. Lü *et al.* [2010] have studied the case of multiple vibrational modes within a linear approximation, finding a Lorentz-like current-induced force arising from the electronic Berry phase [Berry and Robbins, 1993]. In simple situations, the current-induced forces have been also studied within a scattering matrix approach in the context of quantum measurement backaction [Bennett *et al.*, 2010] (see also [Bennett *et al.*, 2011]), and momentum transfer statistics [Kindermann and Beenakker, 2002]. Further studies of slowly varying mechanical modes include *e.g.* recent works on NEMS near continuous mechanical instabilities [Weick *et al.*, 2010; Brüggemann *et al.*, 2012], or the cooling and amplification of mechanical motion by the backaction of

conduction electrons [Naik *et al.*, 2006; Stettenheim *et al.*, 2010; Dundas *et al.*, 2009].

It is an advantage of our approach that it allows us to obtain the various forces exerted by the conduction electrons – namely the average force, a fluctuating force and the velocity dependent forces (appearing as first-order corrections in the NEBO) – in a non-perturbative manner, including their dependence on the system's parameters as well as non-linear effects of the electron-phonon coupling. We derive these current-induced forces in general out-of-equilibrium situations and express them in terms of the scattering matrix of the phase-coherent conductor. Indeed, within the NEBO approximation we can express the forces in terms of two fundamental quantities, the adiabatic S-matrix and the so-called A-matrix, of the system. Thus we extend the Landauer-Büttiker formalism to the study of NEMS, resulting in a unified description of forces and backaction and providing the opportunity to draw general conclusions from symmetry arguments.

Our study includes several general and interesting features of current-induced forces in non-equilibrium situations. The dissipation coefficient acquires a non-equilibrium contribution that can be negative. When the electrons couple to more than one vibrational mode we find that a Lorentz-like force acts on the oscillator and that the mean force exerted by the electrons can become non-conservative. Electronic control over the details of the current-induced forces can be utilized for designing switches on the nanoscale. Additionally, energy transfer between electrons and vibrational modes can cause interesting dynamics with possible applications for molecular motors and refrigerators. In Chapter 4 we study illustrative toy models which capture some of these properties.

We discuss the cooling of a mechanical resonator via coupling to conduction electrons in Chapter 6. There we focus on the regime of slow electrons which absorb single phonons, providing the possibility of reaching the quantum ground state of the oscillator.

### 1.2.2. Switching of anisotropic magnetic molecules

In a similar way to our study of the coupling of electrons to vibrational degrees of freedom, we can also treat the exchange interaction between electrons and a local molecular magnetic moment.

Using the spin degree of freedom in electronic devices has opened new roads in nanoelectronics and data storage [Fert, 2008]. In this context of (molecular) spintronics it is important to have reliable mechanisms for writing and reading the stored information. Specifically, it is essential to have protocols for manipulating and for detecting the orientation of the magnetic moment. To this end it is convenient to take advantage of the coupling between the spins of the electrons, which tunnel from the electrodes, and the localized magnetic moment of the molecule.

We consider current-induced switching in single-molecule junctions containing an anisotropic magnetic molecule. Again, our theory applies in the limit in which the electrons are fast compared to the precession time of the magnetic moments and allows us to describe the current-induced torques including possible implications for designing molecular switches in spintronics. Starting from a microscopic description, we can derive semiclassical equations of motion for the local magnetic moment that have the structure of generalized Landau-Lifshitz-Gilbert (LLG) equations. These ideas are presented in

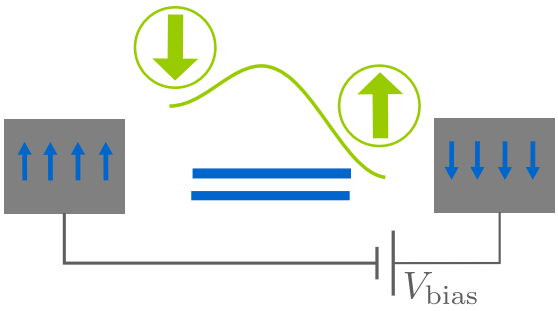


Figure 1.5. Illustration of a molecular switch. An anisotropic magnetic molecule is described by a bistable potential. The spin orientation can be switched by a current between the (possibly spin-polarized) leads.

Chapter 5 of this thesis.

In previous works describing magnetic nanoparticles, LLG equations have been derived in a perturbative way assuming either that the coupling between the electronic spin and the magnetic moment of the nanoparticle is small and/or that tunneling between the leads and the nanoparticle is weak [Katsura *et al.*, 2006; Fransson, 2008; Núñez and Duine, 2008; López-Monís *et al.*, 2012]. In contrast, our microscopic derivation relies entirely on the NEBO approximation which is valid in the high-current limit as described above. As a consequence, our non-perturbative approach allows us to compute how the parameters of the LLG equation depend on the state of the molecular moment as well as on the applied bias and gate voltages.

We find that the strictly adiabatic approximation causes a mean torque exerted by the conduction electrons, while retardation effects result in a renormalization of the precession frequency and Gilbert damping. In addition, equilibrium and non-equilibrium fluctuations of the current cause a fluctuating (Langevin) torque. We can express these torques in terms of the electronic Green's functions and relate them to scattering theory, in the latter case extending earlier work [Tserkovnyak *et al.*, 2002; Brataas *et al.*, 2008, 2011] to include an applied bias voltage. In general out-of-equilibrium situations the conduction electrons can transfer energy to the localized moment by the fluctuations and, in the presence of spin-polarized leads, via a non-conservative (spin-transfer) torque and/or negative damping.

In contrast to the study of mechanical systems, the molecular spin is described by linear equations of motion, affecting the way how the current-induced torques enter the LLG. We note that the dynamics of the molecular spin automatically includes more than one collective degree of freedom and that the non-equilibrium spin-transfer torque is an analog of the non-conservative forces encountered in the study of the mechanical systems. We apply this study of current-induced torques to the description of a molecular switch consisting of an (uniaxially) anisotropic magnetic molecule. We exploit the Langevin equation to identify the relevant switching mechanisms and to derive the current-induced switching rates. The switching between the two spin configurations can be driven either

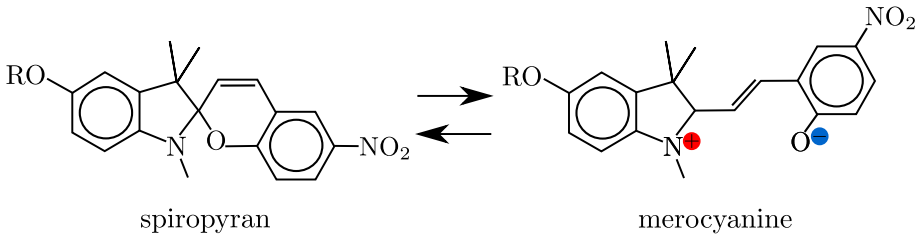


Figure 1.6. Switching between the ring-closed (three-dimensional) spiropyran and the ring-open (planar), zwitterionic merocyanine.

by the fluctuations or, in the presence of spin-polarized leads, by the spin-transfer torque. Again, both the switching and the read-out of the molecular switch can be accomplished completely electronically via changing the applied voltages and measuring the current-voltage characteristics, respectively.

### 1.2.3. Graphene functionalized with molecular switches

In order to incorporate molecular switches as building blocks in technologically relevant electronic applications it is essential to produce devices which are easily scalable and to contact them to the outside world, allowing for electronic transport measurements. We study the latter in order to read out the switching state of certain molecular switches which functionalize a layer of graphene.

In particular, photo-induced conformational changes of molecules are possible candidates for the usage in functional molecular devices. An interesting example for such photochromic switches are spiropyrans which can be reversibly switched between two conformational states, a ring-closed and an open form. The chemical transformation between these two conformations can be driven thermally or by irradiation with light. As indicated in Fig. 1.6, in the reaction a bond between a carbon and an oxygen atom breaks, which is accompanied by a significant change in geometry and electronic configuration between the two isomers, namely the ring-closed spiropyran and the ring-open merocyanine. In particular, due to its zwitterionic form the latter has a large dipole moment [Whelan *et al.*, 2010] which may open new design possibilities for applications.

For possible technological applications it is of major importance to study how the molecular switches interact with a substrate. For instance, the substrate can modify the switching process, *e.g.*, by steric hindrance or by quenching of excitations [Piantek *et al.*, 2009; Bronner *et al.*, 2011]. Conversely, the switch may cause a reversible modification of the substrate. As an example, the optical absorption of carbon nanotubes functionalized with spiropyrans has recently been observed to depend on the switching state [Malic *et al.*, 2011].

In this thesis we discuss a particularly interesting substrate, namely the monolayer of carbon atoms arranged in a honeycomb lattice known as graphene [Neto *et al.*, 2009]. Here we focus on its electronic properties in order to read out the switching state of the attached molecules. Due to its conduction properties and the strictly 2d nature of

graphene, it appears promising to use this – still novel – material as a detector [Schedin *et al.*, 2007] for the conformational state of attached molecular switches. In Chapter 7 we provide a theory of the electronic transport properties of a graphene layer functionalized with the spiropyran-merocyanine system. The light-induced reversible switching between these two isomers affects the carriers in graphene through the associated change in the molecular dipole moment, so that the conductivity may serve as an all-electrical read-out of the molecular switching state.

We present results for both the quasiclassical (Boltzmann) and the quantum-coherent regimes of transport and discuss how the conductance is affected by changing the molecular switching state. In mesoscopic conductors, the universal conductance fluctuations make the conductance a sensitive function of the precise impurity configuration [Al'tshuler and Spivak, 1985; Feng *et al.*, 1986]. In our study of graphene decorated with switches we find that such quantum interference effects also cause a particularly large sensitivity of the conductance of graphene to the molecular switching state. Quite generally, we find a linear sensitivity of the conductance on the molecular dipole moment whenever quantum interference effects play an essential role which contrasts with a quadratic (and thus typically weaker) dependence when quantum interference is absent.

Before we enter into a more detailed discussion of these projects, we use Chapter 2 to sketch some essential formalisms which we will need throughout this thesis. This includes brief introductions to the description of transport phenomena in terms of scattering matrices and of Green's functions.

# 2. Formalism

In this chapter we provide the tools which are needed throughout this thesis for the theoretical description of transport phenomena in mesoscopic systems. We give a brief introduction to scattering theory in Section 2.1. A complementary description of nanoscopic conductors coupled to leads is given in Section 2.2 in terms of Green's functions. Finally, in Section 2.3 we briefly comment on the Wigner representation which is used in our study of slowly varying potentials.

## 2.1. Scattering theory

A powerful and popular approach to mesoscopic transport, in which current flow is viewed as a problem of scattering theory, was introduced by Landauer [1957, 1970]. In this approach the conductance of the device is related to the probability that electrons are transmitted through it, as sketched in Fig. 2.1. Generalizations to multi-channel [Büttiker *et al.*, 1985] and multi-terminal [Büttiker, 1986] setups led to the well-known Landauer-Büttiker formula for current and conductance.

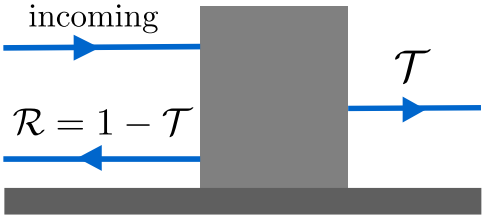


Figure 2.1. Sketch of a tunneling barrier. An incident electron wave is partly reflected and partly transmitted.

We begin this section with a discussion of the transverse quantization of momenta in a constriction connected to electron reservoirs and the corresponding quantization of conductance. Then we show how the in- and outcoming waves are related through the scattering (S-) matrix, which encapsulates the transmission and reflection amplitudes of the problem. This is the foundation for calculating transport properties of the device, as we sketch for the current at the end of this section.

Our discussion is informed by [Büttiker, 1992; Imry and Landauer, 1999] and the presentation in the books by Nazarov and Blanter [2010] and Datta [1995].

### 2.1.1. Quantum-point contact and conductance quantization

As an introductory example to the field we consider a quantum-point contact in a two-dimensional electron gas as studied experimentally by van Wees *et al.* [1988] and Wharam *et al.* [1988]. The idealized setup consists of a waveguide which is connected to electronic reservoirs as illustrated in Fig. 2.2.

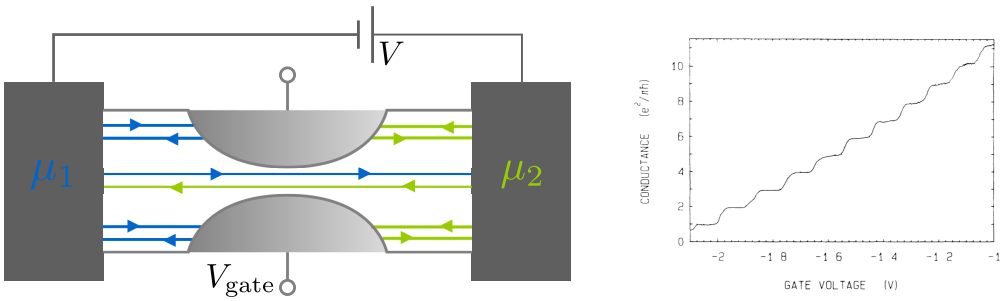


Figure 2.2. (left) Illustration of the setup. The waveguide is in contact with reservoirs at different chemical potentials with $\mu_1 - \mu_2 = eV$. The width of the constriction can be tuned by an external voltage $V_{\text{gate}}$. Inside the constriction, transmitted right-moving electrons are equilibrated with the left reservoir and vice versa. (right) Point-contact conductance as a function of the gate voltage. Plateaus of $2e^2/h$ are clearly visible. *Figure taken from [van Wees* et al.*, 1988].*

We assume that the transverse dimensions of the waveguide vary adiabatically along the channel so that transverse and longitudinal motions decouple. The wave functions in such a waveguide factorize into

$$\psi_n(\boldsymbol{x}) = \psi(x)\,\phi_n(\boldsymbol{x}_\perp), \tag{2.1}$$

where $x$ is the coordinate along the transport direction and $\boldsymbol{x}_\perp$ denotes the transverse direction. Due to the lateral confinement, the wave function $\phi_n(\boldsymbol{x}_\perp)$ vanishes at the transverse boundaries such that the transverse motion of the electron is quantized. Thus $\phi_n(\boldsymbol{x}_\perp)$ corresponds to the wave function of a particle in a box with the channel-dependent energy $\epsilon_n(x) = (\pi\hbar n)^2/[2mL_y^2(x)]$. Within this adiabatic approximation, the plane waves $\psi(x)$ satisfies

$$\left[-\frac{\hbar^2}{2m}\frac{\partial^2}{\partial x^2} + \epsilon_n(x)\right]\psi(x) = \epsilon\,\psi(x). \tag{2.2}$$

Due to the adiabatically varying constriction, the $n$ channels in the quantum point contact do not mix and all the channels are either completely closed (probability of reflection $\mathcal{R}_n = 1$) or fully open (probability of transmission $\mathcal{T}_n = 1 - \mathcal{R}_n = 1$). Only the latter channels, which are shown in the central part of the sketch in Fig. 2.2, contribute to the net transport. Hence, the current for quantized transverse motion reads

$$I = 2e \sum_{n(\text{open})} \int \frac{\mathrm{d}k}{2\pi}\, v(k) f_n(k), \tag{2.3}$$

where the factor 2 accounts for spin-degeneracy and $v = \hbar k/m$ is the electron velocity. Right-moving electrons emanate from the left reservoir, and vice versa, hence their

distribution function is given by the Fermi-Dirac distribution of the corresponding reservoir $\alpha$, namely

$$f_\alpha(\epsilon) = \frac{1}{\mathrm{e}^{(\epsilon-\mu_\alpha)/\mathrm{k_B}T}+1}. \tag{2.4}$$

Throughout this thesis we are interested in electronic transport driven by voltage differences rather than temperature gradients, hence we allow for different chemical potentials $\mu_\alpha$ but assume all reservoirs to be at the same temperature $T$. Accordingly, Eq. (2.3) becomes

$$I = \frac{2e}{h}\sum_{n(\mathrm{open})}\int \mathrm{d}\epsilon\,[f_1(\epsilon)-f_2(\epsilon)] = \frac{2e^2}{h}N_{\mathrm{open}}\,V, \tag{2.5}$$

where we have assumed small temperatures and used $\partial_k\epsilon = \hbar v$ and $\mu_1 - \mu_2 = eV$. Note that the number of open channels depends on the width of the waveguide. From equating $\epsilon_n(x)$ with the Fermi energy $\epsilon_\mathrm{F} = (\hbar k_\mathrm{F})^2/(2m)$ one obtains that $N_{\mathrm{open}}$ is the largest integer larger than $k_\mathrm{F}L_y^{\mathrm{min}}/\pi$, with $L_y^{\mathrm{min}}$ the minimal width of the constriction.

The quantization of the conductance is in striking agreement with the measurements by van Wees *et al.* [1988] and Wharam *et al.* [1988] in a two-dimensional electron gas in a GaAs-AlGaAs heterostructure at low temperatures. The quantum-point contact under study has been defined by electrostatic depletion of the 2DEG and the mean free path has been ensured to be much smaller than the dimensions of the constriction. Fig. 2.2 depicts how the conductance $G = \mathrm{d}I/\mathrm{d}V$ changes in quantized steps of $2e^2/h$ as a function of the gate voltage (and thus the number of open channels), in agreement with Eq. (2.5). The quantum point contact is a particular example of a transport setup, with the special property that all channels are either completely open or closed. In fact, we are interested in the transport through a general mesoscopic structure which is connected via leads to reservoirs, which we describe next.

### 2.1.2. Scattering states and the S-matrix

While the example of the quantum point contact is special, it does point the way to a general theory of coherent transport in electronic nanostructures. This general theory is based on the idea that one can separate the mesoscopic conductor into leads and a scattering region, as illustrated in Fig. 2.3. The leads are modeled as ideal waveguides and support a finite number of propagating transverse channels, much as in the example of the point contact. On the other hand, we will not make any specific assumptions about the scattering region other than the simplification of neglecting electron-electron interactions. By current conservation, it is sufficient to compute the current in the leads. Consequently, we can map the problem of coherent transport through a mesoscopic device to scattering theory. The current flowing in a particular lead depends on the current injected into this lead from the corresponding reservoir, on the part of this injected current which is reflected back into the same lead, as well as on the currents which are injected from other leads and scattered into this lead. Thus the required information is concisely contained in the S matrix of this scattering system.

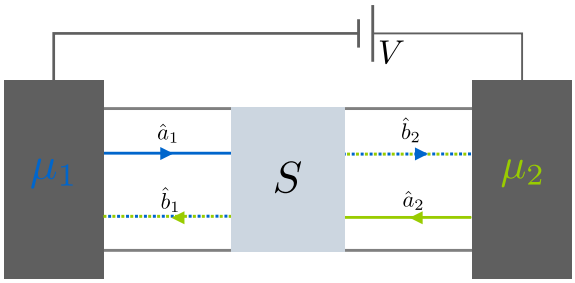


Figure 2.3. Illustration of a two-terminal setup. The scattering region (drawn light blue) is connected through leads (ideal waveguides) to the reservoirs, which differ in their chemical potentials $\mu_1 - \mu_2 = eV$. The annihilation operators for carriers in incoming ($\hat{a}_i$) and outgoing ($\hat{b}_i$) channels in the two leads $i = 1, 2$ are related through the S-matrix.

In fact, the scattering states provide a convenient basis for expressing the wave functions of the problem. Inside lead $\alpha$ the scattering state originating from channel $m$ in reservoir $\alpha$ reads

$$\psi_{\alpha m}(\boldsymbol{x}_\alpha) = \sum_n \frac{1}{\sqrt{2\pi\hbar v_n(\epsilon)}} \phi_n(\boldsymbol{x}_{\perp,\alpha}) \left[\delta_{mn} \mathrm{e}^{\mathrm{i}k_{\alpha n} x_\alpha} + S_{\alpha n,\alpha m} \mathrm{e}^{-\mathrm{i}k_{\alpha n} x_\alpha}\right]. \tag{2.6}$$

It is a superposition of the plane wave originating from reservoir $\alpha$ and the outgoing plane waves from the scattering region. Note that we use a local coordinate system such that positive $x_\alpha$ point from the corresponding reservoir towards the scatterer, and we write $\boldsymbol{x}_{\perp,\alpha} = (y_\alpha, z_\alpha)$. In all other leads $\beta \neq \alpha$ this scattering state consists of the partially transmitted waves originating from $\alpha$,

$$\psi_{\alpha m}(\boldsymbol{x}_\beta) = \sum_n \frac{1}{\sqrt{2\pi\hbar v_n(\epsilon)}} S_{\beta n,\alpha m} \phi_n(\boldsymbol{x}_{\perp,\beta}) \mathrm{e}^{-\mathrm{i}k_{\beta n} x_\beta}. \tag{2.7}$$

Here $S_{\beta n,\alpha m}$ are elements of the scattering matrix, $\phi_n(\boldsymbol{x}_{\perp,\alpha})$ denote the transverse wave functions with energy $\epsilon_n$, and the wave vectors $k_n = \sqrt{2m(\epsilon - \epsilon_{\alpha n})/\hbar}$ are fixed by the energy $\epsilon$ of the scattering state.

The operators $\hat{a}^\dagger_{\alpha m}(\epsilon)$ $[\hat{a}_{\alpha m}(\epsilon)]$ create (annihilate) an electron with energy $\epsilon$ in the incoming scattering state originating from reservoir $\alpha$. These operators obey the usual fermionic anticommutation relations,

$$\left\{\hat{a}^\dagger_{\alpha m}(\epsilon), \hat{a}_{\beta n}(\epsilon')\right\} = \delta_{\alpha\beta}\delta_{mn}\delta(\epsilon - \epsilon'), \tag{2.8}$$

$$\left\{\hat{a}^\dagger_{\alpha m}(\epsilon), \hat{a}^\dagger_{\beta n}(\epsilon')\right\} = \left\{\hat{a}_{\alpha m}(\epsilon), \hat{a}_{\beta n}(\epsilon')\right\} = 0, \tag{2.9}$$

where $\{.,.\}$ denotes an anticommutator. Similarly, one can introduce annihilation (creation) operators $\hat{b}_{\alpha m}(\epsilon)$ $[\hat{b}^\dagger_{\alpha m}(\epsilon)]$ for electrons in the outgoing states in probe $\alpha$, also obeying the usual anticommutation relations. These two sets of operators are related via

the scattering matrix,

$$\hat{\boldsymbol{b}}_\alpha(\epsilon) = \sum_\beta S_{\alpha\beta}(\epsilon)\, \hat{\boldsymbol{a}}_\beta(\epsilon), \tag{2.10}$$

where the vector $\hat{\boldsymbol{a}}_\alpha(\epsilon)$ $[\hat{\boldsymbol{b}}_\alpha(\epsilon)]$ contains the elements $\hat{a}_{\alpha m}(\epsilon)$ $[\hat{b}_{\alpha m}(\epsilon)]$ of the transport channels $m = 1, ..., N_\alpha$. $S_{\alpha\beta}$ are the blocks of the scattering matrix describing the transmission from reservoir $\beta$ through the scattering region to $\alpha$ (for $\alpha \neq \beta$) while the diagonal blocks $S_{\alpha\alpha}$ contain the information about reflection to the same reservoir. In Fig. 2.3 the situation is illustrated for two channels in a two-terminal setup.

Conservation of the number of particles implies that the S-matrix is unitary,

$$S\, S^\dagger = 1. \tag{2.11}$$

Moreover, time-reversal implies the relation

$$S_{\alpha m,\beta n}(\boldsymbol{B}) = S_{\beta n,\alpha m}(-\boldsymbol{B}), \tag{2.12}$$

where $\boldsymbol{B}$ denotes a magnetic field. In particular this implies $S = S^T$ for time-reversal invariant systems with $\boldsymbol{B} = 0$.

### 2.1.3. Landauer Büttiker formula

The current through lead $\alpha$ is expressed in terms of the distribution functions for incoming and outgoing electrons as

$$I_\alpha = \frac{2e}{h} \int \mathrm{d}\epsilon \, \left[ f_\alpha^{\mathrm{in}}(\epsilon) - f_\alpha^{\mathrm{out}}(\epsilon) \right], \tag{2.13}$$

where the electron velocity has been canceled against the corresponding factor in the density of states, as discussed above. The filling factor of incoming particles originating from the reservoir $\alpha$ is given by the Fermi distribution function of reservoir $\alpha$,

$$f_\alpha^{\mathrm{in}}(\epsilon) = \langle \hat{\boldsymbol{a}}_\alpha^\dagger(\epsilon) \cdot \hat{\boldsymbol{a}}_\alpha(\epsilon) \rangle = f_\alpha(\epsilon), \tag{2.14}$$

see also Eq. (2.3). Using Eq. (2.10), we can relate the distribution function for the outgoing particles $f_\alpha^{\mathrm{out}}$ with the known distribution function of the leads so that we obtain

$$f_\alpha^{\mathrm{out}} = \langle \hat{\boldsymbol{b}}_\alpha^\dagger(\epsilon) \cdot \hat{\boldsymbol{b}}_\alpha(\epsilon) \rangle = \sum_\beta \sum_{m,n} f_\beta(\epsilon)\, |S_{\alpha m,\beta n}|^2, \tag{2.15}$$

where $|S_{\alpha m,\beta n}|^2$ gives the fraction of electrons entering the scatterer through lead $\beta$ in channel $n$ and leaving it via lead $\alpha$ in channel $m$.[1] Therefore we obtain

$$\begin{aligned} I_\alpha &= \frac{2e}{h} \int \mathrm{d}\epsilon \sum_\beta \sum_{mn} f_\beta(\epsilon) \, \left[ \delta_{\alpha\beta}\delta_{mn} - |S_{\alpha m,\beta n}|^2 \right] \\ &= \frac{2e}{h} \int \mathrm{d}\epsilon \sum_\beta f_\beta(\epsilon)\, \mathrm{Tr} \left[ \delta_{\alpha\beta} - S_{\alpha\beta}^\dagger S_{\alpha\beta} \right], \end{aligned} \tag{2.16}$$

[1] The probability of reflection back to lead $\alpha$ into channel $m$ is given by $\mathcal{R}_{\alpha m} = \sum_n |S_{\alpha m,\alpha n}|^2$.

where the trace Tr(...) is over the lead-channels. This is the general multi-channel multi-terminal Landauer-Büttiker expression for the current. Note that by current-conservation $\sum_\alpha I_\alpha = 0$, as encapsulated in the unitarity of the S-matrix.

The situation simplifies for a two-terminal setup as illustrated in Fig. 2.3. Then the expression above becomes

$$I_\alpha = \frac{2e}{h} \int \mathrm{d}\epsilon \, [f_1(\epsilon) - f_2(\epsilon)] \, \mathrm{Tr}[t^\dagger t], \tag{2.17}$$

where we have used the unitarity of $S$ and the $N_R \times N_L$ transmission matrix $t = S_{RL}$ describes the transmission through the scatterer. Assuming zero temperature, this yields for the zero-bias conductance

$$G = \frac{2e^2}{h} \mathrm{Tr}[t^\dagger t]. \tag{2.18}$$

Alternatively one can replace the trace by a sum over all transmission eigenvalues $\mathcal{T}_m$ of the matrix $t^\dagger t$. Note that this expression for the conductance is a generalization of the result in Eq. (2.5) to situations in which the channels are neither completely open nor completely closed.

## 2.2. Green's functions

Throughout the thesis we will often use Green's functions in order to describe the dynamics of electrons. In this section we briefly outline the basic properties which we will use in the following chapters. We have benefitted from the pedagogical discussion in the books by Haug and Jauho [2008] and Rammer [2007].

### 2.2.1. Definitions & contour ordering

We are interested in the quantum amplitude for propagation time $t'$ to time $t$. In a general non-equilibrium situation this time evolution is concisely described by the contour-ordered Green's function [Schwinger, 1961; Keldysh, 1965]

$$\mathcal{G}(t, t') = -\mathrm{i}\langle \mathcal{T}_\mathrm{c}[\psi(t)\psi^\dagger(t')]\rangle. \tag{2.19}$$

Here $\mathcal{T}_\mathrm{c}$ orders the fermionic annihilation (creation) operators $\psi$ ($\psi^\dagger$) according to the position of their time arguments on the Schwinger-Keldysh contour, see Fig. 2.4. It is convenient to write this propagator in the matrix form

$$\boldsymbol{\mathcal{G}}(t, t') = \begin{pmatrix} \mathcal{G}^{11}(t, t') & \mathcal{G}^{12}(t, t') \\ \mathcal{G}^{21}(t, t') & \mathcal{G}^{22}(t, t') \end{pmatrix}. \tag{2.20}$$

Here the indices of $\mathcal{G}^{ab}(t, t')$ indicate that the time $t$ ($t'$) belongs to branch $a$ ($b$), where $a, b = 1, 2$ and 1 (2) labels the upper (lower) branch of the Keldysh contour.

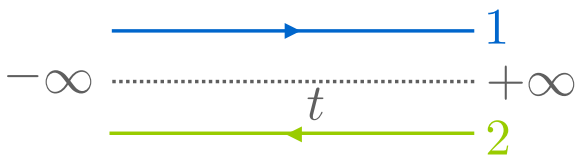


Figure 2.4. The Schwinger-Keldysh contour. It evolves from $t = -\infty$ to $+\infty$ and returns to $-\infty$.

$\mathcal{G}^{12}(t,t') = \mathcal{G}^{<}(t,t')$ and $\mathcal{G}^{21}(t,t') = \mathcal{G}^{>}(t,t')$ are refered to as lesser and greater Green's functions and are given by

$$\mathcal{G}^{<}_{\nu\nu'}(t,t') = +\mathrm{i}\langle\psi^{\dagger}_{\nu'}(t')\psi_{\nu}(t)\rangle, \tag{2.21}$$

$$\mathcal{G}^{>}_{\nu\nu'}(t,t') = -\mathrm{i}\langle\psi_{\nu'}(t)\psi^{\dagger}_{\nu'}(t')\rangle, \tag{2.22}$$

respectively. The propagators on the diagonal are the time-ordered and anti-time-ordered Green's functions. It is often more convenient to work in the representation introduced by Larkin and Ovchinnikov [1975],

$$\boldsymbol{\mathcal{G}} = \frac{1}{2}\begin{pmatrix} 1 & 1 \\ 1 & -1 \end{pmatrix}\begin{pmatrix} \mathcal{G}^{11} & \mathcal{G}^{12} \\ \mathcal{G}^{21} & \mathcal{G}^{22} \end{pmatrix}\begin{pmatrix} 1 & 1 \\ -1 & 1 \end{pmatrix} = \begin{pmatrix} \mathcal{G}^{\mathrm{R}} & \mathcal{G}^{\mathrm{K}} \\ 0 & \mathcal{G}^{\mathrm{A}} \end{pmatrix}, \tag{2.23}$$

where the Keldysh Green's function is given by $\mathcal{G}^{\mathrm{K}} = \mathcal{G}^{>} + \mathcal{G}^{<}$ and we have dropped the time arguments for convenience. The retarded Green's function is defined as

$$\mathcal{G}^{R}_{\nu\nu'}(t,t') = -\mathrm{i}\theta(t-t')\langle\{\psi_{\nu}(t), \psi^{\dagger}_{\nu'}(t')\}\rangle, \tag{2.24}$$

where $\{.,.\}$ denotes the anticommutator. The advanced Green's function $\mathcal{G}^{A}$,

$$\mathcal{G}^{A}_{\nu\nu'}(t,t') = \mathrm{i}\theta(t'-t)\langle\{\psi_{\nu}(t), \psi^{\dagger}_{\nu'}(t')\}\rangle, \tag{2.25}$$

describes the time-reversed propagation. Here the presence of a particle in state $\nu$ at $t$ depends on the state $\nu'$ at the future time $t'$. Accordingly, the retarded and advanced Green's functions are related through $\mathcal{G}^{R}_{\nu\nu'}(t,t') = [\mathcal{G}^{A}(t',t)_{\nu'\nu}]^{*}$. We also note the relation

$$\mathcal{G}^{R} - \mathcal{G}^{A} = \mathcal{G}^{>} - \mathcal{G}^{<}. \tag{2.26}$$

In the following chapters we will use the Green's functions which appear in Eq. (2.26) in order to describe the occupation of a given quantum state and its temporal dynamics in the context of quantum transport. In particular we consider systems, for instance a quantum dot, which are in contact to leads, and study their transport properties, as illustrated in Fig. 2.5. To be specific, we consider the Hamiltonian

$$H = H_L + H_D + H_T, \tag{2.27}$$

where the first two terms represent the Hamiltonians of the leads and the dot, and the last term describes the tunneling between leads and dot. These constituents and the Green's functions involved will be discussed below.

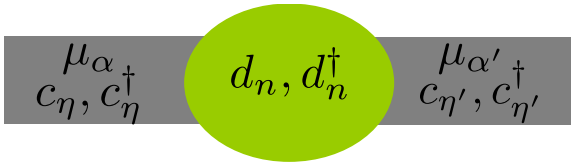


Figure 2.5. Illustration of a mesoscopic structure coupled to leads.

### 2.2.2. Free particles in thermal equilibrium

The leads act as reservoirs for non-interacting electrons kept at fixed chemical potentials $\mu_\alpha$. They can be described by a Hamiltonian of free particles,

$$H_L = \sum_\eta (\epsilon_\eta - \mu_\alpha)\, c_\eta^\dagger c_\eta \,, \tag{2.28}$$

where we represent the electrons in the leads by the creation (annihilation) operators $c_\eta^\dagger$ ($c_\eta$), and $\eta = (\alpha, n, k_{\alpha n})$ is a general 'lead' index, $\eta = 1, \ldots, N_0$ with $N_0 = \sum_\alpha N_\alpha$ with channels $n = 1, \ldots, N_\alpha$, and longitudinal momenta $k_{\alpha n}$. The temporal dynamics is described by the Schrödinger equation, and consequently the Green's functions are solutions to

$$(\mathrm{i}\partial_t - H_L)\, \mathcal{G}^{R(A)}_{\eta\eta'}(t, t') = \delta_{\eta\eta'}\delta(t - t'). \tag{2.29}$$

This can be verified using that the time evolution of the operators is given by $-\mathrm{i}\partial_t \psi_\eta(t) = [H_L, \psi_\eta](t)$.[2] It is easy to see that the (Fourier transform of the) corresponding solution is given by

$$\mathcal{G}^{R(A)}_{0\eta\eta'}(\epsilon) = \frac{\delta_{\eta\eta'}}{\epsilon - \epsilon_\eta \pm \mathrm{i}0^+}, \tag{2.30}$$

where the subscript 0 indicates the free Green's function. The occupation of state $\eta$ is given by $\langle \psi_\eta^\dagger \psi_\eta \rangle = -\mathrm{i}\mathcal{G}^<_{0\eta\eta}(0) = \int \frac{\mathrm{d}\epsilon}{2\pi} f_\alpha(\epsilon_\eta) \left[-2\mathrm{Im}\mathcal{G}^R_{0\eta\eta}\right]$. In thermal equilibrium, the lesser Green's function reads

$$\mathcal{G}^<_{0\eta\eta'}(t - t') = i\delta_{\eta\eta'} f_\alpha(\epsilon_\eta) \mathrm{e}^{-i(t-t')\epsilon_\eta}, \tag{2.31}$$

with the Fermi-Dirac distribution $f_\alpha(\epsilon)$ defined in Eq. (2.4). We note that for free particles the spectral function, given by $-2\mathrm{Im}\mathcal{G}^R = \mathcal{G}^A - \mathcal{G}^R$, is proportional to a delta distribution, see Eq. (2.30).

### 2.2.3. Coupling to leads: the self-energy

In this section we discuss the equations of motion for propagators of a dot which is connected to non-interacting electronic reservoirs (possibly at different chemical potentials), see Fig. 2.5. The coupling to leads can cause a shift and a broadening of the

[2] Note that $\hbar$ is set to one for notational simplicity.

dot's electronic levels; this hybridization with the leads will be expressed in terms of self-energies, as will be pointed out in the remainder of this section. For a more detailed discussion we refer to the book by Haug and Jauho [2008].

The benefit of the Larkin-Ovchinnikov representation, see Eq. (2.23), is that the self-energy $\mathbf{\Sigma}$ also has a tridiagonal structure so that the Dyson equation takes the form

$$\boldsymbol{\mathcal{G}} = \begin{pmatrix} \mathcal{G}_0^R & \mathcal{G}_0^K \\ 0 & \mathcal{G}_0^A \end{pmatrix} + \begin{pmatrix} \mathcal{G}^R & \mathcal{G}^K \\ 0 & \mathcal{G}^A \end{pmatrix} \begin{pmatrix} \Sigma^R & \Sigma^K \\ 0 & \Sigma^A \end{pmatrix} \begin{pmatrix} \mathcal{G}_0^R & \mathcal{G}_0^K \\ 0 & \mathcal{G}_0^A \end{pmatrix}, \tag{2.32}$$

where $\mathcal{G}_0$ is the free Green's function. This provides prescriptions how to connect the different Green's functions, as we briefly outline now. Note that we have suppressed all time arguments and that products of propagators correspond to convolutions in the time domain. Matrix multiplication yields

$$\mathcal{G}^{R(A)} = \mathcal{G}_0^{R(A)} + \mathcal{G}^{R(A)}\Sigma^{R(A)}\mathcal{G}_0^{R(A)} \tag{2.33}$$

$$\mathcal{G}^K = \mathcal{G}_0^K + \mathcal{G}^R\Sigma^R\mathcal{G}_0^K + \mathcal{G}^R\Sigma^K\mathcal{G}_0^A + \mathcal{G}^K\Sigma^A\mathcal{G}_0^A. \tag{2.34}$$

These relations between the Green's functions are often also refered to as Langreth's rules.

These propagators will be studied in more detail next. In particular, we show how the Green's functions of the dot are affected by the coupling to the leads. The generic Hamiltonian for the quantum dot reads

$$H_D = \sum_{mm'} d_m^\dagger \left[h_0\right]_{mm'} d_{m'}, \tag{2.35}$$

where the hermitian $M \times M$ matrix $h_0$ contains information about the $M$ electronic levels of the dot. (In the next chapter we will also include an additional coupling to further local degrees of freedom.) The operator $d^\dagger$ ($d$) creates (annihilates) an electron in the dot and the indices $m$, $m'$ ($= 1, \ldots, M$) label the electronic levels.

Finally, the Hamiltonian $H_T$ represents the tunneling between the leads and the levels in the dot,

$$H_T = \sum_{\eta,m} (c_\eta^\dagger w_{\eta m} d_m + \text{h.c.}) \,. \tag{2.36}$$

Due to this coupling with the leads the energy levels will be broadened (and eventually shifted).

In the next chapter we will express the physical quantities, the current and the forces exerted by it, in terms of the Green's function of the dot. First, we define the retarded Green's functions

$$\mathcal{G}_{n,\eta}^R(t,t') = -\mathrm{i}\theta(t-t')\langle\{d_n(t), c_\eta^\dagger(t')\}\rangle, \tag{2.37}$$

$$\mathcal{G}_{n,n'}^R(t,t') = -\mathrm{i}\theta(t-t')\langle\{d_n(t), d_{n'}^\dagger(t')\}\rangle, \tag{2.38}$$

where $\mathcal{G}^R_{n,\eta}$ contains operators from both the island and the leads and $\mathcal{G}^R_{n,n'}$ is the Green's function of the dot. The time evolution of the former is described by the Dyson equation

$$(-\mathrm{i}\partial_{t'} - \epsilon_\eta)\,\mathcal{G}^R_{n,\eta}(t,t') = \sum_{n'} \mathcal{G}^R_{nn'}(t,t')w^\dagger_{n'\eta}. \tag{2.39}$$

Here, the time derivative acts on the second time argument. We solve this equation by multiplying from the right with the free electronic Green's function of the uncoupled non-interacting leads $\mathcal{G}^R_{0\eta_1\eta}$, given by Eq. (2.30). Then we obtain

$$\mathcal{G}^R_{n,\eta}(t,t') = \int \mathrm{d}t_1 \sum_{n_1\eta_1} \mathcal{G}^R_{nn_1}(t,t_1)w^\dagger_{n_1\eta_1}\mathcal{G}^R_{0\eta_1\eta}(t_1-t'). \tag{2.40}$$

Similarly, the time evolution of the retarded Green's function of the dot obeys a Dyson equation containing $\mathcal{G}^R_{n,\eta}$. We decouple these equations by multiplying (2.40) with the coupling matrix and summing over all states in the leads:

$$\sum_\eta \mathcal{G}^R_{n\eta}(t,t_1)w_{\eta n'} = \int \mathrm{d}t_1 \sum_{n_1} \mathcal{G}^R_{nn_1}(t,t_1)\Sigma^R_{n_1n'}(t_1,t'), \tag{2.41}$$

where we have introduced the self-energy

$$\Sigma^R_{nn'}(t,t') = \sum_{\eta\eta'} w^\dagger_{n\eta}\mathcal{G}^R_{0\eta\eta'}(t-t')w_{\eta'n'}. \tag{2.42}$$

This allows us to write

$$\begin{aligned}-\mathrm{i}\partial_{t'}\mathcal{G}^R_{mm'}(t,t') =& \delta(t-t')\delta_{mm'} + \sum_{m_1}\int \mathrm{d}t_1 \mathcal{G}^R_{mm_1}(t,t_1)\Sigma^R_{m_1m'}(t_1,t') \\ &+ \sum_{m_1} \mathcal{G}^R_{mm_1}(t,t')(h_0)_{m_1m'}\,,\end{aligned} \tag{2.43}$$

which is equivalent to Eq. (2.33).

Thus, indeed all information about the leads is contained in the self-energy $\Sigma^R_{m_1m'}(t_1,t')$, as given by Eq. (2.42). Later we will particularly use its Fourier transform

$$\Sigma^R(\epsilon) = -\mathrm{i}\sum_\alpha \Gamma^\alpha(\epsilon), \tag{2.44}$$

$$\Gamma^\alpha(\epsilon) = \pi W^\dagger(\epsilon)\Pi_\alpha W(\epsilon), \tag{2.45}$$

where $\Pi_\alpha$ is a projection operator onto lead $\alpha$ and we have absorbed square root factors of the density of states in the leads into the (possibly energy-dependent) coupling matrix $W$ for notational simplicity. We will return to these expressions in the next chapter when we derive the current-induced forces in a NEMS in terms of the dot's Green's functions.

Combining Eq. (2.33) and Eq. (2.34) we obtain with Eq. (2.26) for the lesser Green's function

$$\begin{aligned}\mathcal{G}^< =& \mathcal{G}^<_0 + \mathcal{G}^R\Sigma^R\mathcal{G}^<_0 + \mathcal{G}^<\Sigma^A\mathcal{G}^A_0 + \mathcal{G}^R\Sigma^<\mathcal{G}^A_0 \\ =& \left(1+\mathcal{G}^R\Sigma^R\right)\mathcal{G}^<_0\left(1+\Sigma^A\mathcal{G}^A_0\right) + \mathcal{G}^R\Sigma^<\mathcal{G}^A_0\left(1+\Sigma^A\mathcal{G}^A_0\right) + \mathcal{G}^<\Sigma^A\mathcal{G}^A_0\Sigma^A\mathcal{G}^A_0.\end{aligned} \tag{2.46}$$

Here we have iterated by re-inserting the expression for $\mathcal{G}^<$ into the right hand side. Since the leads are non-interacting, we can use $\left(1+\mathcal{G}^R\Sigma^R\right)\mathcal{G}_0^< = \mathcal{G}^R(\mathcal{G}_0^R)^{-1}\mathcal{G}_0^< = 0$, see [Haug and Jauho, 2008]. Accordingly, Eq. (2.46), becomes

$$\mathcal{G}^<_{mm'}(t,t') = \int \mathrm{d}t_1 \int \mathrm{d}t_2 \sum_{mm_1} \mathcal{G}^R_{mm_1}(t,t_1)\Sigma^<_{m_1m_2}(t_1,t_2)\mathcal{G}^A_{m_2m'}(t_2,t'), \tag{2.47}$$

where we have restored all time and state indices. Here we use the lesser self-energy $\Sigma^<_{nn'}(t,t') = \sum_{\eta\eta'} w^\dagger_{n\eta}\mathcal{G}^<_{0\eta\eta'}(t-t')w_{\eta'n'}$, with the lesser Green's function of the leads $\mathcal{G}^<_{0\eta\eta'}(t-t')$ given by Eq. (2.31). Note that $w$ and $w^\dagger$ do not depend on time and hence the self energies depend only on time differences. Accordingly, its Fourier transform takes the form

$$\Sigma^<(\epsilon) = 2\mathrm{i}\sum_\alpha f_\alpha(\epsilon)\Gamma^\alpha(\epsilon)\,. \tag{2.48}$$

### 2.2.4. Current

Within this formalism we can now give an expression for the current in terms of the Green's functions of the dot and the corresponding self-energies. The electronic current through lead $\alpha$ is given by

$$I_\alpha = -e\langle\dot{N}_\alpha\rangle = \mathrm{i}e\sum_{n,\eta\in\alpha} w_{\eta n}\langle c^\dagger_\eta(t)d_n(t)\rangle + \text{h.c.}, \tag{2.49}$$

with $N_\alpha = \sum_{\eta\in\alpha} c^\dagger_\eta c_\eta$. Consequently, we introduce the lesser Green's function

$$\mathcal{G}^<_{n\eta}(t,t') = \mathrm{i}\langle c^\dagger_\eta(t')d_n(t)\rangle \tag{2.50}$$

which is, according to Langreth's rules (see Section 2.2.3), given by

$$\mathcal{G}^<_{n\eta}(t,t') = \int \mathrm{d}t_1 \sum_{n_1\eta_1} w^\dagger_{n_1\eta_1}\left[\mathcal{G}^R_{nn_1}(t,t_1)\mathcal{G}^<_{0\eta_1\eta}(t_1-t') + \mathcal{G}^<_{nn_1}(t,t_1)\mathcal{G}^A_{0\eta_1\eta}(t_1-t')\right]. \tag{2.51}$$

Using the expressions for the self-energies the current becomes

$$I_\alpha(t) = e\int \mathrm{d}t'\,\mathrm{tr}\left\{\mathcal{G}^R(t,t')\Sigma^<_\alpha(t',t) + \mathcal{G}^<(t,t')\Sigma^A_\alpha(t',t)\right\} + \text{h.c.} \tag{2.52}$$

$$= e\int \mathrm{d}t'\,\mathrm{tr}\left\{\mathcal{G}^>(t,t')\Sigma^<_\alpha(t',t) - \mathcal{G}^<(t,t')\Sigma^>_\alpha(t',t)\right\}, \tag{2.53}$$

and is thus completely expressed in terms of the Green's functions of the dot and its self-energies.

## 2.3. Wigner representation

It is often helpful to use the Wigner representation of the Green's functions. This is motivated by the fact that the Green's functions $\boldsymbol{\mathcal{G}}(t_1,t_2)$ oscillate rapidly with the

relative time $\tau = t_1 - t_2$. At the same time, they frequently depend only weakly on the central time $t = (t_1 + t_2)/2$. In order to separate these fast and slow time scales easily it is convenient to use so-called mixed or Wigner coordinates, see for instance [Haug and Jauho, 2008; Rammer, 2007].

In Wigner coordinates, in this section denoted by a tilde, a general function $A(t_1, t_2)$ depending on two time arguments reads

$$\tilde{A}(\tau, t) = A(t + \tau/2, t - \tau/2). \tag{2.54}$$

In order to perform an adiabatic expansion of such a function, it is convenient to consider its Wigner transform,

$$\tilde{A}(\epsilon, t) = \int \mathrm{d}\tau \, \mathrm{e}^{\mathrm{i}\epsilon\tau} \tilde{A}(\tau, t) \,, \tag{2.55}$$

in which a Fourier transform is taken with respect to the relative time. In particular we will deal with a the convolution, $C(t_1, t_2) = \int \mathrm{d}t_3 \, A(t_1, t_3) B(t_3, t_2)$, which is, in mixed coordinates, given by

$$\tilde{C}(\tau, t) = \int \mathrm{d}t_3 \, \tilde{A}(t_1 - t_3, t + \frac{t_3 - t_2}{2}) \tilde{B}(t_3 - t_2, t + \frac{t_3 - t_1}{2}). \tag{2.56}$$

In order to obtain its Wigner transform we expand $\tilde{A}(t_1 - t_3, t + \frac{t_3 - t_2}{2})$ in the central time $t$,

$$\tilde{A}(t_1 - t_3, t + \frac{t_3 - t_2}{2}) = \sum_{n=0}^{\infty} \frac{1}{n!} \left( \frac{t_3 - t_2}{2} \right)^n \partial_t^{(n)} \tilde{A}(t_1 - t_3, t), \tag{2.57}$$

and perform a similar expansion for $\tilde{B}$. Using that the Fourier transform of a convolution factorizes, we obtain for the Wigner transform of the convolution

$$\begin{aligned} \tilde{C}(\epsilon, t) &= \exp\left[ \frac{\mathrm{i}}{2} \left( \partial_\epsilon^{\tilde{A}} \partial_t^{\tilde{B}} - \partial_t^{\tilde{A}} \partial_\epsilon^{\tilde{B}} \right) \right] \tilde{A}(\epsilon, t) \tilde{B}(\epsilon, t) \\ &\simeq \tilde{A}(\epsilon, t) \tilde{B}(\epsilon, t) + \frac{\mathrm{i}}{2} \partial_\epsilon \tilde{A}(\epsilon, t) \partial_t \tilde{B}(\epsilon, t) - \frac{\mathrm{i}}{2} \partial_t \tilde{A}(\epsilon, t) \partial_\epsilon \tilde{B}(\epsilon, t), \end{aligned} \tag{2.58}$$

where we have dropped higher order derivatives in the last line, exploiting the slow variation with $t$.

## 2.4. Summary

In this chapter we have sketched the formalisms which we will use throughout this thesis in order to describe the systems under study. We have briefly outlined how a mesoscopic conductor can be treated in terms of the scattering matrix, resulting in the famous Landauer-Büttiker formula for the conductance. Additionally, non-equilibrium Green's functions are common in order to cope with electronic transport properties. We have

introduced the basic ingredients, namely the various Green's functions in the Keldysh framework. In particular, we have described the coupling of the conductor to electronic reservoirs in terms of the self-energy. We will utilize these tools in the next chapters for the description of transport properties and current-induced forces. For the latter we will encounter a separation of timescales, which will be treated within the so-called Wigner representation, which we have briefly described at the end of the present chapter.

# 3. Current-induced forces in mesoscopic systems

In this chapter we investigate the interplay between the current flowing through a general mesoscopic conductor and slow mechanical degrees of freedom. In these nanoelectromechanical systems (NEMS) the conduction electrons exert forces on the mechanical modes, which we study, as well as the backaction on the electronic transport.

We consider the limit in which the vibrational dynamics is much slower than the typical electronic timescales. Thus the electrons moving through the device experience an approximately static configuration of the mechanical degrees of freedom. In this limit it is appropriate to use a non-equilibrium Born-Oppenheimer (NEBO) approximation, which allows us to describe the vibrational dynamics in terms of a Langevin equation containing forces which are exerted by the current on the mechanical modes.


Figure 3.1. Sketch of a NEMS.

Subsequent to a short introduction, we describe the theoretical model and derive the equations of motion of the mechanical degrees of freedom in Section 3.2. We show how a Langevin equation emerges naturally from a microscopic model when employing the NEBO approximation and derive the current-induced forces in terms of the microscopic parameters. In Section 3.3 we employ the scattering matrix approach to quantum transport to develop a unified theory of NEMS out of equilibrium. In particular, we show that the current-induced forces can be written in terms of parametric derivatives of the scattering matrix (S-matrix) of the system, and state general properties that can be derived from S-matrix symmetry considerations. We complete the discussion of NEMS in terms of S-matrices by providing a corresponding expression for the charge current in in Section 3.4.

The results presented here are adopted from [Bode *et al.*, 2011] and [Bode *et al.*, 2012d].

## 3.1. Introduction

We consider the limit in which the electrons propagate through the nanostructure rapidly, observing a quasistatic configuration of the vibrational modes, but affecting their dynamics profoundly at the same time [Naik *et al.*, 2006; Steele *et al.*, 2009; Lassagne *et al.*, 2009; Stettenheim *et al.*, 2010]. This limit allows us to treat the vibrational degrees of freedom as classical entities embedded in a quantum coherent electronic environment: pictorially,

many electrons pass through the nanostructure during one vibrational period, impinging randomly on the modes. In this limit, it is natural to assume that the dynamics of the vibrational modes, represented by collective coordinates $X_\nu$, will be governed by a set of coupled Langevin equations

$$M_\nu \ddot{X}_\nu + \frac{\partial U}{\partial X_\nu} = F_\nu - \sum_{\nu'} \gamma_{\nu\nu'} \dot{X}_{\nu'} + \xi_\nu \,. \tag{3.1}$$

Here we have grouped the purely elastic contribution on the left hand side (LHS) of Eq. (3.1), $M_\nu$ is the effective mass of mode $\nu$, and $U(\boldsymbol{X})$ an elastic potential. On the right hand side (RHS) we have collected the current-induced forces: the main result of this chapter are expressions for these forces in terms of the scattering matrix and its parametric derivatives. These current-induced forces include the mean force $F_\nu(\boldsymbol{X})$, the stochastic force $\xi_\nu$, and two kinds of velocity-dependent forces (dissipative friction force and effective "Lorentz" force) encoded by the matrix $\gamma_{\nu\nu'}(\boldsymbol{X})$.

Theoretically, these forces have been studied previously within different formalisms, as we have outlined in the introduction, Section 1.2.1. In the preceding chapter we have introduced the basic ingredients which we need for the description of transport through mesoscopic structures. Note that our discussion of scattering theory, Section 2.1, resulting in the famous Landauer-Büttiker formula for the conductance of mesoscopic conductors [Landauer, 1957, 1970; Büttiker *et al.*, 1985; Büttiker, 1986], did not include time-dependent scattering; the application to time-dependent scattering is the topic of this chapter. For time-dependent phenomena, scattering matrix expressions have been obtained for quantum pumping [Brouwer, 1998; Avron *et al.*, 2001], a process by which a direct current is generated through temporal variations of relevant parameters of the system, such as a gate voltage or a magnetic field. The case of pumping in an out-of-equilibrium, biased system has remained largely unexplored so far [Entin-Wohlman *et al.*, 2002; Moskalets and Büttiker, 2005].

We fully express the current-induced forces in terms of a scattering matrix formalism, for arbitrary (albeit adiabatic) out-of-equilibrium situations, thus providing the tools for a systematic approach to study the interplay between electronic and mechanical degrees of freedom in NEMS. Our formalism allows us to retain the non-linearities of the problem, which are essential for even a qualitative description of the dynamics, while turning the problem of calculating the current-induced forces into a scattering problem for which standard techniques can be applied.

## 3.2. Microscopic derivation of the Langevin equation

We start our discussion with a description of the model and a derivation of analytical expressions for the current-induced forces within the NEBO approximation in terms of non-equilibrium Green's functions.

### 3.2.1. Model

We model the system as a mesoscopic quantum dot connected to multiple leads and coupled to vibrational degrees of freedom, as illustrated in Fig. 3.1. Throughout this discussion we consider non-interacting electrons and we set $\hbar = 1$. The Hamiltonian for the full system reads

$$H = H_L + H_T + H_D + H_X \,, \tag{3.2}$$

where the different terms are introduced in the following.

The dot is coupled to leads which are modeled as non-interacting electronic reservoirs at fixed chemical potentials. The corresponding Hamiltonian $H_L$ is given by Eq. (2.28). The coupling between the different leads and the dot is described by the tunneling Hamiltonian $H_T$, see Eq. (2.36). The dot's levels hybridize with the leads due to this coupling as discussed to some extent in the preceding chapter (see Section 2.2.3). We describe the quantum dot itself by $M$ electronic levels coupled to $N$ slow collective degrees of freedom $\hat{\boldsymbol{X}} = (\hat{X}_1, \ldots, \hat{X}_N)$. This is contained in the dot's Hamiltonian

$$H_D = \sum_{mm'} d_m^\dagger \left[ h_0(\hat{\boldsymbol{X}}) \right]_{mm'} d_{m'} \tag{3.3}$$

which describes the electronic levels of the dot and their dependence on the collective modes' coordinates $\hat{X}_\nu$ ($\nu = 1, \ldots, N$) by the hermitian $M \times M$ matrix $h_0(\hat{\boldsymbol{X}})$.[1] The operator $d^\dagger$ ($d$) creates (annihilates) an electron in the dot and the indices $m$, $m'$ ($= 1, \ldots, M$) label the electronic levels. Note that here we allow $h_0$ to be a general function of $\hat{\boldsymbol{X}}$ and that our analysis is valid for any coupling strength. The Hamiltonian

$$H_X = \sum_\nu \left[ \frac{\hat{P}_\nu^2}{2M_\nu} + U(\hat{\boldsymbol{X}}) \right] \tag{3.4}$$

describes the free evolution of the mechanical degrees of freedom of the dot.

### 3.2.2. Non-equilibrium Born-Oppenheimer approximation

We use as a starting point the Heisenberg equations of motion for the mechanical modes which can be cast as

$$M_\nu \ddot{\hat{X}}_\nu + \frac{\partial U}{\partial \hat{X}_\nu} = -\sum_{m,m'} d_m^\dagger \left[ \Lambda^\nu(\hat{\boldsymbol{X}}) \right]_{mm'} d_{m'} \,, \tag{3.5}$$

where we have introduced the $\hat{\boldsymbol{X}}$-dependent matrices

$$\Lambda^\nu \left( \hat{\boldsymbol{X}} \right) = \frac{\partial h_0}{\partial \hat{X}_\nu} \,. \tag{3.6}$$

[1] In the present discussion we assume that the tunneling, described by $H_T$, is unaffected by the coupling to the localized degrees of freedom. In order to describe for instance STM/AFM-setups, straightforward generalizations have to be incorporated, involving $\hat{\boldsymbol{X}}$-dependent tunnel amplitudes in Eq. (2.36).

The RHS of Eq. (3.5) contains the current-induced forces, expressed through the electronic operators $d$ of the quantum dot. We now proceed to calculate these forces within a non-equilibrium Born-Oppenheimer (NEBO) approximation, in which the dynamics of the collective modes is assumed to be slow. In this limit, we can treat the mechanical degrees of freedom as classical, acting as a slow classical field on the fast electronic dynamics.

The NEBO approximation consists of averaging the RHS of Eq. (3.5) over times long compared to the electronic time scales, but short in terms of the oscillator dynamics. In this approximation, the force operator is represented by its (average) expectation value $\langle d^\dagger \Lambda d \rangle_{\boldsymbol{X}(t)}$, evaluated for a given trajectory $\boldsymbol{X}(t)$ of the mechanical degrees of freedom, plus fluctuations containing both Johnson-Nyquist and shot noise. These fluctuations give rise to a Langevin force $\boldsymbol{\xi}$. Hence, Eq. (3.5) becomes

$$M_\nu \ddot{X}_\nu + \frac{\partial U}{\partial X_\nu} = \mathrm{tr}[\mathrm{i}\Lambda^\nu \mathcal{G}^<(t,t)] + \xi_\nu \,, \tag{3.7}$$

where the trace "tr" is taken over the dot levels, and we have introduced the lesser Green's function

$$\mathcal{G}^<_{mm'}(t,t') = \mathrm{i}\langle d^\dagger_{m'}(t') d_m(t) \rangle_{\boldsymbol{X}(t)} \,. \tag{3.8}$$

The variance of the stochastic force $\xi_\nu$ is governed by the symmetrized fluctuations of the operator $d^\dagger \Lambda d$. Given that the electronic fluctuations happen on short time scales, $\xi_\nu$ is locally correlated in time,

$$\langle \xi_\nu(t) \xi_{\nu'}(t') \rangle = D_{\nu\nu'}(\boldsymbol{X}) \delta(t-t') \,, \tag{3.9}$$

as we describe below. (An alternative but equivalent derivation, is based on a saddle point approximation for the Keldysh action, see *e.g.* the review by Kamenev and Levchenko [2009].) Since we are dealing with non-interacting electrons, $D(\boldsymbol{X})$ can be expressed in terms of single particle Green's functions using Wick's theorem, as we detail below. These expressions for the current-induced forces show that we need to evaluate the electronic Green's function for a given classical trajectory $\boldsymbol{X}(t)$. In doing so, we can exploit that the mechanical degrees of freedom are assumed to be slow compared to the electrons. Thus, we can approximate the Green's function by its solution to first order in the velocities $\dot{\boldsymbol{X}}(t)$.

We now proceed with this derivation, starting with the time evolution of the retarded Green's function,

$$\mathcal{G}^R_{mm'}(t,t') = -\mathrm{i}\theta(t-t') \langle \{ d_m(t), d^\dagger_{m'}(t') \} \rangle_{\boldsymbol{X}(t)} \,, \tag{3.10}$$

where $\{.,.\}$ indicates the anticommutator. We note that since we consider non-interacting electrons, we can restore the lesser and greater Green's functions (or the advanced Green's function $\mathcal{G}^A$) at the end of the calculation by standard manipulations, which we have outlined in Section 2.2. The Dyson equation for the retarded Green's function can then be written, in matrix form, as

$$-\mathrm{i}\partial_{t'} \mathcal{G}^R(t,t') = \delta(t-t') + \int \mathrm{d}t_1 \mathcal{G}^R(t,t_1) \Sigma^R(t_1,t') + \mathcal{G}^R(t,t') h_0(\boldsymbol{X}) \,. \tag{3.11}$$

The coupling to the leads is incorporated in the self-energy $\Sigma^R(t_1, t')$, which we have discussed in some detail in Section 2.2.3; see Eq. (2.42) in particular.

To perform the adiabatic expansion, it is convenient to work in the Wigner representation, in which fast and slow time scales are easily identifiable. We can use this representation for the Green's function $\mathcal{G}^R$, since the slow mechanical motion implies that $\mathcal{G}^R(t_1, t_2)$ varies slowly with the central time $t = (t_1 + t_2)/2$ and oscillates fast with the relative time $\tau = t_1 - t_2$. Generally, the Wigner transform of a function $A(t_1, t_2)$ depending on two time arguments, is given by Eq. (2.55), which reads

$$\tilde{A}(\epsilon, t) = \int \mathrm{d}\tau \, \mathrm{e}^{\mathrm{i}\epsilon\tau} A(t + \tau/2, t - \tau/2).$$

The Wigner transform of a convolution $C(t_1, t_2) = \int \mathrm{d}t_3 \, A(t_1, t_3)B(t_3, t_2)$ is given by

$$\tilde{C} \simeq \tilde{A}\tilde{B} + \frac{\mathrm{i}}{2}\partial_\epsilon \tilde{A}\partial_t \tilde{B} - \frac{\mathrm{i}}{2}\partial_t \tilde{A}\partial_\epsilon \tilde{B},$$

as discussed in Section 2.3. Here we have repeated Eq. (2.58) for the convenience of the reader and dropped higher order derivatives, exploiting the slow variation with $t$. Therefore, using Eq. (2.58) we can rewrite the Dyson equation (3.11) as

$$1 \simeq \mathcal{G}^R \left(\epsilon - \Sigma^R - h_0\right) - \frac{\mathrm{i}}{2}\partial_\epsilon \mathcal{G}^R \partial_t h_0 - \frac{\mathrm{i}}{2}\partial_t \mathcal{G}^R \left(1 - \partial_\epsilon \Sigma^R\right) , \tag{3.12}$$

where the Green's functions are now in the Wigner representation. Unless otherwise denoted by explicitly stating the variables, here and in the remainder of this chapter all functions are in the Wigner representation. Dropping all time derivatives in Eq. (3.12), one obtains the strictly adiabatic Green's function

$$G^R(\epsilon, \boldsymbol{X}) = \left[\epsilon - h_0(\boldsymbol{X}) - \Sigma^R(\epsilon)\right]^{-1} . \tag{3.13}$$

Our notation is such that $\mathcal{G}$ denotes *full* Green's functions, while $G$ denotes the strictly adiabatic (or *frozen*) Green's functions that are evaluated for a fixed value of $\boldsymbol{X}$ (so that all derivatives with respect to central time in Eq. (3.12) can be dropped). From now on, $\mathcal{G}^{(R,A,<,>)}$ denote the Green's functions in the Wigner representation, with arguments $(\epsilon, t)$, and $\mathcal{G}^A = (\mathcal{G}^R)^\dagger$. The self-energy is given by $\Sigma^R(\epsilon) = -\mathrm{i}\pi W^\dagger(\epsilon)W(\epsilon)$ where $W$ denotes the coupling matrix to the leads, see Eq. (2.44) in the previous chapter. Thus, from (3.13) it is easy to see that

$$W^\dagger W = \frac{1}{2\pi\mathrm{i}}[(G^R)^{-1} - (G^A)^{-1}] . \tag{3.14}$$

The following two other identities will be used repeatedly:

$$\partial_{X_\nu} G^R = G^R \Lambda^\nu G^R, \tag{3.15}$$

$$-\partial_\epsilon G^R = G^R(1 - \partial_\epsilon \Sigma^R)G^R. \tag{3.16}$$

These relations are obtained by differentiating $G^R\left[\epsilon - h_0(\boldsymbol{X}) - \Sigma^R(\epsilon)\right] = 1$ with respect to $X_\nu$ and $\epsilon$, respectively, multiplying the result with $G^R$ and using the definition (3.6). Finally, with the help of Eqs. (3.15) and (3.16), we obtain to first order in $\dot{X}_\nu$

$$\mathcal{G}^R \simeq G^R + \frac{\mathrm{i}}{2}\sum_\nu \dot{X}_\nu \left(\partial_\epsilon G^R \Lambda^\nu G^R - G^R \Lambda^\nu \partial_\epsilon G^R\right). \tag{3.17}$$

$\mathcal{G}^<$ and $\mathcal{G}^R$ are related through Langreth's rule, Eq. (2.47), which states $\mathcal{G}^<(t,t') = \int \mathrm{d}t_1 \int \mathrm{d}t_2\, \mathcal{G}^R(t,t_1)\Sigma^<(t_1,t_2)\mathcal{G}^A(t_2,t')$. Note that in the Wigner representation the lesser self-energy $\Sigma^<(\epsilon)$ depends only on $\epsilon$ and is independent of the central time, *cf.* Eq. (2.48). Expanding Eq. (2.47) up to the leading adiabatic correction according to Eq. (2.58), we obtain $\mathcal{G}^<$ to first order in $\dot{\boldsymbol{X}}$,

$$\mathcal{G}^< = G^< + \frac{\mathrm{i}}{2}\dot{\boldsymbol{X}}\cdot\left[(\partial_\epsilon G^<)\boldsymbol{\Lambda} G^A - G^R\boldsymbol{\Lambda}\partial_\epsilon G^< + (\partial_\epsilon G^R)\boldsymbol{\Lambda}G^< - G^<\boldsymbol{\Lambda}\partial_\epsilon G^A\right]. \tag{3.18}$$

The frozen lesser Green's function is

$$G^< = G^R\Sigma^< G^A = 2\pi\mathrm{i}\sum_\alpha f_\alpha\, G^R W^\dagger \Pi_\alpha W G^A, \tag{3.19}$$

we use $G^A = [G^R]^\dagger$, $f_\alpha$ is the Fermi distribution, and $\Pi_\alpha$ is a projector on lead $\alpha$, see also Eq. (2.45) and Eq. (2.48). We will also encounter the strictly adiabatic greater Green's function, which is given by

$$G^> = -2\pi i\sum_\alpha (1-f_\alpha)\, G^R W^\dagger \Pi_\alpha W G^A. \tag{3.20}$$

In order to obtain this expression we have used the general relation between the various Green's functions $G^R - G^A = G^> - G^<$, see Eq. (2.26), as well as Eqs. (3.14) and (3.19).

### 3.2.3. Current-induced forces in terms of Green's functions

We can now collect the results from the previous section and identify the current-induced forces appearing in the Langevin equation (3.1). Except for the stochastic noise force, the current induced forces are encoded in $\mathrm{tr}(\mathcal{G}^<\Lambda^\nu)$. In the strictly adiabatic limit, *i.e.*, retaining only the first term on the RHS of Eq. (3.18), $\mathcal{G}^< \simeq G^<$, we obtain the mean force

$$F_\nu(\boldsymbol{X}) = -\int \frac{\mathrm{d}\epsilon}{2\pi\mathrm{i}}\ \mathrm{tr}\left[\Lambda^\nu G^<\right]. \tag{3.21}$$

The leading order correction in Eq. (3.18) gives a velocity-dependent contribution to the current induced forces, which determines the tensor $\gamma_{\nu\nu'}$. After integration by parts, we find

$$\gamma_{\nu\nu'} = \int \frac{\mathrm{d}\epsilon}{2\pi}\mathrm{tr}\left(G^<\Lambda^\nu\partial_\epsilon G^R\Lambda^{\nu'} - G^<\Lambda^{\nu'}\partial_\epsilon G^A\Lambda^\nu\right). \tag{3.22}$$

This tensor can be split into symmetric and anti-symmetric contributions, $\gamma = \gamma^s + \gamma^a$, which define a dissipative term $\gamma^s$ and an orbital, effective magnetic field $\gamma^a$ in the

space of the collective modes. The latter interpretation is based on the fact that the corresponding force takes a Lorentz-like form, as we will discuss below. Using Eq. (2.26), and noting that $2\int d\epsilon G^< \partial_\epsilon G^< = \int d\epsilon \partial_\epsilon (G^<)^2 = 0$, we obtain the explicit expressions

$$\gamma^s_{\nu\nu'}(\boldsymbol{X}) = \int \frac{\mathrm{d}\epsilon}{2\pi} \mathrm{tr}\left\{\Lambda^\nu G^< \Lambda^{\nu'} \partial_\epsilon G^>\right\}_s , \tag{3.23}$$

$$\gamma^a_{\nu\nu'}(\boldsymbol{X}) = -\int \frac{\mathrm{d}\epsilon}{2\pi} \mathrm{tr}\left\{\Lambda^\nu G^< \Lambda^{\nu'} \partial_\epsilon \left(G^A + G^R\right)\right\}_a . \tag{3.24}$$

Here we have introduced the notation $\{M_{\nu\nu'}\}_{s,a} = (M_{\nu\nu'} \pm M_{\nu'\nu})/2$ for symmetric and anti-symmetric parts of an arbitrary matrix $M$.

At last, the stochastic force $\xi_\nu$ is given by the thermal and non-equilibrium fluctuations of the force operator $-d^\dagger \Lambda^\nu d$ in Eq. (3.5). Thus, the symmetrized noise correlator reads

$$\begin{aligned}\langle \xi_\nu(t)\xi_{\nu'}(t')\rangle =& \frac{1}{2}\sum_{mm'nn'} \big[\Lambda^\nu_{mm'}\Lambda^{\nu'}_{nn'}\langle d^\dagger_m(t) d_{m'}(t) d^\dagger_n(t') d_{n'}(t')\rangle \\ &+ \Lambda^{\nu'}_{nn'}\Lambda^{\nu}_{mm'}\langle d^\dagger_n(t') d_{n'}(t') d^\dagger_m(t) d_{m'}(t)\rangle\big] \\ =& \mathrm{tr}\{\Lambda^\nu \mathcal{G}^>(t,t')\Lambda^{\nu'}\mathcal{G}^<(t',t)\}_s ,\end{aligned} \tag{3.25}$$

where we have used Wick's theorem and $\mathcal{G}^>_{mm'}(t,t') = -\mathrm{i}\langle d_m(t) d^\dagger_{m'}(t')\rangle_{\boldsymbol{X}(t)}$ is the full greater Green's function. As indicated by the fluctuation-dissipation theorem, the fluctuating force is of the same order in the adiabatic expansion as the velocity dependent force. Thus, we can evaluate the expression for the correlator of the fluctuating force, Eq. (3.25), to lowest order in the adiabatic expansion, so that we obtain Eq. (3.9), with

$$D_{\nu\nu'}(\boldsymbol{X}) = \int \frac{\mathrm{d}\epsilon}{2\pi} \mathrm{tr}\left\{\Lambda^\nu G^< \Lambda^{\nu'} G^>\right\}_s , \tag{3.26}$$

in terms of the strictly adiabatic lesser and greater Green's functions.

This formalism gives the tools needed to describe the dynamics of the vibrational modes in the presence of a bias for an arbitrary number of modes and dot levels. When expressions (3.21) - (3.24) are inserted back in Eq. (3.1), they define a non-linear Langevin equation due to their non-trivial dependences on $\boldsymbol{X}(t)$ .

## 3.3. S-matrix theory of current-induced forces

Scattering matrix approaches to mesoscopic transport generally involve expressions in terms of the elastic S-matrix, cp. the discussion in Section 2.1. For our problem, the S-matrix is elastic only in the strictly adiabatic limit, in which it is evaluated for a fixed value of $\boldsymbol{X}$.

### 3.3.1. Adiabatic expansion of the S-matrix

As pointed out by Moskalets and Büttiker [2004, 2005], this is not sufficient for general out of equilibrium situations, even when $\boldsymbol{X}(t)$ varies adiabatically in time. In their

work, they calculated, within a Floquet formalism, the leading correction to the strictly adiabatic S-matrix. We follow here the same approach, rephrased in terms of the Wigner representation. The full S-matrix can be written as [Aleiner *et al.*, 2002]

$$\mathcal{S}(\epsilon,t) = 1 - 2\pi\mathrm{i}\left[W\mathcal{G}^R W^\dagger\right](\epsilon,t)\,. \tag{3.27}$$

To go beyond the frozen approximation, we expand $\mathcal{S}$ to leading order in $\dot{\boldsymbol{X}}$,

$$\mathcal{S}(\epsilon,t) \simeq S(\epsilon,\boldsymbol{X}(t)) + \sum_\nu \dot{X}_\nu(t) A_\nu(\epsilon,\boldsymbol{X}(t))\,, \tag{3.28}$$

where the strictly adiabatic S-matrix is given by

$$S(\epsilon,\boldsymbol{X}) = 1 - 2\pi\mathrm{i} W(\epsilon) G^R(\epsilon,\boldsymbol{X}) W^\dagger(\epsilon)\,. \tag{3.29}$$

Note that, in line with the notation established before for the Green's functions, the strictly adiabatic S-matrix is denoted by $S$ while the full S-matrix is denoted by $\mathcal{S}$. The leading correction defines the matrix $A$, which, similar to $S$, has definite symmetry properties. In particular, if the system is time-reversal invariant, the adiabatic S-matrix is even under time reversal while $A$ is odd. For a given problem, the A-matrix has to be obtained along with $S$.

We can now derive a Green's function expression for the matrix $A$ [Vavilov *et al.*, 2001; Arrachea and Moskalets, 2006]. Comparing Eq. (3.28) with the expansion to the same order of $\mathcal{S}$ in terms of adiabatic Green's functions we obtain

$$A_\nu(\epsilon,\boldsymbol{X}) = \pi\partial_\epsilon\left[W(\epsilon)G^R(\epsilon,\boldsymbol{X})\right]\Lambda^\nu(\boldsymbol{X})G^R(\epsilon,\boldsymbol{X})W^\dagger(\epsilon) \tag{3.30}$$

$$- \pi W(\epsilon)G^R(\epsilon,\boldsymbol{X})\Lambda^\nu(\boldsymbol{X})\partial_\epsilon\left[G^R(\epsilon,\boldsymbol{X})W^\dagger(\epsilon)\right]\,. \tag{3.31}$$

This follows straightforwardly from performing explicitly the convolution in Eq. (3.27) and keeping terms up to linear order in the velocity $\dot{\boldsymbol{X}}$. Current conservation constrains both the frozen and full scattering matrices to be unitary. From the unitarity of the frozen S-matrix, $S^\dagger S = 1$, we obtain the useful relation

$$\frac{\partial S^\dagger}{\partial X_\nu} S + S^\dagger \frac{\partial S}{\partial X_\nu} = 0\,, \tag{3.32}$$

which we will use repeatedly in the following sections. On the other hand, unitarity of the full S-matrix, $\mathcal{S}^\dagger\mathcal{S} = 1$, imposes a relation between the A-matrix and the frozen S-matrix. To first order in the velocity $\dot{\boldsymbol{X}}$ we have

$$1 = SS^\dagger + SA^\dagger + AS^\dagger + \frac{\mathrm{i}}{2}\left(\frac{\partial S}{\partial\epsilon}\frac{\partial S^\dagger}{\partial t} - \frac{\partial S}{\partial t}\frac{\partial S^\dagger}{\partial\epsilon}\right)\,, \tag{3.33}$$

where $A(\epsilon,\boldsymbol{X}) = \sum_\nu A_\nu(\epsilon,\boldsymbol{X})\dot{X}_\nu$. Therefore, $S$ and $A$ are related through

$$A_\nu S^\dagger + S A_\nu^\dagger = \frac{\mathrm{i}}{2}\left(\frac{\partial S}{\partial X_\nu}\frac{\partial S^\dagger}{\partial\epsilon} - \frac{\partial S}{\partial\epsilon}\frac{\partial S^\dagger}{\partial X_\nu}\right)\,. \tag{3.34}$$

In the next section we will see that the A-matrix is essential to express the current-induced dissipation and "Lorentz" forces, Eqs. (3.23) and (3.24).

### 3.3.2. Current-induced forces

After exploiting the slow variation of the scattering matrix with time we can now express the results for the current-induced forces of the preceding section in terms of the $S$- and $A$-matrices.

#### Mean Force

The mean force exerted by the electrons on the oscillator is given by Eq. (3.21). Using Eq. (3.19) we can express $G^<$ in terms of $G^R$ and $G^A$ and obtain

$$F_\nu(\boldsymbol{X}) = -\int \mathrm{d}\epsilon \sum_\alpha f_\alpha \mathrm{tr}\left(\Pi_\alpha W G^A \Lambda^\nu G^R W^\dagger\right), \tag{3.35}$$

where we have used also the cyclic invariance of the trace. In order to write the expression inside the trace in terms of the S-matrix, we note that $2\pi\mathrm{i}G^A W^\dagger W G^R = G^A - G^R$, implied by Eq. (3.14), so that

$$W G^A \Lambda^\nu G^R W^\dagger = (1 + 2\pi\mathrm{i} W G^A W^\dagger) W G^R \Lambda^\nu G^R W^\dagger = \frac{\mathrm{i}}{2\pi} S^\dagger \frac{\partial S}{\partial X_\nu}. \tag{3.36}$$

Here we have used Eq. (3.29) and Eq. (3.15) in the last equality. Note that this relation holds for arbitrary magnitude of $\boldsymbol{X}$. Hence, the mean force, Eq. (3.35), can be expressed directly through scattering matrices $S(\epsilon, \boldsymbol{X})$ as

$$F_\nu(\boldsymbol{X}) = \sum_\alpha \int \frac{\mathrm{d}\epsilon}{2\pi\mathrm{i}} f_\alpha \mathrm{Tr}\left(\Pi_\alpha S^\dagger \frac{\partial S}{\partial X_\nu}\right). \tag{3.37}$$

Note that now the trace (denoted by "Tr") is over lead-space.

An important issue is whether this force is *conservative*, *i.e.*, derivable from a potential. A necessary condition for this is that the "curl" of the force, $\partial_{X_\nu} F_{\nu'} - \partial_{X_{\nu'}} F_\nu$, vanishes. In equilibrium the sum over the lead indices in Eq. (3.37) can be directly performed, since $f_\alpha = f$ for all $\alpha$, and $\sum_\alpha \Pi_\alpha = 1$. Therefore we obtain for the curl

$$\begin{aligned}\frac{\partial F_{\nu'}}{\partial X_\nu} - \frac{\partial F_\nu}{\partial X_{\nu'}} &= \int \frac{\mathrm{d}\epsilon}{2\pi\mathrm{i}} f \ \mathrm{Tr}\left(\frac{\partial S^\dagger}{\partial X_\nu}\frac{\partial S}{\partial X_{\nu'}} - \frac{\partial S^\dagger}{\partial X_{\nu'}} S S^\dagger \frac{\partial S}{\partial X_\nu}\right) \\ &= \int \frac{\mathrm{d}\epsilon}{2\pi\mathrm{i}} f \ \mathrm{Tr}\left(\frac{\partial S^\dagger}{\partial X_\nu}\frac{\partial S}{\partial X_{\nu'}} - \frac{\partial S}{\partial X_{\nu'}}\frac{\partial S^\dagger}{\partial X_\nu}\right) = 0\,,\end{aligned} \tag{3.38}$$

where we have used the unitarity of the S-matrix, the cyclic property of the trace, and Eq. (3.32) in the last line. Thus, the mean force is conservative in thermal equilibrium. In general, however, the mean force will be *non-conservative* in out-of-equilibrium situations, providing a way to exert work on the mechanical degrees of freedom by controlling the external bias potential [Dundas *et al.*, 2009; Todorov *et al.*, 2010; Lü *et al.*, 2010]. Examples will be studied in Chapter 4, where we explicitly study the coupling of two mechanical modes to the conduction electrons, and in Chapter 5 in the context of magnetic systems and spin-transfer torques.

### Stochastic Force

Next, we discuss the fluctuating force $\xi_\nu$ with variance $D_{\nu\nu'}$ given by Eq. (3.26). Following a similar path as described in the previous subsection for the mean force $F_\nu$, we can also express the variance of the fluctuating force in terms of the adiabatic S-matrix. Namely, we explicitly insert the expressions for the Green's functions, Eqs. (3.19) and (3.20), into Eq. (3.26), and obtain with the help of the relation (3.36)

$$D_{\nu\nu'}(\boldsymbol{X}) = \sum_{\alpha\alpha'} \int \frac{\mathrm{d}\epsilon}{2\pi} F_{\alpha\alpha'} \mathrm{Tr} \left\{ \Pi_\alpha \left[ S^\dagger \frac{\partial S}{\partial X_\nu} \right]^\dagger \Pi_{\alpha'} S^\dagger \frac{\partial S}{\partial X_{\nu'}} \right\}_s . \tag{3.39}$$

Here we have introduced the function $F_{\alpha\alpha'}(\epsilon) = f_\alpha(\epsilon)\,[1 - f_{\alpha'}(\epsilon)]$. From Eq. (3.39) it is straightforward to show that $D_{\nu\nu'}$ is positive definite. By performing a unitary transformation to a basis in which $D_{\nu\nu'}$ is diagonal, using $\Pi_\alpha = \Pi_\alpha^2$ and the cyclic invariance of the trace, we obtain the expression

$$D_{\nu\nu}(\boldsymbol{X}) = \sum_{\alpha\alpha'} \int \frac{\mathrm{d}\epsilon}{2\pi} F_{\alpha\alpha'} \mathrm{Tr} \left\{ \left( \Pi_{\alpha'} S^\dagger \frac{\partial S}{\partial X_\nu} \Pi_\alpha \right)^\dagger \Pi_{\alpha'} S^\dagger \frac{\partial S}{\partial X_\nu} \Pi_\alpha \right\}_s , \tag{3.40}$$

which is evidently positive.

We note that we were able to express both the mean force and the correlator of the stochastic force in terms of the frozen S-matrix only. This is no longer the case for the first correction to the strictly adiabatic approximation, given by Eqs. (3.23) and (3.24). We focus on these contributions next.

### Damping Matrix

We start here with the first of the terms, which are proportional to the velocity $\dot{\boldsymbol{X}}$, the symmetric matrix $\gamma^s$. This term is responsible for dissipation of the mechanical system into the electronic bath. The result for $\gamma^s$ is given below in Eq. (3.49), and we detail its – somewhat lengthy – derivation now.

With the aid of Eqs. (3.19) and (3.20), the expression for $\gamma^s$ given in Eq. (3.23) can be written explicitly in terms of retarded and advanced Green's functions as

$$\begin{aligned} \gamma^s_{\nu\nu'} =& 2\pi \sum_{\alpha\alpha'} \int \mathrm{d}\epsilon\, f_\alpha(-\partial_\epsilon f_{\alpha'}) \mathrm{tr} \left\{ \Lambda^\nu G^R W^\dagger \Pi_\alpha W G^A \Lambda^{\nu'} G^R W^\dagger \Pi_{\alpha'} W G^A \right\}_s \\ &+ 2\pi \sum_{\alpha\alpha'} \int \mathrm{d}\epsilon\, F_{\alpha\alpha'} \mathrm{tr} \left\{ \Lambda^\nu G^R W^\dagger \Pi_\alpha W G^A \Lambda^{\nu'} \partial_\epsilon \left( G^R W^\dagger \Pi_{\alpha'} W G^A \right) \right\}_s . \end{aligned} \tag{3.41}$$

It is instructive to split the factor $F_{\alpha\alpha'}$ into a symmetric and an antisymmetric part under exchange of the lead indices, $F_{\alpha\alpha'} = F^s_{\alpha\alpha'} + F^a_{\alpha\alpha'}$, with

$$F^s_{\alpha\alpha'} \equiv \frac{1}{2}(f_\alpha + f_{\alpha'} - 2 f_\alpha f_{\alpha'}) \qquad \text{and} \qquad F^a_{\alpha\alpha'} \equiv \frac{1}{2}(f_\alpha - f_{\alpha'}) . \tag{3.42}$$

Correspondingly, we split the second line of Eq. (3.41) into symmetric and antisymmetric parts in the lead indices. Then we can write

$$\begin{aligned}\gamma^s_{\nu\nu'} =& 2\pi \sum_{\alpha\alpha'} \int \mathrm{d}\epsilon \big[f_\alpha(-\partial_\epsilon f_{\alpha'}) - \frac{1}{2}\partial_\epsilon F^s_{\alpha\alpha'}\big] \mathrm{tr}\left\{\Lambda^\nu G^R W^\dagger \Pi_\alpha W G^A \Lambda^{\nu'} G^R W^\dagger \Pi_{\alpha'} W G^A\right\}_s \\ &+ 2\pi \sum_{\alpha\alpha'} \int \mathrm{d}\epsilon F^a_{\alpha\alpha'} \mathrm{tr}\left\{\Lambda^\nu G^R W^\dagger \Pi_\alpha W G^A \Lambda^{\nu'} \partial_\epsilon \left(G^R W^\dagger \Pi_{\alpha'} W G^A\right)\right\}_s , \end{aligned} \tag{3.43}$$

where we have used the symmetries of the term proportional to $F^s_{\alpha\alpha'}$ and have integrated by parts noting that $F^s_{\alpha\alpha'}$ vanishes for $\epsilon \to \pm\infty$.

Since in equilibrium $F^a_{\alpha\alpha'} = F^a_{\alpha\alpha} = 0$ and the second line of Eq. (3.43) vanishes, we can now regroup terms into an "equilibrium" and a purely non-equilibrium contribution $\gamma^s = \gamma^{s,eq} + \gamma^{s,ne}$. Thus, using the cyclic invariance of the trace and Eq. (3.36), the first line of Eq. (3.43) can be written as

$$\begin{aligned}\gamma^{s,eq}_{\nu\nu'} &= \frac{1}{4}\sum_{\alpha\alpha'} \int \frac{\mathrm{d}\epsilon}{2\pi} \partial_\epsilon (f_\alpha + f_{\alpha'}) \mathrm{Tr}\left\{\Pi_\alpha S^\dagger \frac{\partial S}{\partial X_\nu} \Pi_{\alpha'} S^\dagger \frac{\partial S}{\partial X_{\nu'}}\right\}_s \\ &= \frac{1}{2}\sum_{\alpha} \int \frac{\mathrm{d}\epsilon}{2\pi} (-\partial_\epsilon f_\alpha) \mathrm{Tr}\left(\Pi_\alpha \frac{\partial S^\dagger}{\partial X_\nu} \frac{\partial S}{\partial X_{\nu'}}\right) , \end{aligned} \tag{3.44}$$

where we have used that $\sum_{\alpha'} \Pi_{\alpha'} = 1$ , $S^\dagger S = 1$, and Eq. (3.32) in the last line. Note that in general, $\gamma^{s,eq}$ also depends on the applied bias voltage, but gives the only contribution to the damping matrix when in equilibrium.

To express $\gamma^{s,ne}$, given by the second line of Eq. (3.43), in terms of S-matrix quantities, we rewrite this contribution as

$$\begin{aligned}&\gamma^{s,ne}_{\nu\nu'} \\ &= \int \frac{\mathrm{d}\epsilon}{2\mathrm{i}} \sum_\alpha f_\alpha \mathrm{tr}\left\{\Pi_\alpha \left[S^\dagger \frac{\partial S}{\partial X_\nu} W G^A \Lambda^{\nu'} \partial_\epsilon (G^R W^\dagger) - \partial_\epsilon (W G^A) \Lambda^{\nu'} G^R W^\dagger\right]\right\}_s , \end{aligned} \tag{3.45}$$

where we have exploited $\sum_\alpha \Pi_\alpha = 1$ and the identity (3.36). The evaluation of the commutator, denoted by [. , .], is lengthy but can be done straightforwardly with the help of Eq. (3.14). Finally, we obtain

$$\gamma^{s,ne}_{\nu\nu'} = \int \frac{\mathrm{d}\epsilon}{2\pi i} \sum_\alpha f_\alpha \mathrm{Tr}\left\{\Pi_\alpha \left(\frac{\partial S^\dagger}{\partial X_\nu} A_{\nu'} - A^\dagger_{\nu'} \frac{\partial S}{\partial X_\nu}\right)\right\}_s , \tag{3.46}$$

in terms of the A-matrix defined in Eq. (3.31). Here we have used the identity

$$\begin{aligned}\frac{1}{\pi}\frac{\partial S^\dagger}{\partial X_\nu} A_{\nu'} =& 2\pi \mathrm{i} W G^A \Lambda^\nu G^A W^\dagger \frac{\partial (W G^R)}{\partial \epsilon} \Lambda^{\nu'} G^R W^\dagger \\ &- W G^A \Lambda^\nu (G^A - G^R) \Lambda^{\nu'} \frac{\partial (G^R W^\dagger)}{\partial \epsilon} . \end{aligned} \tag{3.47}$$

Note that $\gamma^{s,ne}_{\nu\nu'}$ vanishes in equilibrium, as can be shown using the properties of the $S$ and $A$ matrices: Since the sum over leads can be directly performed in equilibrium, expression (3.46) involves

$$\begin{aligned}&\mathrm{Tr}\left\{\frac{\partial S^\dagger}{\partial X_\nu}A_{\nu'}-A^\dagger_{\nu'}\frac{\partial S}{\partial X_\nu}\right\}_s=-\mathrm{Tr}\left\{\frac{\partial S}{\partial X_\nu}S^\dagger\left(A_{\nu'}S^\dagger+SA^\dagger_{\nu'}\right)\right\}_s\\&=-\frac{\mathrm{i}}{2}\mathrm{Tr}\left\{\frac{\partial S}{\partial X_\nu}S^\dagger\left(\frac{\partial S}{\partial X_{\nu'}}\frac{\partial S^\dagger}{\partial\epsilon}-S\frac{\partial S^\dagger}{\partial\epsilon}\frac{\partial S}{\partial X_{\nu'}}S^\dagger\right)\right\}_s=0,\end{aligned}\tag{3.48}$$

where we have used the unitarity of $\mathcal{S}$ and the cyclic invariance of the trace multiple times. In the first equality, we inserted $S^\dagger S=1$ and used Eq. (3.32), the second equality follows by inserting the identity (3.34) and using again (3.32).

Finally, combining all terms we obtain an S-matrix expression for the full damping matrix $\gamma^s$,

$$\begin{aligned}\gamma^s_{\nu\nu'}(\boldsymbol{X})=&-\sum_\alpha\int\frac{\mathrm{d}\epsilon}{4\pi}\partial_\epsilon f_\alpha\mathrm{Tr}\left\{\Pi_\alpha\frac{\partial S^\dagger}{\partial X_\nu}\frac{\partial S}{\partial X_{\nu'}}\right\}_s\\&+\sum_\alpha\int\frac{\mathrm{d}\epsilon}{2\pi\mathrm{i}}f_\alpha\mathrm{Tr}\left\{\Pi_\alpha\left(\frac{\partial S^\dagger}{\partial X_\nu}A_{\nu'}-A^\dagger_{\nu'}\frac{\partial S}{\partial X_\nu}\right)\right\}_s.\end{aligned}\tag{3.49}$$

Note that in equilibrium, by the relation $-\partial_\epsilon f=f(1-f)/T$ and using Eq. (3.32), the fluctuating force $D$ and damping $\gamma^s$ are related via

$$D_{\nu\nu'}=2T\gamma^{s,eq}_{\nu\nu'}=2T\gamma^s_{\nu\nu'}\tag{3.50}$$

as required by the fluctuation-dissipation theorem. Our result for $\gamma^{s,eq}_{\nu\nu'}$ is analogous to the S-matrix expression obtained for dissipation in ferromagnets in thermal equilibrium, dubbed Gilbert damping [Brataas *et al.*, 2008]. We will encounter magnetic systems, both in and out-of equilibrium, in more detail in Chapter 5.

Following a similar set of steps as shown above for the variance $D_{\nu\nu'}$ in Eq. (3.40), one sees that $\gamma^{s,eq}_{\nu\nu'}$ has positive eigenvalues. On the other hand, the sign of $\gamma^{s,ne}_{\nu\nu'}$ is not fixed, allowing the possibility of negative eigenvalues of $\gamma^s$. The possibility of negative damping is, therefore, a pure non-equilibrium effect. Several recent papers found negative damping in specific out of equilibrium models [Clerk and Bennett, 2005; Hussein *et al.*, 2010; Lü *et al.*, 2011], further examples will be discussed in the next chapter.

### Lorentz force

The contribution to the Langevin equation $-\sum_{\nu'}\gamma^a_{\nu\nu'}\dot{X}_{\nu'}$ acts like a Lorentz force and we want to express the corresponding effective magnetic field[2] in terms of the S- and A-matrices in the following.

[2] Consider for example a two-dimensional problem, $\boldsymbol{X}=(X_1,X_2)$, in which the antisymmetric part of the velocity dependent force accordingly reads $\begin{pmatrix}0&-\gamma^a_{12}\\\gamma^a_{12}&0\end{pmatrix}\begin{pmatrix}\dot{X}_1\\\dot{X}_2\end{pmatrix}$. This corresponds to the Lorentz force $-e\dot{\boldsymbol{X}}\times\boldsymbol{B}$ when $\boldsymbol{B}=(\gamma^a_{12}/e)\hat{\boldsymbol{e}}_3$ is identified as an effective magnetic field.

Using Eq. (3.19) for the lesser Green's function, this effective magnetic field can be written as

$$\gamma^a_{\nu\nu'} = \mathrm{i}\int \mathrm{d}\epsilon \sum_\alpha f_\alpha \mathrm{Tr}\left\{\Pi_\alpha W G^A \Lambda^\nu \left(\partial_\epsilon G^R + \partial_\epsilon G^A\right)\Lambda^{\nu'} G^R W^\dagger\right\}_a . \tag{3.51}$$

In order to relate this to the scattering matrix, we note that taking the derivative of the A-matrix with respect to $X_{\nu'}$ yields $[\partial_{X_{\nu'}} A_\nu]_a = 2\pi[W G^R \Lambda^{\nu'}(\partial_\epsilon G^R)\Lambda^\nu G^R W^\dagger]_a$, using Eqs. (3.15) and (3.31). Therefore we obtain

$$\left[S^\dagger \frac{\partial A_\nu}{\partial X_{\nu'}}\right]_a = -2\pi\left[W G^A \Lambda^\nu (\partial_\epsilon G^R)\Lambda^{\nu'} G^R W^\dagger\right]_a , \tag{3.52}$$

which allows us to write $\gamma^a$ in terms of the S-matrix as

$$\gamma^a_{\nu\nu'}(\boldsymbol{X}) = \sum_\alpha \int \frac{\mathrm{d}\epsilon}{2\pi\mathrm{i}} f_\alpha \mathrm{Tr}\left\{\Pi_\alpha\left(S^\dagger \frac{\partial A_\nu}{\partial X_{\nu'}} - \frac{\partial A^\dagger_\nu}{\partial X_{\nu'}} S\right)\right\}_a . \tag{3.53}$$

If the system is time-reversal invariant, $\gamma^a$ vanishes in thermal equilibrium. The latter implies $\sum_\alpha \Pi_\alpha f_\alpha = f$, so that Eq. (3.53) involves only

$$\mathrm{Tr}\left\{S^\dagger \frac{\partial A_\nu}{\partial X_{\nu'}} - \frac{\partial A^\dagger_\nu}{\partial X_{\nu'}} S\right\} = \mathrm{Tr}\left\{\frac{\partial A^T_\nu}{\partial X_{\nu'}} S^* - S^T \frac{\partial A^*_\nu}{\partial X_{\nu'}}\right\} = \mathrm{Tr}\left\{-\frac{\partial A_\nu}{\partial X_{\nu'}} S^\dagger + S\frac{\partial A^\dagger_\nu}{\partial X_{\nu'}}\right\},$$

yielding $\gamma^a = 0$ due to the cyclic invariance of the trace. In the last equality, we have used $S = S^T$ and $A = -A^T$ as implied by time-reversal invariance.

Out of equilibrium, $\gamma^a$ generally does not vanish even for time reversal symmetric conductors, since the current effectively breaks time reversal symmetry.

## 3.4. Current

So far we have focused on the effect of the electrons on the mechanical degrees of freedom. For a complete picture, we also need to consider the reverse effect of the mechanical vibrations on the electronic current. In the strictly adiabatic limit, this obviously has to reduce to the Landauer-Büttiker formula for the transport current. Considering the leading adiabatic correction to the current in equilibrium is closely related to the phenomenon of quantum pumping, and we will see that our results in this limit essentially reduce to Brouwer's S-matrix formula for the pumping current [Brouwer, 1998]. Our full result is, however, more general since it gives the leading adiabatic correction to the current in arbitrary *non-equilibrium* situations [Moskalets and Büttiker, 2005].

The current through lead $\alpha$ is given by Eq. (2.53),

$$I_\alpha(t) = e\int \mathrm{d}t'\,\mathrm{tr}\left\{\mathcal{G}^R(t,t')\Sigma^<_\alpha(t',t) + \mathcal{G}^<(t,t')\Sigma^A_\alpha(t',t)\right\} + \mathrm{h.c.}\,,$$

as we have discussed in Section 2.2.4. Again we use the separation of time scales and go to the Wigner representation, yielding

$$I_\alpha = e\int \frac{\mathrm{d}\epsilon}{2\pi}\,\mathrm{tr}\left\{\mathcal{G}^R\Sigma_\alpha^< + \mathcal{G}^<\Sigma_\alpha^A - \tfrac{\mathrm{i}}{2}\left(\partial_t\mathcal{G}^R\partial_\epsilon\Sigma_\alpha^< + \partial_t\mathcal{G}^<\partial_\epsilon\Sigma_\alpha^A\right)\right\} + \text{h.c.}\,. \tag{3.54}$$

We split the current into an adiabatic contribution $I_\alpha^0$ and a term proportional to the velocity $\dot{X}_\mu$: $I_\alpha = I_\alpha^0 + I_\alpha^1$. Next we will express these quantities in terms of the scattering matrix.

### 3.4.1. Landauer-Büttiker current

The strictly adiabatic contribution to the current is given by

$$I_\alpha^0(\boldsymbol{X}) = e\int \frac{\mathrm{d}\epsilon}{2\pi}\,\mathrm{tr}\left\{\left(G^R - G^A\right)\Sigma_\alpha^< + G^<\left(\Sigma_\alpha^A - \Sigma_\alpha^R\right)\right\}\,, \tag{3.55}$$

where we have collected the purely adiabatic terms from Eqs. (3.17) and (3.18). Inserting the expressions for the self-energies Eqs. (2.44) and (2.48), we can express this as

$$I_\alpha^0(\boldsymbol{X}) = e\int \mathrm{d}\epsilon\sum_\beta f_\beta \mathrm{i}\,\mathrm{Tr}\left\{W\left[\delta_{\alpha\beta}(G^R - G^A) + 2\pi\mathrm{i}G^RW^\dagger\Pi_\beta WG^A\right]W^\dagger\Pi_\alpha\right\}, \tag{3.56}$$

where we used Eq. (3.19). Inserting the adiabatic S-matrix, Eq. (3.29) yields

$$I_\alpha^0(\boldsymbol{X}) = e\int \frac{\mathrm{d}\epsilon}{2\pi}\sum_\beta f_\beta \mathrm{Tr}\left\{\left[\delta_{\alpha\beta} - S\Pi_\beta S^\dagger\right]\Pi_\alpha\right\} \tag{3.57}$$

$$= e\int \frac{\mathrm{d}\epsilon}{2\pi}\sum_\beta \left(f_\alpha - f_\beta\right)\,\mathrm{Tr}\left\{S\Pi_\beta S^\dagger\Pi_\alpha\right\}\,, \tag{3.58}$$

where we used $\sum_\beta S\Pi_\beta S^\dagger = 1$ in the last line. We hence recover the usual expression for the Landauer-Büttiker current [Büttiker *et al.*, 1985], Eq. (2.16), which we discussed in Section 2.1. Note that the total adiabatic current depends implicitly on time through $\boldsymbol{X}(t)$, and is conserved at every instant of time, $\sum_\alpha I_\alpha^0(\boldsymbol{X}) = 0$. In the next chapter we will demonstrate how the $\boldsymbol{X}$-dependence of the current can be used for monitoring the dynamics of the oscillator.

To obtain the *dc* current, we need to average $I_\alpha$ over the Langevin dynamics of the mechanical degrees of freedom. Alternatively, we can average the current expression with the probability distribution of $\boldsymbol{X}$, which can be obtained from the corresponding Fokker-Planck equation, as done, *e.g.*, in [Mozyrsky *et al.*, 2006; Brüggemann *et al.*, 2012]. Similar remarks would apply to calculations of the current noise. We will deal with the Fokker-Planck equation to some extent in Chapter 5 when we study the switching dynamics of anisotropic magnetic molecules.

### 3.4.2. First order correction

Now we turn to the first order correction to the adiabatic approximation [Moskalets and Büttiker, 2005], restricting our considerations to the wide-band limit. The contribution to the current (3.54) which is linear in the velocity reads

$$\begin{aligned} & I_\alpha^1(\boldsymbol{X}) \\ &= -e\int\frac{\mathrm{d}\epsilon}{2\pi\mathrm{i}}\sum_\mu \dot{X}_\mu \,\mathrm{tr}\left\{(\partial_\epsilon G^R)\Lambda^\mu G^R\Sigma_\alpha^< + \left[\left(\partial_\epsilon G^<\right)\Lambda^\mu G^A - G^R\Lambda^\mu(\partial_\epsilon G^<)\right]\Sigma_\alpha^A\right\} + \mathrm{h.c.} \\ &= -e\int \mathrm{d}\epsilon\sum_\nu \dot{X}_\nu \sum_\beta f_\beta\Big\{\frac{\delta_{\alpha\beta}}{\mathrm{i}\pi}\,\mathrm{tr}\big[(\partial_\epsilon G^R)\Lambda^\nu G^R W^\dagger\Pi_\alpha W\big] \\ &\quad + \mathrm{tr}\big[G^R W^\dagger\Pi_\beta W G^A\big(W^\dagger\Pi_\alpha W(\partial_\epsilon G^R)\Lambda^\nu - \Lambda^\nu\partial_\epsilon(G^A W^\dagger\Pi_\alpha W)\big)\big]\Big\} + \mathrm{h.c.}, \end{aligned} \tag{3.59}$$

after integration by parts and using the cyclic invariance of the trace. Again, we have inserted Eq. (3.19) for the lesser Green's function, and expressions (2.44) and (2.48) for the self-energies. In the wide band limit, the identity

$$(\mathrm{i}/2)\partial_\epsilon\partial_{X_\nu}S + A_\nu = W(\partial_\epsilon G^R)\Lambda^\nu G^R W^\dagger \tag{3.60}$$

holds, so that we can write

$$I_\alpha^1(\boldsymbol{X}) = -e\int\frac{\mathrm{d}\epsilon}{2\pi}\,\dot{\boldsymbol{X}}\cdot\sum_\beta f_\beta \mathrm{Tr}\left[\left(\frac{\mathrm{i}}{2}\frac{\partial^2 S}{\partial\epsilon\partial\boldsymbol{X}} + \boldsymbol{A}\right)\Pi_\beta S^\dagger\Pi_\alpha\right] + \mathrm{h.c.}\,. \tag{3.61}$$

After straightforward manipulations we integrate by parts, so that we can split this expression as

$$\begin{aligned} I_\alpha^1(\boldsymbol{X}) = &-\frac{e}{2\pi}\int \mathrm{d}\epsilon\dot{\boldsymbol{X}}\cdot\sum_\beta \partial_\epsilon f_\beta \mathrm{ImTr}\left\{\Pi_\alpha\frac{\partial S}{\partial\boldsymbol{X}}\Pi_\beta S^\dagger\right\} \\ &+\frac{e}{2\pi}\int \mathrm{d}\epsilon\dot{\boldsymbol{X}}\cdot\sum_\beta f_\beta\ \mathrm{ReTr}\left\{\mathrm{i}\Pi_\alpha\frac{\partial S}{\partial\boldsymbol{X}}\Pi_\beta\frac{\partial S^\dagger}{\partial\epsilon} - 2\Pi_\alpha\boldsymbol{A}\Pi_\beta S^\dagger\right\}. \end{aligned} \tag{3.62}$$

In equilibrium, the second term vanishes due to the identity Eq. (3.34) and the first term agrees with Brouwer's formula for the pumping current [Brouwer, 1998]. As for the strictly adiabatic contribution, the *dc* current is obtained by averaging over the probability distribution of $\boldsymbol{X}$.

## 3.5. Summary

In this chapter we have described slowly varying mechanical modes coupled to electrons flowing through a nanostructure. These mechanical modes are described by a Langevin equation containing current-induced forces. Under general non-equilibrium conditions they include

- an average force (which can be non-conservative out of equilibrium),
- the damping (with possibly negative eigenvalues, corresponding to energy-transfer from the current to the oscillator),
- a non-dissipative velocity dependent ("Lorentz"-) force which is present even for time reversal invariant systems, and
- a fluctuating force originating from noise of the current flow.

We have also calculated how the backaction of these forces affects the current through the device. The dependence of the current on the vibrational dynamics allows one to study the current-induced forces by monitoring the electronic transport; this holds already for the strictly adiabatic current. In equilibrium the first order correction reduces to the well-known expression for the pumping current. When more than one mechanical mode couples to the conduction electrons this yields the possibility of transferring charge through the devices even in the absence of an applied bias voltage.

We have calculated the current-induced forces and the current in a non-equilibrium Born-Oppenheimer approximation. Starting from a Green's functions approach we have related the resulting expressions to scattering theory. Going beyond the strictly adiabatic limit, we have realized that in general non-equilibrium situations the forces cannot be expressed solely by the frozen S-matrix but an additional fundamental quantity, the A-matrix, is needed for the description.

A number of examples which illustrate the description of the various current-induced forces, which we have derived here, will be considered in the following chapter.

# 4. Current-induced forces: Examples

In this chapter we are going to apply our general formalism of current-induced forces to several simple models which illustrate the peculiar nature of the NEMS. We consider models which are inspired *e.g.* by quantum dots, which are coupled to two electrodes, or molecules in a break junction. The vibrational modes can be excited by the current flowing through the system which in turn is affected by the mechanical motion.

We consider three model systems of increasing complexity. In Section 4.1 we study a single electronic level coupled to a single vibrational mode, like the one illustrated in Fig. 4.1 (a). In Section 4.2 we exploit the situation which is illustrated in Fig. 4.1 (b): a structure consisting of two electronic levels which couple to another vibrational mode. We find that the A-matrix, derived in Chapter 3, is needed for the description of this setup and we find the possibility of negative damping which can be controlled electronically. As a last example for a NEMS, we consider the coupling of the electrons with two vibrational modes in Section 4.3. Specifically, we find that in out-of-equilibrium situations the current-induced forces can destabilize the mechanical vibrations and cause limit-cycle dynamics. We also study how signatures of the dynamics can be extracted from the current.

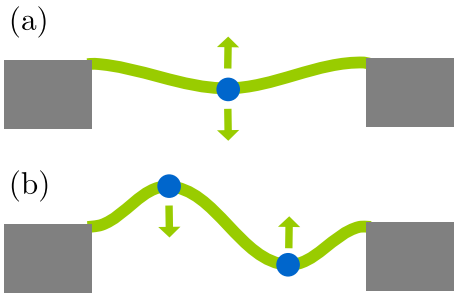


Figure 4.1. Exemplary vibrational modes considered in the main text.

The results presented in this chapter have been published in [Bode *et al.*, 2011] and [Bode *et al.*, 2012d].

## 4.1. Resonant Level

To connect with the existing literature, we treat as a first example the simplest case within our formalism: a resonant electronic level coupled to a single vibrational mode and attached to two leads on the left ($L$) and right ($R$). This model has been discussed in detail for zero temperature by Mozyrsky *et al.* [2006] and Pistolesi *et al.* [2008]. It provides a simple description on how current-induced forces can be used to manipulate a molecular switch. Here we derive finite-temperature expressions for the current-induced forces for a generic coupling between electronic and mechanical degrees of freedom, starting from the scattering matrix of the system, and show how they reduce to the known results for zero temperature and linear coupling.

We consider a single electronic level which is coupled to one mechanical mode, $N = M = 1$, denoting the mode coordinate by $X$, the energy of the dot level by $\tilde{\epsilon}(X)$, and the number of channels in the left and right leads by $N_L$ and $N_R$, respectively. The Hamiltonian of the dot can then be written as

$$H_D = \tilde{\epsilon}(X) d^\dagger d \tag{4.1}$$

and the hybridization matrix as $W^\dagger = \left(\boldsymbol{W}^L, \boldsymbol{W}^R\right)^\dagger$, with $\boldsymbol{W}^\alpha = (W_1^\alpha, \dots W_{N_\alpha}^\alpha)$ and $\alpha = L,\, R$. Hence the frozen S-matrix, Eq. (3.29), is given by

$$S = 1 - \frac{2\pi \mathrm{i}}{\mathcal{L}} \begin{pmatrix} \boldsymbol{W}^L \left(\boldsymbol{W}^L\right)^\dagger & \boldsymbol{W}^L \left(\boldsymbol{W}^R\right)^\dagger \\ \boldsymbol{W}^R \left(\boldsymbol{W}^L\right)^\dagger & \boldsymbol{W}^R \left(\boldsymbol{W}^R\right)^\dagger \end{pmatrix}, \tag{4.2}$$

where $\mathcal{L}(\epsilon, X) = \epsilon - \tilde{\epsilon}(X) + \mathrm{i}\Gamma$, $\Gamma = \Gamma_L + \Gamma_R$, and $\Gamma_\alpha = \pi \left(\boldsymbol{W}^\alpha\right)^\dagger \cdot \boldsymbol{W}^\alpha$. Rotating to an eigenbasis of the lead channels, this S-matrix does not mix channels within the same lead, and hence we can project the S-matrix into a single non-trivial channel in each lead, to obtain

$$S = 1 - \frac{2i}{\mathcal{L}} \begin{pmatrix} \Gamma_L & \sqrt{\Gamma_L \Gamma_R} \\ \sqrt{\Gamma_L \Gamma_R} & \Gamma_R \end{pmatrix}. \tag{4.3}$$

To calculate the mean force from Eq. (3.37), we need an explicit expression for the relation (3.36). This can be easily calculated to be

$$S^\dagger \frac{\partial S}{\partial X} = -\frac{\partial \tilde{\epsilon}}{\partial X} \frac{2\mathrm{i}}{|\mathcal{L}|^2} \begin{pmatrix} \Gamma_L & \sqrt{\Gamma_L \Gamma_R} \\ \sqrt{\Gamma_L \Gamma_R} & \Gamma_R \end{pmatrix} \tag{4.4}$$

and hence

$$F(X) = -\int \frac{\mathrm{d}\epsilon}{\pi} \left[ \frac{f_L \Gamma_L + f_R \Gamma_R}{|\mathcal{L}|^2} \right] \frac{\partial \tilde{\epsilon}}{\partial X}. \tag{4.5}$$

Analogously, the variance of the stochastic force, Eq. (3.39), becomes

$$D(X) = 2 \int \frac{\mathrm{d}\epsilon}{\pi} \sum_{\alpha\alpha'} \frac{\Gamma_\alpha \Gamma_{\alpha'} F_{\alpha\alpha'}}{|\mathcal{L}|^4} \left[ \frac{\partial \tilde{\epsilon}}{\partial X} \right]^2. \tag{4.6}$$

It only remains to calculate the dissipation coefficient $\gamma$. Since there is only one collective mode, $\nu = 1$, $\gamma$ is a scalar and hence $\gamma^a = 0$. Moreover, for energy-independent hybridization we have that $\partial_\epsilon G^R = -(G^R)^2$, and the A-matrix (3.31) can be written as

$$A_\nu = -\pi W G^R [G^R, \Lambda^\nu] G^R W^\dagger. \tag{4.7}$$

Being the commutator of scalars, in this case $A_1 = 0$ and from Eq. (3.49), $\gamma^s$ must be positive and is given by Eq. (3.44). (For an alternative derivation of the positiveness of the friction coefficient in a resonant-level system, see Hyldgaard [2003]). After some algebra, we obtain

$$\left(\frac{\partial S}{\partial X}\right)^\dagger \frac{\partial S}{\partial X} = 4 \left[ \frac{\partial \tilde{\epsilon}}{\partial X} \right]^2 \frac{\Gamma}{|\mathcal{L}|^2} \begin{pmatrix} \Gamma_L & \sqrt{\Gamma_L \Gamma_R} \\ \sqrt{\Gamma_L \Gamma_R} & \Gamma_R \end{pmatrix}. \tag{4.8}$$

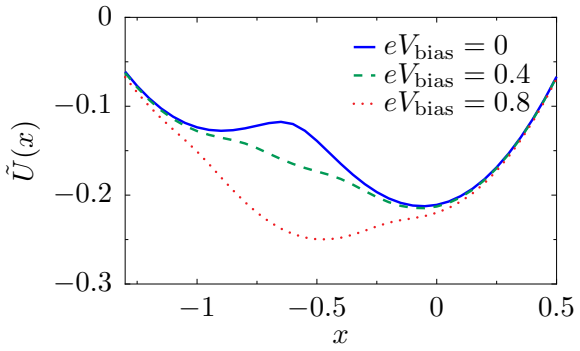


Figure 4.2. Resonant level. The shape of the effective potential $\tilde{U}(X)$ can be tuned by the bias voltage. We consider the level to be in the middle of the current window ($eV_{\rm gate} = 0$) and the parameters $\hbar\omega_0 = 0.01$ and $\Gamma = 0.1$. The dimensionless coordinate is $x = (M\omega_0^2/\lambda)X$ and energies are measured in units of $\lambda^2/(M\omega_0^2)$.

and hence the damping coefficient becomes

$$\gamma(X) = -\frac{\mathrm{d}\epsilon}{\pi}\Gamma\frac{\Gamma_L\partial_\epsilon f_L + \Gamma_R\partial_\epsilon f_R}{|\mathcal{L}|^4}\left[\frac{\partial\tilde{\epsilon}}{\partial X}\right]^2 . \tag{4.9}$$

We can evaluate the remaining integrals analytically in the zero-temperature limit [Mozyrsky *et al.*, 2006; Pistolesi *et al.*, 2008]. In the following we assume $\mu_L \geq \mu_R$. The average force is given by

$$F(X) = -\frac{1}{\pi}\frac{\partial\tilde{\epsilon}}{\partial X}\sum_\alpha \frac{\Gamma_\alpha}{\Gamma}\left[\arctan\left(\frac{\mu_\alpha - \tilde{\epsilon}}{\Gamma}\right) + \frac{\pi}{2}\right] . \tag{4.10}$$

Similarly we obtain the dissipation coefficient

$$\gamma^s(X) = \frac{\Gamma}{\pi}\left[\frac{\partial\tilde{\epsilon}}{\partial X}\right]^2 \sum_\alpha \frac{\Gamma_\alpha}{\left[(\mu_\alpha - \tilde{\epsilon})^2 + \Gamma^2\right]^2} , \tag{4.11}$$

together with the fluctuation kernel

$$D(X) = \frac{\Gamma_L\Gamma_R}{\pi\Gamma^3}\left[\frac{\partial\tilde{\epsilon}}{\partial X}\right]^2 \left[\arctan\left(\frac{\mu - \tilde{\epsilon}}{\Gamma}\right) + \frac{\Gamma(\mu - \tilde{\epsilon})}{(\mu - \tilde{\epsilon})^2 + \Gamma^2}\right]\Bigg|_{\mu=\mu_R}^{\mu=\mu_L} . \tag{4.12}$$

The position of the dot electronic level can be adjusted by an external gate voltage

$$eV_{\rm gate} = \frac{\mu_L + \mu_R}{2} - \epsilon_0 , \tag{4.13}$$

where the factor $(\mu_L + \mu_R)/2$ is included for convenience, to measure energies from the center of the conduction window. The difference in chemical potential between the leads is adjusted via a bias voltage

$$eV_{\rm bias} = \mu_L - \mu_R . \tag{4.14}$$

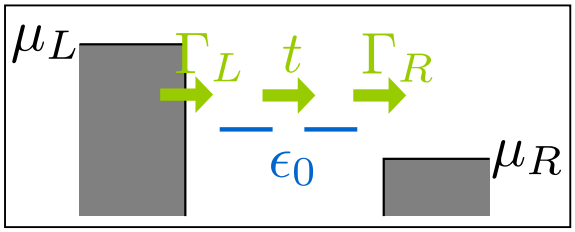


Figure 4.3. Sketch of the two-level model. Electrons tunnel through two degenerate energy levels between left and right leads. Both the hopping between the two levels and the position of the levels are affected the coupling to the vibrational modes.

For a single vibrational mode, the average current-induced force is necessarily conservative and we can define a corresponding potential. Restricting now our results to linear coupling, we write the local level as $\tilde{\epsilon}(X) = \epsilon_0 + \lambda X$. This situation is illustrated in Fig. 4.1 (a). We show the corresponding effective potential $\tilde{U}(X) = (M\omega_0^2/2)X^2 - \int \mathrm{d}X F(X)$ which describes both the elastic and the current-induced forces at zero temperature and various bias voltages in Fig. 4.2. Already this simple example shows that the current-induced forces can affect the mechanical motion qualitatively. Indeed, the effective potential $\tilde{U}(X)$ can become multistable even for a purely harmonic elastic force and depends sensitively on the applied bias voltage.

## 4.2. Two-level model

For the resonant level model discussed so far, the A-matrix vanishes and the damping is necessarily positive. We now consider a model which allows for negative damping, see also [Metelmann and Brandes, 2011]. Our toy model could be inspired by a double dot on a suspended carbon nanotube or an $H_2$ molecule in a break junction, which we have mentioned in the introduction. The model is depicted schematically in Fig. 4.3.

The bare dot Hamiltonian corresponds to degenerate electronic states $\epsilon_0$, localized on the left and right atoms or quantum dots, with tunnel coupling $t$ in between,

$$H_0 = \epsilon_0\, \sigma^0 + t\, \sigma^1, \tag{4.15}$$

where we denote by $\sigma^\mu$ (with $\mu = 0, \ldots, 3$) the usual Pauli matrices acting in the two-site basis.[1] We consider a single oscillator mode with coordinate $X$ that couples linearly to the difference in the occupation of the levels. In our previous notation, this means $\Lambda^1 = \lambda_1 \sigma^3$. The shift of the electronic levels is given by $\tilde{\epsilon}_\pm(X) = \epsilon_0 \pm \lambda_1 X$. This is shown schematically in Fig. 4.1 (b) and further illustrated in Fig. 4.4. The hybridization

[1] The Pauli matrices are given by

$$\sigma^0 = \begin{pmatrix} 1 & 0 \\ 0 & 1 \end{pmatrix}, \qquad \sigma^1 = \begin{pmatrix} 0 & 1 \\ 1 & 0 \end{pmatrix}, \qquad \sigma^2 = \begin{pmatrix} 0 & -\mathrm{i} \\ \mathrm{i} & 0 \end{pmatrix}, \qquad \sigma^3 = \begin{pmatrix} 1 & 0 \\ 0 & -1 \end{pmatrix}.$$

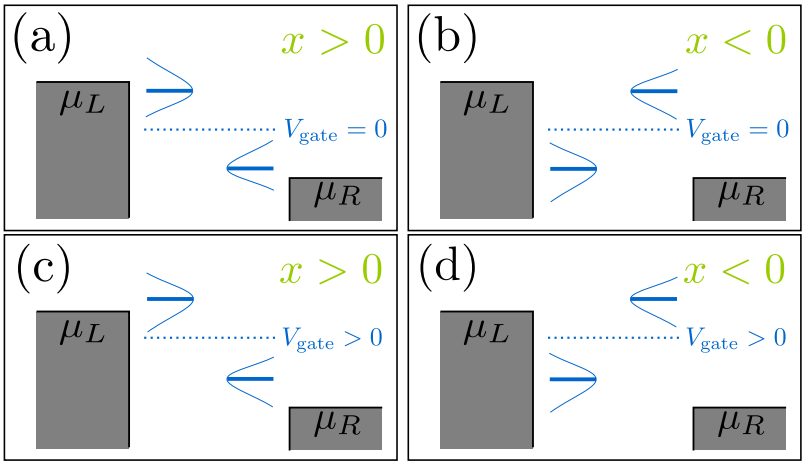


Figure 4.4. Cartoon of the positions of the electronic levels in the dot with respect to the Fermi levels of the leads, depending on the sign of $x$ and the existence of a gate voltage at zero temperature. The levels are broadened due to the hybridization with the leads $\Gamma$. When $x > 0$, "left" and "right" levels approach the Fermi levels of left and right leads respectively. (a) For $eV_{\text{gate}} = 0$ the levels align simultaneously for left and right. (b) The alignment of the levels is inverted. (c) and (d) A finite $eV_{\text{gate}}$ produces an asymmetry between left and right.

matrices are given by $\Gamma^\alpha = \frac{1}{2}\Gamma_\alpha(\sigma^0 \pm \sigma^3)$, where the $+(-)$ refers to $\alpha = L(R)$. We can deduce the tunneling matrix $W$ in terms of the hybridization matrices,

$$W = \sqrt{\Gamma_L/\pi}\,\frac{\sigma^0 + \sigma^3}{2} + \sqrt{\Gamma_R/\pi}\,\frac{\sigma^0 - \sigma^3}{2}\,. \tag{4.16}$$

In the wide-band limit, we approximate $W$ and $\Gamma_\alpha$ to be independent of energy. The retarded adiabatic Green's function takes the form

$$G^R(\epsilon, X) = \frac{1}{\Delta}\begin{pmatrix} \epsilon - \tilde{\epsilon}_+ + \mathrm{i}\Gamma_R & t \\ t & \epsilon - \tilde{\epsilon}_- + \mathrm{i}\Gamma_L \end{pmatrix}, \tag{4.17}$$

with the abbreviation $\Delta(X) = (\epsilon - \tilde{\epsilon}_- + \mathrm{i}\Gamma_L)(\epsilon - \tilde{\epsilon}_+ + \mathrm{i}\Gamma_R) - t^2$.

For simplicity, we restrict our attention to symmetric couplings to the leads, $\Gamma_L = \Gamma_R = \Gamma/2$. Hence the frozen S-matrix and the A-matrix become

$$S(\epsilon, X) = 1 - \frac{\mathrm{i}\Gamma}{\Delta}\begin{pmatrix} \epsilon - \tilde{\epsilon}_+ + \mathrm{i}\Gamma/2 & t \\ t & \epsilon - \tilde{\epsilon}_- + \mathrm{i}\Gamma/2 \end{pmatrix}, \tag{4.18}$$

$$A(\epsilon, X) = i\lambda_1 \frac{\Gamma\, t}{\Delta^2}\,\sigma^2\,. \tag{4.19}$$

We can now give explicit expressions for the current-induced forces. The explicit expressions are lengthy and are given in Appendix A.1, namely in Eqs. (A.1) and (A.2)

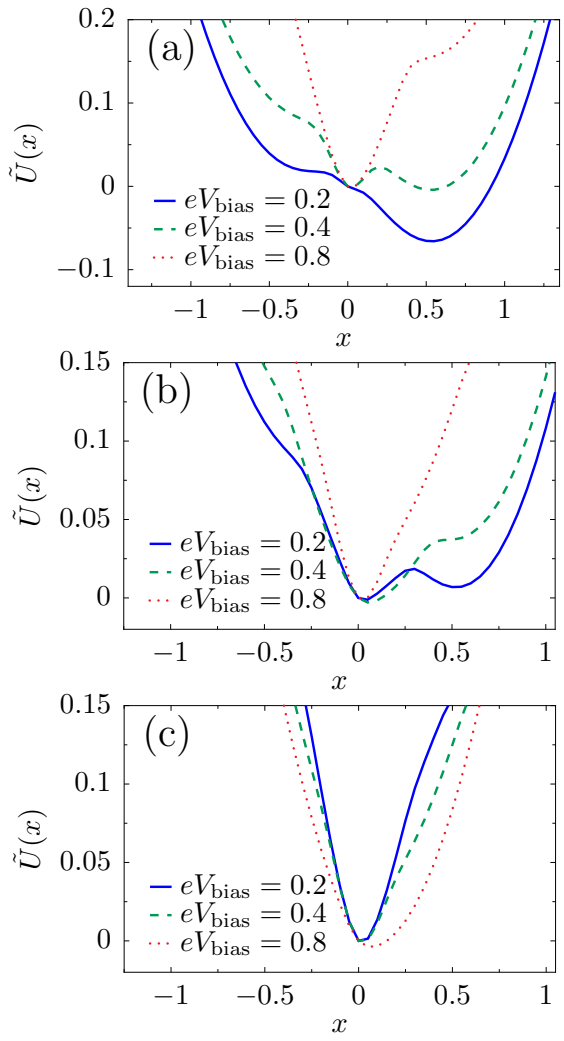


Figure 4.5. Effective potential for the mechanical motion in the two-level model. The shape of the potential can be tuned by changing the bias and gate voltages: (a) $eV_{\mathrm{gate}} = 0$, (b) $eV_{\mathrm{gate}} = 0.2$ and (c) $eV_{\mathrm{gate}} = 0.4$. We consider the parameters $\hbar\omega_0 = 0.01$, $t = 0.1$ and $\Gamma = 0.1$. The dimensionless coordinate is $x = (M\omega_0^2/\lambda_1)X$ and energies are measured in units of $\lambda_1^2/(M\omega_0^2)$.

for the mean force and damping matrix, respectively. The variance of the fluctuating force can be calculated accordingly. The average force given in Eq. (A.1) combines with the elastic force to give rise to the effective potential $\tilde{U}(X)$ depicted, for zero temperature, in Fig. 4.5. As in the case studied in the previous section, the system can exhibit various levels of multistability when changing the bias.

The results for the friction coefficient, given in Eq. (A.2), are shown in Fig. 4.6 as a function of the dimensionless oscillator coordinate $x$ for zero temperature. The contribution $\gamma^{s,eq}$ to the friction coefficient is peaked at

$$eV_{\text{gate}} \pm eV_{\text{bias}}/2 = \pm\sqrt{(\lambda_1 X)^2 + t^2}, \tag{4.20}$$

as depicted in Figs. 4.6 (a) and (c). Neglecting the coupling to the leads, our toy model can be considered as a two-level system with level-spacing $2\sqrt{(\lambda_1 X)^2 + t^2}$. Thus, the peaks occur when one of the electronic levels of the dot enters the conduction window. When this happens, small changes in the oscillator coordinate $X$ can have a large impact on the occupation of the levels. This effect is more pronounced when the dot's levels pass the Fermi levels that they are directly attached to [corresponding to $X > 0$ for current flowing from left to right, see Fig. 4.6 (a) and Fig. 4.4 (a), (b)]. The broadening of the peaks is due to the hybridization with the leads, $\Gamma/2$. When $eV_{\text{gate}} = 0$, two peaks are expected symmetrically about $X = 0$, as shown in Fig. 4.6 (a) [see also Figs. 4.4 (a) and (b)]. The effect of a finite gate voltage $eV_{\text{gate}}$ is two-fold: it shifts the non-interacting electronic levels of the dot away from the middle of the conduction window, and hence the shifted levels $\tilde{\epsilon}_\pm$ pass the Fermi levels of right and left leads at different values of $X$, Figs. 4.4 (c) and (d). Therefore in this case four peaks are expected, with two larger peaks located at $X > 0$, and two smaller peaks located at $X < 0$. This is shown in Fig. 4.6 (c). The height of the peaks in this case is reduced with respect to the case $eV_{\text{gate}} = 0$, since for a given peak, only one of the dot's levels is in resonance with one of the leads. Note that four real values of $X$ can be obtained only if $(eV_{\text{gate}} \pm eV_{\text{bias}}/2)^2 > t^2$, cp. Eq. (4.20). A situation with $(eV_{\text{gate}} - eV_{\text{bias}}/2)^2 < t^2$ while $(eV_{\text{gate}} + eV_{\text{bias}}/2)^2 > t^2$ is shown in 4.6 (c) (red-dotted line), where two peaks are present for $X_\pm = \pm 1/\lambda_1\sqrt{(eV_{\text{gate}} + eV_{\text{bias}}/2)^2 - t^2}$ [the small peak at $X_-$ is not displayed in Fig. 4.6 (c)], plus a peak at $X = 0$.

For this model, the A-matrix is generally non-vanishing, which can result in negative damping for out-of-equilibrium situations. This is due to a negative contribution of $\gamma^{s,ne}$ to the total damping. This is visualized in Figs. 4.6 (b) and (d). Negative damping is possible when both dot levels are inside the conduction window, restricting the region in $X$ over which negative damping can occur. Indeed, when only one level is within the conduction window, the system effectively reduces to the resonant level model for which, as we showed in the previous section, the friction coefficient $\gamma^s$ is always positive. When current flows from left to right, negative damping occurs only for positive values of the oscillator coordinate $X$, as shown in Figs. 4.6 (b) and (d). This is consistent with a level-inversion picture, as discussed recently by Lü *et al.* [2011]. Pictorially, the electron-vibron coupling causes a splitting in energy of the left and right levels. When $X > 0$, electrons can go "down the ladder" formed by the energy levels by passing energy to the oscillator and hence amplifying the vibrations. For $X < 0$, electrons

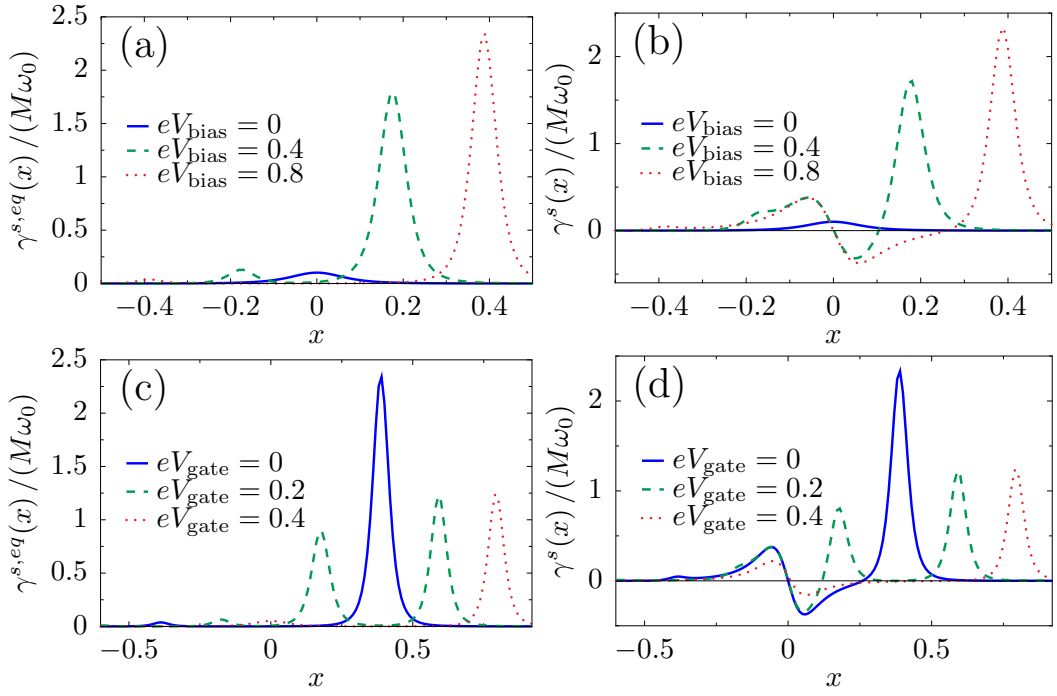


Figure 4.6. Damping vs. mechanical displacement in the two-level model. (a) Contribution $\gamma^{s,eq}$ to the friction coefficient for various bias voltages at fixed gate voltage $eV_{\rm gate} = 0$. (b) At the same gate voltage, the total damping, $\gamma^s = \gamma^{s,eq} + \gamma^{s,ne}$, exhibits a region of negative damping due to the contribution of $\gamma^{s,ne}$. (c) $\gamma^{s,eq}$ for various gate voltages with the bias voltage $eV_{\rm bias} = 0.8$. Note that for both $eV_{\rm gate} = 0.2$ and $eV_{\rm gate} = 0.4$, one small peak for negative $x$ falls outside of the shown range of $x$. (d) Again, the full damping $\gamma^s$ exhibits regions of negative damping. We choose $\hbar\omega_0 = 0.01$, $\Gamma = 0.1$ and $t = 0.1$. The dimensionless coordinate is $x = (M\omega_0^2/\lambda_1)X$ and energies are measured in units of $\lambda_1^2/(M\omega_0^2)$.

can pass between the two dots only by absorbing energy from the vibrations, causing additional non-equilibrium damping. For small broadening of the dot levels due to the coupling to the leads, this effect is expected to be strongest when the vibration-induced splitting $\lambda_1 X$ becomes of the same order as the strength of the hopping $t$. When $X$ grows further, the increasing detuning of the dot levels reduces the current and hence the non-equilibrium damping [see Figs. 4.6 (b) and (d) and Figs. 4.7 (a), (b)]. The coexistence of a multistable potential together with regions of negative damping can lead to interesting non-linear behavior for the dynamics of the oscillator. In particular, and as we show in the next example, limit-cycle solutions are possible, in the spirit of a Van der Pol oscillator [Hanggi and Riseborough, 1983].

In order to complete the discussion we also calculate the current. The pumping contribution is proportional to the velocity $\dot{X}$ and thus small. Therefore we show here results only for the dominant adiabatic part of the current, which is given by

$$I^0 = \frac{e}{h} \int \mathrm{d}\epsilon \frac{2t^2\Gamma^2(f_L - f_R)}{|\Delta|^2} \,. \tag{4.21}$$

For zero temperature, the behavior of the current is shown in Fig. 4.7 as a function of various parameters. Figs. 4.7 (a) and (b) show the current as a function of the (dimensionless) oscillator coordinate $x$ for two different values of gate potential for which the system exhibits multistability by developing several metastable equilibrium positions. For $V_{\mathrm{gate}} = 0$ and independently of bias, the current shows a maximum at the local minimum of the effective potential $x = 0$, while $I^0 \approx 0$ for another possible local minimum at $x \approx 0.5$ [compare with Fig. 4.5 (a)]. The true equilibrium value of $x$ can be tuned *via* the bias potential, showing the possibility of perfect switching. For finite gate potential however, the current is depleted from $x = 0$ with diminishing bias. Figs. 4.7 (c) and (d) show the current as a function of gate or bias voltage for fixed representative values of the oscillator coordinate $x$. The current changes stepwise as the number of levels inside the conduction window changes, coinciding with the peaks in the friction coefficient illustrated in Fig. 4.6. In an experimental setting, the measured *dc* current would involve an average over the probability distribution of the coordinate $x$, given by the solution of the Fokker-Planck equation associated to the Langevin equation (3.1).

## 4.3. Two vibrational modes

As a final example, we present a simple model which allows for both a non-conservative force and an effective "Lorentz" force, in addition to negative damping. For this it is necessary to couple the two electronic orbitals of the previous example, see Eq. (4.15), to at least two oscillatory modes which we assume to be degenerate. The relevant vibrations in this case can be thought of as a center-of-mass vibration $X_1$ between the leads, and a stretching mode $X_2$. (It should be noted that this is for visualization purposes only. In reality, for an $H_2$ molecule, the stretching mode is a high energy mode when compared to a transverse and a rotational mode, see Djukic *et al.* [2005]. Nevertheless, the $H_2$ molecule does indeed have two near-degenerate low energy vibrational modes, corresponding to

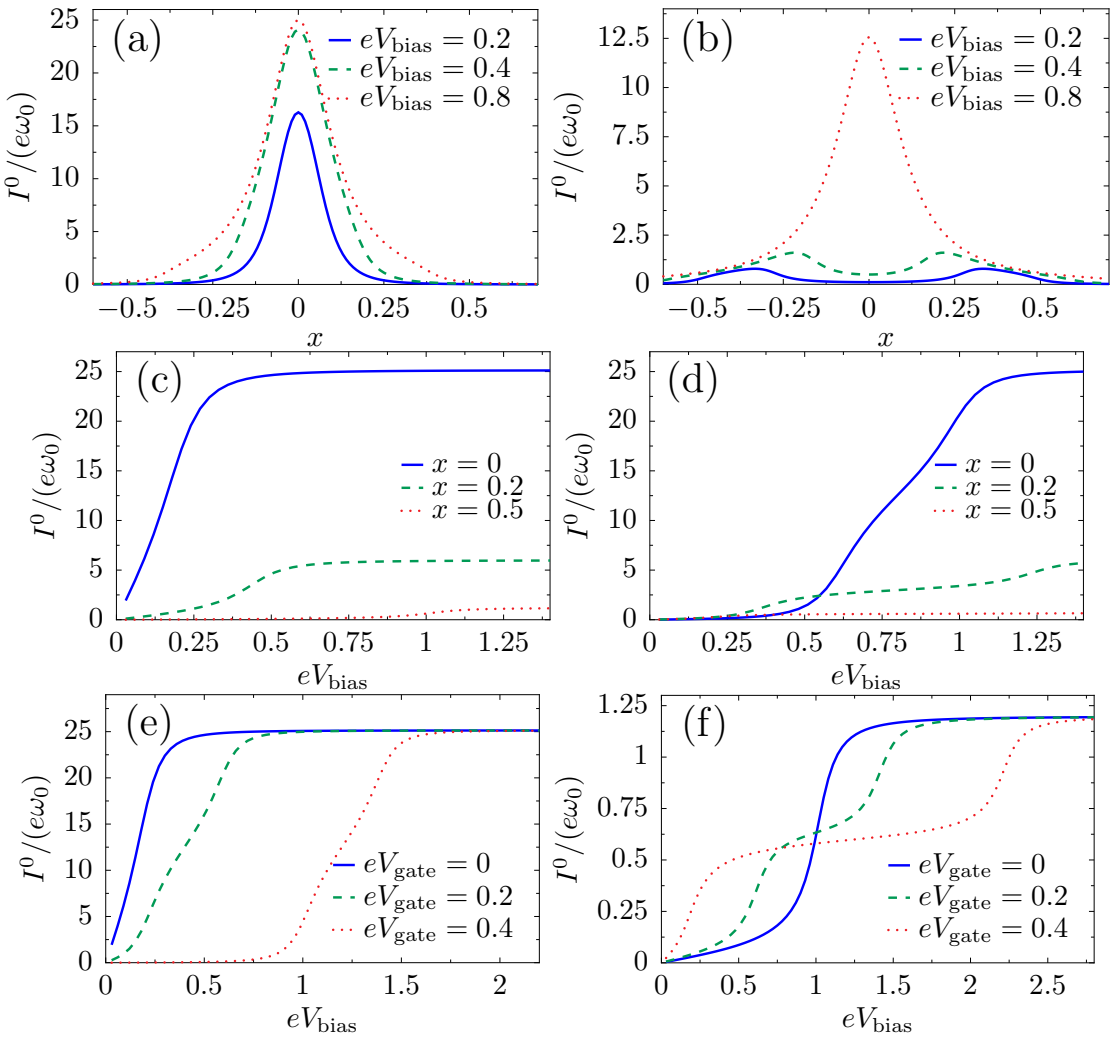


Figure 4.7. Dependence of the current in the two-level model on various parameters. Current as function of mechanical displacement for (a) $V_{\rm gate} = 0$ and (b) $V_{\rm gate} = 0.4$; as function of bias for (c) $V_{\rm gate} = 0$, (d) $V_{\rm gate} = 0.4$, (e) $x = 0$ and (f) $x = 0.5$. We choose $\hbar\omega_0 = 0.01$, $\Gamma = 0.1$ and $t = 0.1$. The dimensionless coordinate is $x = (M\omega_0^2/\lambda_1)X$ and energies are measured in units of $\lambda_1^2/(M\omega_0^2)$.

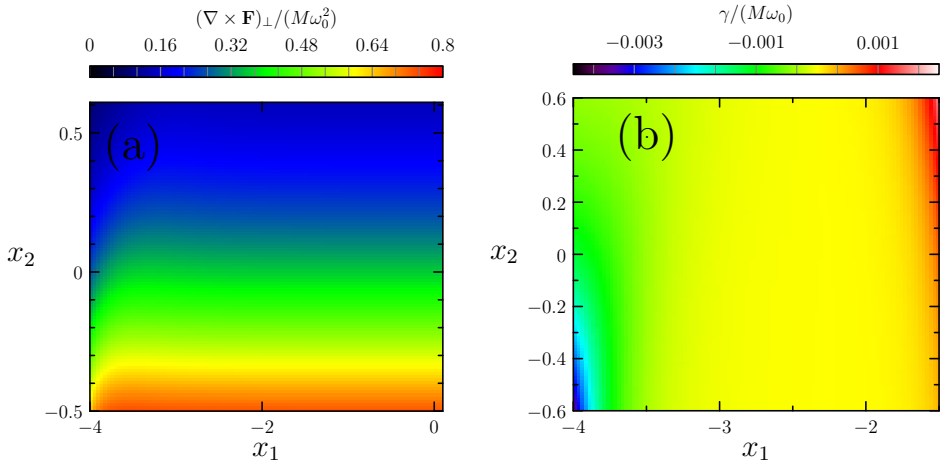


Figure 4.8. Curl of the average force and damping coefficient for the model with two vibrational modes: (a) The curl of the current-induced mean force $\boldsymbol{F}$ is, in a non-equilibrium situation, generally non-zero, indicating that the force is non-conservative. (b) One of the two eigenvalues of $\gamma^s$. Remarkably, it undergoes sign changes. A dissipation matrix $\gamma^s$ which is non-positive definite implies destabilization of the static equilibrium solution found at lower bias potentials, in this case driving the system into a limit-cycle, see main text and Fig. 4.9. The parameters used are such that $\lambda_1/\lambda_2 = 3/2$. The elastic modes are degenerate with $\hbar\omega_0 = 0.014$, $\Gamma_{L,R} = \frac{1\pm0.8}{2}(\sigma^0 \pm \sigma^z)$, and the hopping between the orbitals is $t = 0.9$. The dimensionless coordinates are $x_i = (M\omega_0^2/\lambda)X_i$ and energies are given in units of $\lambda^2/(M\omega_0^2)$, where $\lambda = (\lambda_1 + \lambda_2)/2$.

rigid vibrations between the leads and a rigid rotation relative to the axis defined by the two leads.) The stretch mode modulates the hopping parameter,

$$t \to \tilde{t}(X_2) = t + \lambda_2 X_2 \,, \tag{4.22}$$

while the center of mass mode $X_1$ is modeled as coupling linearly to the density,

$$\epsilon_0 \to \tilde{\epsilon}(X_1) = \epsilon_0 + \lambda_1 X_1 \,, \tag{4.23}$$

hence $\Lambda^1 = \lambda_1 \sigma^0$ and $\Lambda^2 = \lambda_2 \sigma^1$. We work in the wide-band limit, but allow for asymmetric coupling to the leads. The retarded Green's function becomes

$$G^R(\epsilon, X_1, X_2) = \frac{1}{\Delta} \begin{pmatrix} \epsilon - \tilde{\epsilon} + \mathrm{i}\Gamma_R & \tilde{t} \\ \tilde{t} & \epsilon - \tilde{\epsilon} + \mathrm{i}\Gamma_L \end{pmatrix} , \tag{4.24}$$

where now $\Delta(X_1, X_2) = (\epsilon - \tilde{\epsilon} + \mathrm{i}\Gamma_L)(\epsilon - \tilde{\epsilon} + \mathrm{i}\Gamma_R) - \tilde{t}^2$. The frozen S-matrix can be easily calculated to be

$$S(\epsilon, X_1, X_2) = 1 - \frac{2i}{\Delta} \begin{pmatrix} (\epsilon - \tilde{\epsilon} + \mathrm{i}\Gamma_R)\,\Gamma_L & \tilde{t}\sqrt{\Gamma_L \Gamma_R} \\ \tilde{t}\sqrt{\Gamma_L \Gamma_R} & (\epsilon - \tilde{\epsilon} + \mathrm{i}\Gamma_L)\,\Gamma_R \end{pmatrix} . \tag{4.25}$$

The A-matrices also take a simple form for this model. Since $\Lambda^1$ is proportional to the identity operator,

$$A_1(\epsilon, X_1, X_2) = -\pi \lambda_1 \, W G_R \, [G_R, \sigma^0] \, G_R W^\dagger = 0 \,. \tag{4.26}$$

On the other hand, the A-matrix associated with $X_2$ is non-zero and given by

$$A_2(\epsilon, X_1, X_2) = -\mathrm{i}\lambda_2 \, \frac{\sqrt{\Gamma_1 \Gamma_2}}{\Delta^2} \, \sigma^2 \,. \tag{4.27}$$

From this we can compute the average force, damping, pseudo-Lorentz force, and noise terms. These are listed in Appendix A.2. At zero temperature, it is possible to obtain analytical expressions for these current-induced forces. Studying the dynamics of the modes $X_{1,2}(t)$ implies solving the two coupled Langevin equations given by Eq. (3.1), after inserting the expressions for the forces given in Appendix A.2. Within our formalism we are able to study the full non-linear dynamics of the problem, which brings out a plethora of new qualitative behavior. In particular, analyses which linearize the current-induced force about a static equilibrium point would predict run-away modes due to negative damping and non-conservative forces [Lü *et al.*, 2010]. Taking into account non-linearities allows one to find the new stable attractor of the motion. Indeed, we find that these linear instabilities typically result in dynamical equilibrium, namely limit-cycle dynamics. We note in passing that limit-cycle dynamics in a nanoelectromechanical system was also discussed recently by Metelmann and Brandes [2011].

We have studied the zero-temperature dynamics of our two-level, two-mode system for different ranges of parameters. In Fig. 4.8 we map out the values of the curl of the mean force, $(\nabla \times F)_\perp$, indicating that the force is non-conservative throughout parameter

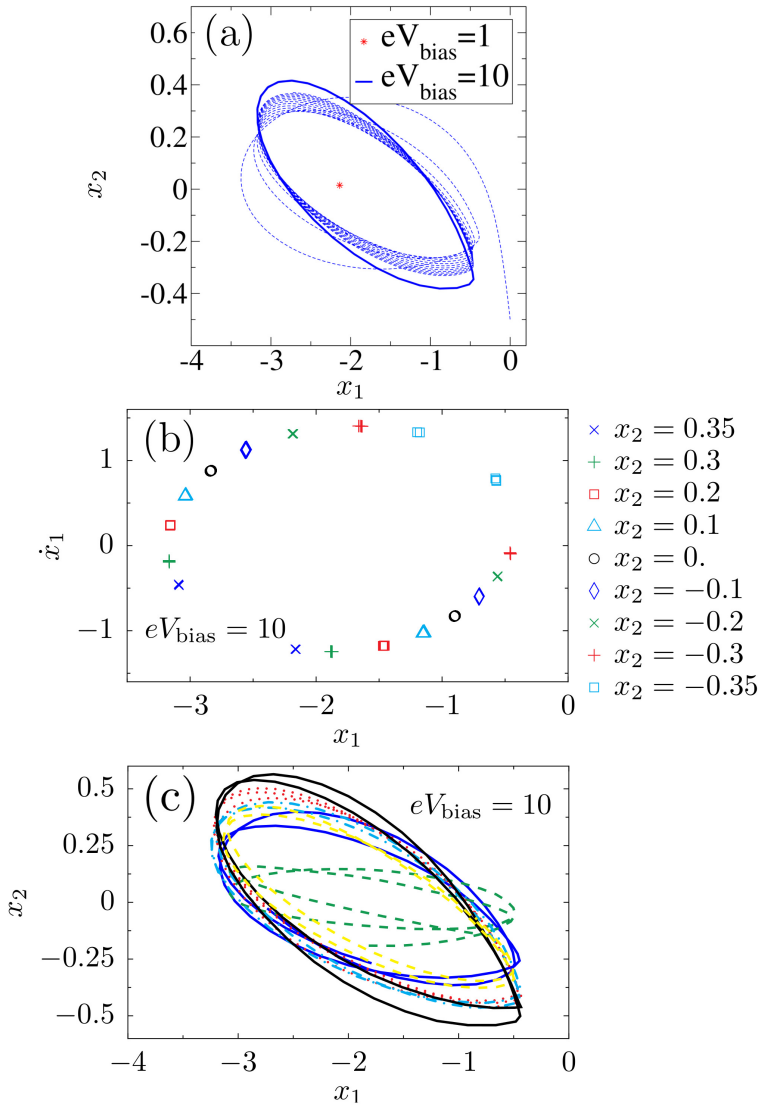


Figure 4.9. Limit-cycle dynamics for the model with two vibrational modes. (a) Limit cycle (blue solid line) and its approach (blue dotted line) at large bias vs. stable oscillations at low bias (red asterisk) in the Langevin dynamics without fluctuating force. (b) At large bias voltages, Poincaré sections of the four dimensional phase space show the presence of a limit-cycle in the Langevin dynamics without fluctuating force. (c) Several periods of typical trajectories (for different initial conditions after a transient) in the presence of the fluctuating forces $\boldsymbol{\xi}$ are shown. The same general parameters as in Fig. 4.8 are used here.

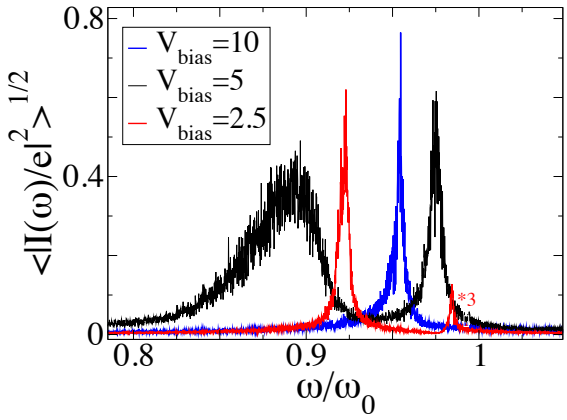


Figure 4.10. Current-current correlation function in the presence of noise for the system with two vibrational modes. The limit-cycle is signaled by a single peak ($V_{\text{bias}} = 10$, see Fig. 4.9), as opposed to two peaks in the absence of a limit-cycle ($V_{\text{bias}} = 2.5$, 5). Increasing the bias potential increases the noise levels but the peaks are still easily recognizable. The results are obtained by averaging over times long enough compared with the characteristic oscillation times. The same general parameters as in Fig. 4.8 are used here.

space. We also plot one of the two eigenvalues of the dissipation matrix $\gamma^s$, showing that it can take negative values in some regions of the parameter space.

We find that it is possible to drive the system into a limit-cycle by varying the bias potential. The existence of this limit-cycle is shown in Fig. 4.9 (a) and (b), where we show how a limit-cycle is approached and the corresponding various Poincaré sections of the non-linear system without fluctuations. Fig. 4.9 (b) shows the trajectory in phase space of the (dimensionless) oscillator coordinate $x_1$ after the dynamical equilibrium is reached, for several cuts of the (dimensionless) coordinate $x_2$. Each cut shows two points in $x_1$ phase space, indicating the entry and exit of the trajectory. Each point in the plot actually consists of several points that fall on top of each other, corresponding to every time the coordinate $x_2$ has the value indicated in the legend of Fig. 4.9 (b). This shows the periodicity of the solution of the non-linear equations of motion for $x_1$, $x_2$ for the particular bias chosen. Surveying over the various values of $x_2$ reveals a closed trajectory in the parametric coordinate space $x_1$, $x_2$. Remarkably, signatures of the limit-cycle survive the inclusion of the Langevin force. Fig. 4.9 (c) depicts typical trajectories in the oscillator's coordinate space $x_1$, $x_2$ in the presence of the stochastic force, showing fluctuating trajectories around the stable limit-cycle.

Experimentally, the signature of the limit-cycle would be most directly reflected in the current-current correlation function, as depicted in Fig. 4.10. We find that in the absence of a limit-cycle the system is dominated by two characteristic frequencies, shown by the peaks in Fig. 4.10. These frequencies correspond to the shift in energy of the

two degenerate vibrational modes due to the average current-induced forces $F_1$ and $F_2$. When the bias voltage is such that the system enters a limit-cycle, the current-current correlation shows instead only one peak as a function of frequency. This result, as shown in Fig. 4.10, is fairly robust to noise, making the onset of limit-cycle dynamics in principle observable in experiments.

## 4.4. Summary

The theory outlined in Chapter 3 allows us to study the non-linear dynamics generated by the interplay between current and vibrational degrees of freedom within a controlled approximation. This opens up the path for a systematic study of current-induced forces in nanoelectromechanical systems. We have discussed a number of illustrative toy models in this chapter.

As an introductory example we have studied a single electronic level, which is coupled to a single vibrational mode, and through which electrons can flow. We have shown how the current-induced forces can be controlled by gate and bias voltages. For instance, it is possible to create bistabilities in the potential, which is interesting in the context of all-electrical control over molecular switches. In a slightly more advanced model system, inspired *e.g.* by a double-dot or an $H_2$ molecule, we have shown that the damping coefficient can be negative, expressing an unconventional way of energy transfer from the conduction electrons to the mechanical mode. Depending on the kind of coupling, in a system with more than one mechanical mode a Lorentz-like force may arise in addition to the possibly non-conservative mean force resulting in interesting dynamics such as the existence of a limit-cycle.

Due to the backaction on the current, in principle the dynamics of the oscillator can be studied by measuring the transport properties of the device. These examples highlight that it is essential to include the non-linearities of the coupling to the vibrational modes as well as the full dependencies on the externally controllable voltages.

# 5. Current-induced switching in anisotropic magnetic molecules

In this chapter we describe the interaction between a localized magnetic molecule and conduction electrons passing through it, in analogy to the discussion of current-induced forces in the preceding chapters. In particular, we consider current-induced switching in single-molecule junctions containing an anisotropic magnetic molecule, providing possible applications to molecular spintronics. Within our model the conduction electrons couple to the magnetic molecule through the exchange interaction and we consider the regime of high currents in which the molecular spin dynamics is slow compared to the typical timescales of the conduction electrons.

This chapter is organized as follows. We introduce our model of the single-molecule junction containing an anisotropic magnetic molecule in Section 5.2. In the limit of interest, the molecular spin obeys a non-equilibrium Langevin equation which takes the form of a generalized Landau-Lifshitz-Gilbert (LLG) equation and which we derive microscopically by means of the non-equilibrium Born-Oppenheimer approximation. In Section 5.3 we derive S-matrix expressions for the various torques entering into the LLG equation, which generalize previous expressions in the literature to non-equilibrium situations. This Langevin equation is further explored in Section 5.4, considering molecular switches with axial symmetry. Switching of the molecular moment is discussed in Section 5.5, focusing on the effect of fluctuations. There it is convenient to convert the LLG-equation into a Fokker-Planck equation in order to discuss typical switching dynamics. In Section 5.6 we consider spin-torque caused by spin-polarized leads on the magnetic moment, which can also be utilized for molecular switching.


Figure 5.1. Sketch of the single-molecule junction. The electronic spins interact with the localized magnetic moment.

Our discussion closely follows the presentation in [Bode *et al.*, 2012a].

## 5.1. Introduction

The goal of this chapter is to explore the limit in which the electronic processes are fast compared to the collective degrees of freedom, in the context of magnetic molecules. We consider a generic model for an anisotropic magnetic moleculesandwiched between two

metallic (possibly spin-polarized) electrodes at which a bias voltage is applied [Friedman and Sarachik, 2010].

Work on molecular spintronics has focused on single molecule magnets such as $Mn_{12}$ and transition metal complexes. Transport experiments with $Mn_{12}$ concentrated on signatures of the magnetic excitations, as revealed by peaks in the differential conductance [Jo *et al.*, 2006], and a spin-blockade mechanism [Friedman *et al.*, 1996; Heersche *et al.*, 2006]. Research on transition metal complexes, based *e.g.* on Co, also addresses the Kondo effect [Park *et al.*, 2002; Liang *et al.*, 2002; Yu *et al.*, 2005; Romeike *et al.*, 2006; Florens *et al.*, 2011; Parks *et al.*, 2010; Franke *et al.*, 2011]. Related phenomena have been discussed in molecular spin valves, which have been realized in setups with $C_{60}$ [Rocha *et al.*, 2005; Pasupathy *et al.*, 2004], and more recently in $TbPc_2$ setups coupled to nanotubes through supramolecular interactions [Urdampilleta *et al.*, 2011].

We consider the regime where the typical time for dynamics of the molecular magnetic moment is much larger than the dwell time of the electrons flowing through the structure, so that a single electron is subject to a quasistatic configuration of the molecule. Within this *adiabatic* regime it is possible to study the coupled electronic transport and spin dynamics within a non-equilibrium Born-Oppenheimer (NEBO) approximation analogous to the one adopted in NEMS in the equivalent regime, as we have discussed in the preceding chapters. The resulting Landau-Lifshitz-Gilbert equations have been the basis for several previous works in spintronics and nanomagnetism [Katsura *et al.*, 2006; Kupferschmidt *et al.*, 2006; Fransson, 2008; Núñez and Duine, 2008; Basko and Vavilov, 2009; Dunn and Kamenev, 2011; López-Monís *et al.*, 2012; Tserkovnyak *et al.*, 2002; Brataas *et al.*, 2008, 2011; Hals *et al.*, 2010]. In particular the spin-transfer torque exerted by the transport current is well known in the context of layered magnetic structures [Slonczewski, 1996; Berger, 1996; Ralph and Stiles, 2008]. However, in the setup we consider, the different coefficients that govern the dynamics of the molecular magnetic moment show a strong dependence on the bias voltage determined by the electronic structure of the molecule, also determining the behavior of the electronic current.

Note that we consider a generic and standard model for the molecule which applies to a wide type of molecular systems, provided that a sufficiently large current flows through the molecule and that the magnetic moment is sufficiently large to fulfill the adiabatic condition assumed in the NEBO treatment. In particular, good candidates can be the $Mn_{12}$- or $Fe_8$-based devices. These systems are described by microscopic Hamiltonians of the type we consider in this chapter, and have rigid magnetic cores with magnetization $M = 10$ and an anisotropy barrier $DM^2$ of the order of a few meV [Friedman and Sarachik, 2010; Misiorny and Barnas, 2009; Sanvito, 2011]. Classical descriptions of spin dynamics have been presented for these molecules in contact to phononic environments [Zueco and García-Palacios, 2006]. We estimate for the $Mn_{12}$- or $Fe_8$ systems with a rather large magnetic anisotropy that the Born-Oppenheimer approximation can be applied when the current through the device exceeds $\sim 10$nA.

## 5.2. Description of the spin dynamics

We consider a minimal model of an anisotropic magnetic molecule embedded into a single-molecule junction.

### 5.2.1. Model

We assume that transport through the molecule is dominated by a single molecular orbital which is coupled to left ($L$) and right ($R$) leads at different chemical potentials. The spin $\hat{\boldsymbol{s}}$ of the current-carrying electrons couples to a localized molecular spin $\hat{\boldsymbol{M}}$ through exchange. Then, the full Hamiltonian consists of three terms

$$H = H_L + H_T + H_d. \tag{5.1}$$

The Hamiltonian $H_L = \sum_\eta \epsilon_\eta c_\eta^\dagger c_\eta$ models the leads $\alpha = L, R$ as free-electron systems (creation operators $c_\eta^\dagger$ with $\eta = [\alpha, k_\alpha, \sigma]$). We will consider the possibility of spin-polarized leads, assuming a spin-dependent dispersion $\epsilon_\eta$. The tunneling Hamiltonian $H_T = \sum_\eta w_{\eta\sigma} c_\eta^\dagger d_\sigma + \text{h.c.}$ describes the hybridization between the molecular orbital (with creation operator $d_\sigma^\dagger$) and the leads. This coupling to the leads through these two Hamiltonians has been discussed in Section 2.2.3 to some extent. The molecular Hamiltonian is given by

$$H_d = \sum_\sigma \epsilon_0 d_\sigma^\dagger d_\sigma + g_e \hat{\boldsymbol{s}} \cdot \boldsymbol{B} + J \hat{\boldsymbol{s}} \cdot \hat{\boldsymbol{M}} + U(\hat{\boldsymbol{M}}). \tag{5.2}$$

The potential experienced by the molecular spin in the absence of coupling to the external leads is $U(\hat{\boldsymbol{M}}) = g_d \hat{\boldsymbol{M}} \cdot \boldsymbol{B} - D\hat{M}_z^2$. The uniaxial anisotropy of the molecule is parametrized through the anisotropy parameter $D$, with easy-axis anisotropy corresponding to $D > 0$ and easy-plane anisotropy to $D < 0$. The coupling constant $J$ denotes the strength of the exchange interaction between the molecular spin $\hat{\boldsymbol{M}}$ and the electronic spins,

$$\hat{s}_j = \frac{\hbar}{2} \sum_{\sigma,\sigma'} d_\sigma^\dagger \sigma^j_{\sigma\sigma'} d_{\sigma'}, \tag{5.3}$$

where $\sigma^j$ (with $j = x, y, z$) are the usual Pauli matrices.[1] For simplicity, we assume this exchange interaction to be isotropic. The energy of the molecular orbital $\epsilon_0$ can be tuned by a gate voltage and $\boldsymbol{B}$ represents a Zeeman field acting on the electronic and the localized spins with $g$-factors $g_e$ and $g_d$, respectively.

We now discuss this model within the non-equilibrium Born-Oppenheimer (NEBO) approximation in the limit of slow precession of the magnetic moment. Our derivation starts from the Heisenberg equation of motion for the molecular spin,

$$\dot{\hat{M}}_j = \sum_{l,k} \varepsilon_{jlk} [J\hat{s}_l + g_d B_l] \hat{M}_k + D \sum_k \varepsilon_{zjk} [\hat{M}_z \hat{M}_k + \hat{M}_k \hat{M}_z], \tag{5.4}$$

[1] See the footnote on page 44 for the definition of the Pauli matrices.

where $\varepsilon_{jlk}$ is the antisymmetric Levy-Civita tensor. Within the NEBO approximation, we can turn this into an equation of motion for the expectation value $\boldsymbol{M}(t) = \langle \hat{\boldsymbol{M}}(t) \rangle$ of the localized spin,

$$\dot{\boldsymbol{M}} = \boldsymbol{M} \times \left[ -\partial_{\boldsymbol{M}} U(\boldsymbol{M}) - J\boldsymbol{s} + \boldsymbol{\delta\mathcal{B}} \right], \tag{5.5}$$

with $-\partial_{\boldsymbol{M}} U(\boldsymbol{M}) = -g_d \boldsymbol{B} + 2DM_z \hat{\mathbf{e}}_z$. Here, $\boldsymbol{M} = \boldsymbol{M}(t)$ denotes the molecular spin averaged over a time interval large compared to the electronic time scales, but small compared to the precessional dynamics of the molecular spin itself. The corresponding time-averaged electronic spin $\boldsymbol{s} = \boldsymbol{s}(t)$ can be expressed as

$$s_j(t) = \langle \hat{s}_j \rangle_{\boldsymbol{M}(t)} = -\frac{\mathrm{i}\hbar}{2} \mathrm{tr}[\mathcal{G}^<(t,t)\sigma^j]. \tag{5.6}$$

Here $\mathcal{G}^<_{\sigma\sigma'}(t,t') = \mathrm{i}\langle d^\dagger_{\sigma'}(t') d_\sigma(t) \rangle_{\boldsymbol{M}(t)}$ is the electronic lesser Green's function of the molecular orbital. It is important to note that due to the NEBO approximation, the lesser Green's function must be evaluated for a given time dependence of the molecular spin $\boldsymbol{M}(t)$. As a result, the average electronic spin $\boldsymbol{s}(t)$ depends on the molecular spin at earlier times. This will be considered in more detail in the next subsection. The instantaneous contribution gives rise to a force acting on the molecular spin. Retardation effects produce terms proportional to $\dot{\boldsymbol{M}}$, appearing in the equation of motion as Gilbert damping and a change in the gyromagnetic ratio. Additionally, fluctuations of the electron spin give rise to a fluctuating Zeeman field $\boldsymbol{\delta\mathcal{B}}$ acting on the molecular spin.

### 5.2.2. Electronic Green's function in the adiabatic limit

From now on, we again set $\hbar = 1$. We evaluate the electronic lesser Green's function, accounting for the slowly varying molecular spin $\boldsymbol{M}(t)$. The non-equilibrium Born-Oppenheimer approximation was discussed in detail in Chapter 3 which we now apply to the magnetic molecule and give explicitly the expressions for the electronic Green's functions for this model. We consider the corresponding retarded Green's function and – since the electrons are non-interacting– we can obtain $\mathcal{G}^<$ from $\mathcal{G}^R$ at the end of the calculation. Again, we rewrite the Dyson equation in the mixed (Wigner) representation in order to implement the Born-Oppenheimer approximation. Along these lines we obtain the Dyson equation for the retarded Green's function $\mathcal{G}^R = \mathcal{G}^R(\epsilon, t)$ in the Wigner representation, see Eq. (3.12).

In the strictly adiabatic limit we drop the terms proportional to derivatives with respect to the central time. To this order we obtain the frozen Green's function

$$G^R(\epsilon, \boldsymbol{M}) = \left[ \epsilon - \epsilon_0 - \Sigma^R(\epsilon) - \boldsymbol{\sigma} \cdot \boldsymbol{b} \right]^{-1}. \tag{5.7}$$

As discussed in Section 2.2.3, the self-energy $\Sigma^R_{\alpha,\sigma}(\epsilon)$ accounts for the coupling to the (possibly spin-polarized) leads, see Eq. (2.44). In the above equation and in what follows, the Green's functions, as well as the self-energies, are matrices in spin space with elements $\mathcal{G}^R_{\sigma,\sigma'}(\epsilon, t)$ and $\Sigma^R_{\sigma,\sigma'}(\epsilon)$, respectively. It is convenient to introduce an effective magnetic

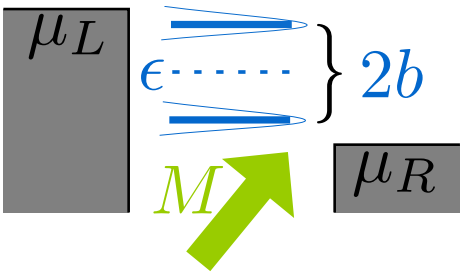


Figure 5.2. Illustration of the setup. The electronic level splits due to the effective magnetic field, given by $b = b(\vartheta)$. The number of levels in the current window depends on $b$, the applied bias voltage $eV = \mu_L - \mu_R$ and the gate voltage $eV_g = (\mu_L + \mu_R)/2 - \epsilon$.

field experienced by the electrons given by

$$\boldsymbol{b}(t) = \frac{1}{2}(J\boldsymbol{M}(t) + g_e\boldsymbol{B}), \tag{5.8}$$

see also Fig. 5.2. Notice that even if we consider a constant external magnetic field, the effective magnetic field is time dependent due to the explicit time dependence of the molecular spin $\boldsymbol{M} = \boldsymbol{M}(t)$.

In next-to-leading order in the Born-Oppenheimer approximation, we keep the time derivatives with respect to central time to linear order. As discussed in Section 3.2, the retarded Green's function becomes to first order in $\dot{\boldsymbol{M}}$

$$\mathcal{G}^R \simeq G^R + \frac{\mathrm{i}}{2}\left[\partial_\epsilon G^R \boldsymbol{\sigma}\cdot\dot{\boldsymbol{b}} G^R - G^R\boldsymbol{\sigma}\cdot\dot{\boldsymbol{b}}\partial_\epsilon G^R\right]. \tag{5.9}$$

The lesser Green's function can now be deduced from the relation Eq. (2.47),[2] which yields

$$\mathcal{G}^< \simeq G^< + \frac{\mathrm{i}}{2}\Big(\partial_\epsilon G^<\boldsymbol{\sigma}\cdot\dot{\boldsymbol{b}}G^A - G^R\boldsymbol{\sigma}\cdot\dot{\boldsymbol{b}}\partial_\epsilon G^< + \partial_\epsilon G^R\boldsymbol{\sigma}\cdot\dot{\boldsymbol{b}}G^< - G^<\boldsymbol{\sigma}\cdot\dot{\boldsymbol{b}}\partial_\epsilon G^A\Big), \tag{5.10}$$

in accordance with the corresponding expression Eq. (3.18). Here we used $G^< = G^R\Sigma^< G^A$ where the lesser self-energy is given explicitly in the Appendix B.1. Note that we suppressed the arguments of the frozen Green's functions, $G^{R,A,<} = G^{R,A,<}(\epsilon, \boldsymbol{M})$.

### 5.2.3. Electron spin

We can now employ this result for the electronic Green's function and evaluate the electron spin. Substituting Eq. (5.10) into Eq. (5.6), we find

$$J\boldsymbol{s}(\boldsymbol{M}) \simeq J\boldsymbol{s}^0(\boldsymbol{M}) + \gamma(\boldsymbol{M})\dot{\boldsymbol{M}}. \tag{5.11}$$

[2] This states $\mathcal{G}^<(t,t') = \int \mathrm{d}t_1 \int \mathrm{d}t_2\, \mathcal{G}^R(t,t_1)\Sigma^<(t_1,t_2)\mathcal{G}^A(t_2,t')$. Here we use $\mathcal{G}^A = [\mathcal{G}^R]^\dagger$.

The first term in Eq. (5.11) contains the average electron spin

$$s_l^0(\boldsymbol{M}) = -\frac{\mathrm{i}}{2}\int \frac{\mathrm{d}\epsilon}{2\pi}\mathrm{tr}[G^<\sigma^l] \tag{5.12}$$

in the strictly adiabatic limit. The correction due to retardation effects associated with the slow dynamics of the molecular spin are captured by the matrix $\gamma(\boldsymbol{M})$, which follows from Eq. (5.10) along the lines of the derivation in Section 3.2 using integration by parts and the relation between the Green's functions $G^> - G^< = G^R - G^A$. It is appropriate to split the resulting matrix into $\gamma_{lk} = \gamma^s_{lk} + \gamma^a_{lk}$ with the shorthand $\gamma^{s,a}_{lk} = (\gamma_{lk} \pm \gamma_{kl})/2$. As we will see, the symmetric part of this matrix,

$$\gamma^s_{lk}(\boldsymbol{M}) = \frac{J^2}{4}\int \frac{\mathrm{d}\epsilon}{2\pi}\mathrm{tr}[\sigma^l\partial_\epsilon G^>\sigma^k G^<]_s, \tag{5.13}$$

describes Gilbert damping of the molecular spin, induced by the coupling to the electrons. The antisymmetric part of the matrix $\gamma$,

$$\gamma^a_{lk}(\boldsymbol{M}) = \frac{J^2}{4}\int \frac{\mathrm{d}\epsilon}{2\pi}\mathrm{tr}[\sigma^l\partial_\epsilon \left(G^R + G^A\right)\sigma^k G^<]_a, \tag{5.14}$$

will induce a coupling renormalization.

Due to the stochastic nature of the current flow through the magnetic molecule (as reflected in thermal as well as shot noise of the current), the electronic spin will also fluctuate, giving rise to a fluctuating torque $\boldsymbol{\delta\mathcal{B}}(t)$ acting on the molecular spin. Note that in the Born-Oppenheimer limit, we can neglect any frequency dependence of this correlation function on the time scales of the molecular spin, so that the fluctuating Zeeman field can be taken as locally correlated in time. Therefore, as discussed in Chapter 3, in the Born-Oppenheimer approximation, the fluctuating Zeeman field $\boldsymbol{\delta\mathcal{B}}$ has the symmetrized correlator $\langle\delta\mathcal{B}_k(t)\delta\mathcal{B}_l(t')\rangle = \tilde{D}_{kl}(\boldsymbol{M})\delta(t-t')$ with

$$\tilde{D}_{kl}(\boldsymbol{M}) = \frac{J^2}{4}\int \frac{\mathrm{d}\epsilon}{2\pi}\mathrm{tr}[\sigma^k G^>\sigma^l G^<]_s. \tag{5.15}$$

Note that accordingly the fluctuations of the spin can be evaluated using the Green's function $G^{<,>}$ to lowest order in $\dot{\boldsymbol{b}}$.

### 5.2.4. Landau-Lifshitz-Gilbert equation

Substituting the expression for the electronic spin, Eq. (5.11), into the equation of motion (5.5) we obtain a Langevin equation of the Landau-Lifshitz-Gilbert type,

$$\dot{\boldsymbol{M}} = \boldsymbol{M}\times\left[-\partial_{\boldsymbol{M}}U - J\boldsymbol{s}^0 - \gamma^s\dot{\boldsymbol{M}} - \gamma^a\dot{\boldsymbol{M}} + \boldsymbol{\delta\mathcal{B}}\right]. \tag{5.16}$$

Note that, unlike in simple versions of a Landau-Lifshitz-Gilbert equation, the effective exchange field $\boldsymbol{s}^0$ as well as the coefficient matrices $\gamma^s$ and $\gamma^a$ still depend on the molecular spin $\boldsymbol{M}$ itself. We can simplify this equation by introducing the vector

$$C_k(\boldsymbol{M}) = \frac{1}{2}\sum_{lm}\epsilon_{klm}\gamma^a_{lm}(\boldsymbol{M}). \tag{5.17}$$

Using that the length of $\boldsymbol{M}$ is conserved, it follows that the antisymmetric part of $\gamma$ merely renormalizes the precession frequency by an overall prefactor

$$\alpha(\boldsymbol{M}) = \frac{1}{1 + \boldsymbol{C} \cdot \boldsymbol{M}}. \tag{5.18}$$

This yields the simplified Landau-Lifshitz-Gilbert equation

$$\dot{\boldsymbol{M}} = \alpha \boldsymbol{M} \times \left[ -\partial_{\boldsymbol{M}} U - J\boldsymbol{s}^0 - \gamma^s \dot{\boldsymbol{M}} + \boldsymbol{\delta\mathcal{B}} \right], \tag{5.19}$$

which we will analyze further in the subsequent sections.

When coupled to spin-polarized leads and when a finite bias voltage is applied, the torque can be non-conservative, yielding the so-called spin-transfer torque [Ralph and Stiles, 2008]. Also the eigenvalues of $\gamma^s$ can become overall negative, providing another mechanism of energy transfer from the electrons to the localized spin.

Since the stochastic spin dynamics is effectively two-dimensional, it generically exhibits similar phenomena as NEMS with more than one vibrational mode, which we have discussed in the previous chapters. Specifically, this includes the non-conservative nature of the average force in general non-equilibrium situations as well as the presence of the antisymmetric contribution to the velocity-dependent force. The latter acts, however, in different ways in the two cases, owing to the different orders of the Langevin equation. In the vibrational context, this term gives rise to an effective Lorentz force, while it merely renormalizes the precession frequency in the context of the magnetic molecule.

## 5.3. Relation to scattering matrix theory

It has already been noted in a series of works by Tserkovnyak *et al.* [2002], Brataas *et al.* [2008, 2011] and Hals *et al.* [2010] that the coefficients in the Landau-Lifshitz-Gilbert equation in lead-ferromagnet-lead structures can be expressed in terms of the scattering matrix of the structure, resulting in expressions for Gilbert damping and the fluctuating torque in thermal equilibrium and for current-induced spin-transfer torques within linear response theory. Here we will provide S-matrix expressions which remain valid in general out-of-equilibrium situations and which include the exchange field and the precession renormalization in addition to the Gilbert damping with the only assumption that the precessional frequency of the localized magnetic moment is slow compared to the electronic time scales. In this section we apply the general discussion from Chapter 3 in order to provide S-matrix expressions for the various entries in the Landau-Lifshitz-Gilbert equation.

For adiabatic parameter variations, the full $\mathcal{S}$-matrix of mesoscopic conductors can be expressed in the Wigner representation as Büttiker [Moskalets and Büttiker, 2004; Arrachea and Moskalets, 2006] introduced an $A$-matrix through

$$\mathcal{S}(\epsilon, t) \simeq S(\boldsymbol{M}(t), \epsilon) + \dot{\boldsymbol{M}}(t) \cdot \boldsymbol{A}(\epsilon, \boldsymbol{M}(t)),$$

repeating Eq. (3.28) from Chapter 3. Note that we expanded the full S-matrix $\mathcal{S}$ to linear order in the velocities $\dot{\boldsymbol{M}}$ of the adiabatic variables, see [Moskalets and Büttiker, 2004;

Arrachea and Moskalets, 2006]. For the model considered here, the frozen $S$-matrix and the $A$-matrix are related to the frozen retarded Green's function $G^R(\epsilon, \boldsymbol{M})$ through

$$S(\epsilon, \boldsymbol{M}) = 1 - 2\pi \mathrm{i} W G^R(\epsilon, \boldsymbol{M}) W^\dagger, \tag{5.20}$$

$$A_k(\boldsymbol{M}, \epsilon) = \pi \frac{J}{2} \Big[ \partial_\epsilon \left( W G^R \right) \sigma^k G^R W^\dagger - W G^R \sigma^k \partial_\epsilon \left( G^R W^\dagger \right) \Big]. \tag{5.21}$$

The average electronic spin $s_l^0(\boldsymbol{M})$ can be written in terms of the frozen S-matrix (5.20) by expressing the lesser Green's function $G^< = G^R \Sigma^< G^A$ in terms of the self-energy $\Sigma^<(\epsilon) = \mathrm{i}\pi \sum_\alpha f_\alpha W^\dagger \Pi_\alpha W$ with $\Pi_\alpha$ a projector on lead $\alpha$, cp. the discussion in Section 2.2.3. Using the identity $2\pi \mathrm{i} W^\dagger W = (G^R)^{-1} - (G^A)^{-1}$, we find

$$J s_k^0(\boldsymbol{M}) = -\sum_\alpha \int \frac{\mathrm{d}\epsilon}{2\pi \mathrm{i}} f_\alpha \ \mathrm{Tr} \left( \Pi_\alpha S^\dagger \frac{\partial S}{\partial M_k} \right) \tag{5.22}$$

for the average electronic spin. Here the trace "Tr" acts in lead-channel space.

The S-matrix expression (5.22) allows us to make some general statements about the average torque acting on the molecular spin. In particular, we can evaluate the curl of the average torque, $\partial_{M_l} s_k^0 - \partial_{M_k} s_l^0$. In Section 3.3.2 we have discussed in some detail that this curl, and hence the spin-transfer torque, vanishes in thermal equilibrium. However, in general out-of-equilibrium situations, the curl will be nonzero, giving rise to finite spin-transfer torque. We will return to this issue when we discuss switching in Section 5.6.

To express the velocity-dependent forces in terms of the scattering matrix in general non-equilibrium situations, we need to go beyond the frozen scattering matrix $S$ and include the $A$ matrix introduced above. The Gilbert-damping coefficients appearing in the Langevin equation (5.19) can then be written as

$$\begin{aligned} \gamma_{kl}^s(\boldsymbol{M}) = & \sum_\alpha \int \frac{\mathrm{d}\epsilon}{4\pi} (-\partial_\epsilon f_\alpha) \mathrm{Tr} \left\{ \Pi_\alpha \frac{\partial S^\dagger}{\partial M_k} \frac{\partial S}{\partial M_l} \right\}_s \\ & + \sum_\alpha \int \frac{\mathrm{d}\epsilon}{2\pi \mathrm{i}} f_\alpha \mathrm{Tr} \left\{ \Pi_\alpha \left( \frac{\partial S^\dagger}{\partial M_k} A_l - A_l^\dagger \frac{\partial S}{\partial M_k} \right) \right\}_s . \end{aligned} \tag{5.23}$$

The eigenvalues of the first line are strictly positive while the sign of the second line is not fixed, giving rise to the possibility of overall *negative* Gilbert damping. Note that the second line is a pure non-equilibrium contribution, as discussed in Section 3.3.2. Similarly, we express the antisymmetric part of $\gamma_{kl}$ as

$$\gamma_{kl}^a(\boldsymbol{M}) = \sum_\alpha \int \frac{\mathrm{d}\epsilon}{2\pi \mathrm{i}} f_\alpha \mathrm{Tr} \left\{ \Pi_\alpha \left( S^\dagger \frac{\partial A_k}{\partial M_l} - \frac{\partial A_k^\dagger}{\partial M_l} S \right) \right\}_a , \tag{5.24}$$

which causes a renormalization of the precession frequency, as discussed above.

Similar to the average spin, we can also express the variance of the fluctuating Zeeman field (5.15) in terms of the frozen $S$-matrix,

$$\tilde{D}_{kl}(\boldsymbol{M}) = \sum_{\alpha\alpha'} \int \frac{\mathrm{d}\epsilon}{2\pi} f_\alpha (1 - f_{\alpha'}) \mathrm{Tr} \left\{ \Pi_\alpha \left( S^\dagger \frac{\partial S}{\partial M_k} \right)^\dagger \Pi_{\alpha'} S^\dagger \frac{\partial S}{\partial M_l} \right\}_s . \tag{5.25}$$

By going to a basis in which $\tilde{D}$ is diagonal and using $\Pi_\alpha = \Pi_\alpha^2$, we find that $\tilde{D}$ is a positive definite matrix, see Section 3.3.2. With this preparation, it is now easy to ascertain that in equilibrium damping and fluctuations are related by the fluctuation-dissipation theorem, $\tilde{D}_{kl} = 2T\gamma^s_{kl}$.

## 5.4. Molecular switches with axial symmetry

From now on we specify to the case of axial symmetry, where both the magnetic field and the polarization of the leads point along the anisotropy axis $\hat{\mathbf{e}}_z$. In this section, we will derive explicit expressions for the current-induced forces, including their dependence on the molecular spin $\boldsymbol{M}$.

We first consider the average torque which is determined by the average electronic spin. Given that there are two basic vectors in the problem, namely $\hat{\mathbf{e}}_z$ and $\hat{\boldsymbol{M}} = \boldsymbol{M}/M$, the spin can be decomposed as

$$\boldsymbol{s}^0(\boldsymbol{M}) = s_M(\boldsymbol{M})\hat{\boldsymbol{M}} + s_z(\boldsymbol{M})\hat{\mathbf{e}}_z + s_t(\boldsymbol{M})(\hat{\mathbf{e}}_z \times \hat{\boldsymbol{M}}). \tag{5.26}$$

Hence, the average torque exerted on the molecular spin by the conduction electrons is

$$-\alpha \boldsymbol{M} \times J\boldsymbol{s}^0 = -\alpha \boldsymbol{M} \times \Big[ s_z\, \hat{\mathbf{e}}_z + s_t\, (\hat{\mathbf{e}}_z \times \hat{\boldsymbol{M}}) \Big], \tag{5.27}$$

which is obtained by inserting Eq. (5.26) into the Landau-Lifshitz-Gilbert equation (5.19). The first term inside the bracket can be derived from a potential, since its curl vanishes. This becomes more evident from the explicit expressions below using that the $\boldsymbol{M}$-dependence of the coefficients stems from the effective magnetic field $\boldsymbol{b}$ experienced by the electrons and that the length of $\boldsymbol{M}$ is conserved. This contribution modifies the precession frequency around the $z$-axis. In contrast, the second term on the right hand side of Eq. (5.27) has a non-vanishing curl, $\nabla_{\boldsymbol{M}} \times \Big[ s_t\, (\hat{\mathbf{e}}_z \times \hat{\boldsymbol{M}}) \Big] \neq 0$, so that $s_t$ introduces a *non-conservative* torque, providing the possibility of energy exchange between the conduction electrons and the molecule.

Concrete expressions for these contributions to the current-induced torque can be obtained from

$$s_z(\boldsymbol{M}) = -\,\mathrm{i} \int \frac{\mathrm{d}\epsilon}{2\pi} [G_z^<(\epsilon, \boldsymbol{M}) + G_b^<(\epsilon, \boldsymbol{M}) \Big( \frac{g_e B}{2} + \mathrm{Re}[\Sigma_s^R] \Big)], \tag{5.28}$$

$$s_t(\boldsymbol{M}) = -\,\frac{\mathrm{i}J}{M} \int \frac{\mathrm{d}\epsilon}{2\pi} G_t^<(\epsilon, \boldsymbol{M}), \tag{5.29}$$

as derived by substituting $G^<$, see Eq. (B.4) in Appendix B, into Eq. (5.12) and taking into account possibly spin-polarized leads with the notation $\Sigma^R_{\alpha,c(s)} = [\Sigma^R_{\alpha,\uparrow} \pm \Sigma^R_{\alpha,\downarrow}]/2$ for the self-energies.

These general expressions simplify significantly for unpolarized leads.[3] In particular, the component $s_t$ of the average torque vanishes, and the remaining conservative contribution

[3] Unpolarized leads correspond to $\Sigma^R_{\alpha,s} = 0$ and one finds that consequently $G_t^<$ and $G_z^<$ vanish, see Eqs. (B.4) and (B.5).

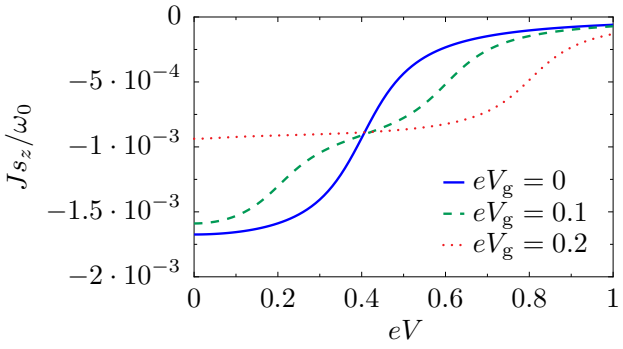


Figure 5.3. Component of the average current-induced torque in a uniaxial situation for unpolarized leads. $Js_z(\boldsymbol{M})$ is plotted as a function of the applied bias voltage for different gate voltages $eV_g$. As discussed in the text, $Js_z$ changes when the number of levels in the current window varies at $V_g \pm eV/2 = \pm b$ (see also Fig. 5.2). The plots are obtained at zero temperature at the potential minimum $\vartheta = 0$ for the values $JM/2 = 0.2$, $\Gamma = 0.1$, $g_eB/2 = 0.002$ and $g_e = g_d$. The precession frequency in the absence of coupling to electron spin and magnetic field is $\epsilon_0 = 2DM = 0.01$. All energies are measured in units of the barrier height without magnetic field $DM^2$.

$s_z$ is then found to be $s_z = s_z^- - s_z^+$ with

$$s_z^{\pm}(\boldsymbol{M}) = \sum_\alpha \frac{\Gamma_\alpha}{\pi\Gamma}\left(\arctan\left[\frac{\mu_\alpha - \tilde{\epsilon} \pm b}{\Gamma/2}\right] + \frac{\pi}{2}\right)\frac{g_eB}{2b}. \tag{5.30}$$

Here we assume the limit of zero temperature and introduce the shorthand $\tilde{\epsilon} = \epsilon_0 + \mathrm{Re}[\Sigma_c]$.

It is instructive to study the dependence of the average torque on bias and gate voltage. Notice that, due to the effective magnetic field $\boldsymbol{b}$ acting on the electron spin, the electronic level splits, like we sketched in Fig. 5.2. Consequently, $b$, the applied bias voltage $eV = \mu_L - \mu_R$, and the gate voltage $eV_g = (\mu_L + \mu_R)/2 - \tilde{\epsilon}$ control the number of levels in the current window. This changes from zero ($eV/2 > eV_g \pm b$) to one ($eV_g + b > eV/2 > eV_g - b$) to two ($eV_g \pm b > eV/2$).[4] The average torque is finite when just one level, corresponding to *e.g.* spin-up electrons, is occupied. In contrast, for sufficiently high bias voltages both spin-up and spin-down electrons participate in the transport so that no net electron spin acts on the molecule. This is illustrated in Fig. 5.3, where the average electronic spin on the molecule is plotted as a function of the applied bias voltage $eV$ for three different values of the molecular level $\epsilon_0$ (as tunable by the gate voltage $eV_g$).

For Gilbert damping and the fluctuating torque, we restrict ourselves to unpolarized leads. This choice is motivated by the fact that switching of the molecular spin (as discussed in the next two sections) is dominated by the average torque for polarized leads (and thus weakly affected by higher orders in the adiabatic expansion) and by

[4] He we assume $eV, eV_g > 0$ for simplicity.

the fluctuating force for unpolarized leads. (We mention in passing that expressions for Gilbert damping and fluctuating force for polarized leads can be readily derived but are rather cumbersome.)

For unpolarized leads, we can split the Gilbert damping tensor into one part proportional to the unit matrix and another proportional to a projector onto the $z$-axis,

$$\boldsymbol{M} \times \gamma^s \dot{\boldsymbol{M}} = \gamma^{s,1} \boldsymbol{M} \times \dot{\boldsymbol{M}} + \gamma^{s,2} (\dot{\boldsymbol{M}} \cdot \hat{\mathbf{e}}_z) \boldsymbol{M} \times \hat{\mathbf{e}}_z, \tag{5.31}$$

where $\gamma^{s,1}$ and $\gamma^{s,2}$ are scalars. The first term in Eq. (5.31) tends to (anti)align the molecular spin with the anisotropy axis while the second modifies the precession frequency. The coefficients $\gamma^{s,1}$ and $\gamma^{s,2}$ are calculated by inserting $G^<$ and $G^>$ from Eq. (B.5) into Eq. (B.8), resulting in

$$\gamma^{s,1}(\boldsymbol{M}) = \int \frac{d\epsilon}{8\pi} \sum_{\alpha\beta} \frac{J^2 \, \Gamma_\alpha \Gamma_\beta (-\partial_\epsilon f_\beta)}{[(\epsilon - \tilde{\epsilon} + b)^2 + (\Gamma/2)^2] \, [(\epsilon - \tilde{\epsilon} - b)^2 + (\Gamma/2)^2]}, \tag{5.32}$$

and

$$\gamma^{s,2}(\boldsymbol{M}) = \int \frac{d\epsilon}{16\pi} \sum_{\alpha\beta} \frac{(g_e B J)^2 \, \Gamma_\alpha \Gamma_\beta (-\partial_\epsilon f_\beta)(\epsilon - \tilde{\epsilon})^2}{[(\epsilon - \tilde{\epsilon} + b)^2 + (\Gamma/2)^2]^2 \, [(\epsilon - \tilde{\epsilon} - b)^2 + (\Gamma/2)^2]^2}. \tag{5.33}$$

The damping coefficient is peaked when the number of levels between $\mu_L$ and $\mu_R$ changes and thus vanishes at large voltages when both levels are in the transport window. We illustrate this dependence of $\gamma^{s,1}$ on gate and bias voltage in Fig. 5.4.

As stated above, the prefactor $\alpha$ in Eq. (5.19) is given by $\alpha(\boldsymbol{M}) = 1/\left(1 + \boldsymbol{C} \cdot \boldsymbol{M}\right)$, with $\boldsymbol{C}$ defined in Eq. (5.17). This is calculated in the same way as the damping coefficients, yielding

$$\boldsymbol{C}(\boldsymbol{M}) = \int \frac{\mathrm{d}\epsilon}{2\pi} \sum_{\alpha} \frac{J^2 \Gamma^2 \, \Gamma_\alpha f_\alpha \, (\epsilon - \tilde{\epsilon})}{[(\epsilon - \tilde{\epsilon} + b)^2 + (\Gamma/2)^2]^2 \, [(\epsilon - \tilde{\epsilon} - b)^2 + (\Gamma/2)^2]^2} \boldsymbol{b}, \tag{5.34}$$

where we have inserted $G^<$ and $G^>$ into Eq. (5.14).

We close this section with the corresponding expression for the variance of the fluctuating Zeeman field, Eq. (5.15), which becomes $\tilde{D}_{kl}(\boldsymbol{M}) = \tilde{D}^1(\boldsymbol{M})\delta_{kl} + \tilde{D}^2(\boldsymbol{M}) b_k b_l$, where

$$\tilde{D}^1(\boldsymbol{M}) = \frac{J^2}{2} \int \frac{\mathrm{d}\epsilon}{2\pi} \sum_{\alpha\beta} \frac{\Gamma_\alpha \Gamma_\beta f_\alpha (1 - f_\beta)}{[(\epsilon - \tilde{\epsilon} + b)^2 + (\Gamma/2)^2] \, [(\epsilon - \tilde{\epsilon} - b)^2 + (\Gamma/2)^2]}, \tag{5.35}$$

$$\tilde{D}^2(\boldsymbol{M}) = J^2 \int \frac{\mathrm{d}\epsilon}{2\pi} \sum_{\alpha\beta} \frac{\Gamma_\alpha \Gamma_\beta f_\alpha (1 - f_\beta) \, (\epsilon - \tilde{\epsilon})^2}{[(\epsilon - \tilde{\epsilon} + b)^2 + (\Gamma/2)^2]^2 \, [(\epsilon - \tilde{\epsilon} - b)^2 + (\Gamma/2)^2]^2}, \tag{5.36}$$

for unpolarized leads. As illustrated in Fig. 5.4, the strength of the fluctuations changes with the number of electronic levels in the transport window and saturates at high bias voltages when both levels lie within.

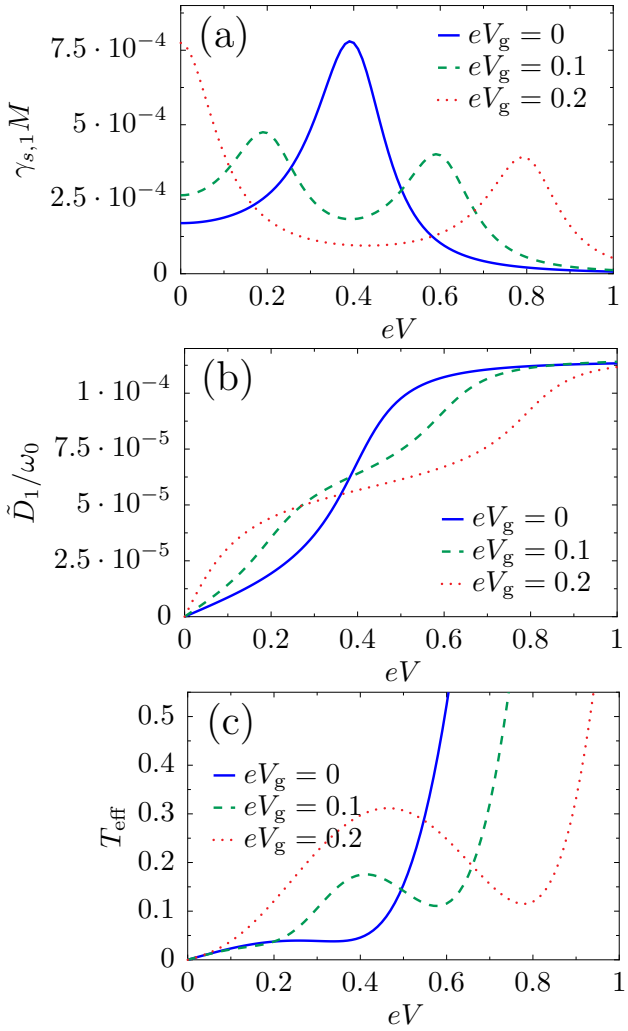


Figure 5.4. Damping and fluctuations as a function of the applied bias voltage. (a) The damping coefficient $\gamma^{s,1}$ is plotted for three different gate voltages. It is peaked when the number of levels in the current region changes from zero to one to two at $V_g \pm eV/2 = \pm b$ (see also Fig. 5.2). (b) At these points the fluctuation kernel $\tilde{D}^1$ increases steplike. The level broadening results from the interaction with the leads encapsulated in $\Gamma$. (c) The effective temperature $T_{\text{eff}} = \tilde{D}^1/(2\gamma^{s,1})$ is shown as a function of the bias voltage. The plots are obtained at the potential minimum $\vartheta = 0$ with the same parameters as in Fig. 5.3. All energies are measured in units of the barrier height without magnetic field $DM^2$.

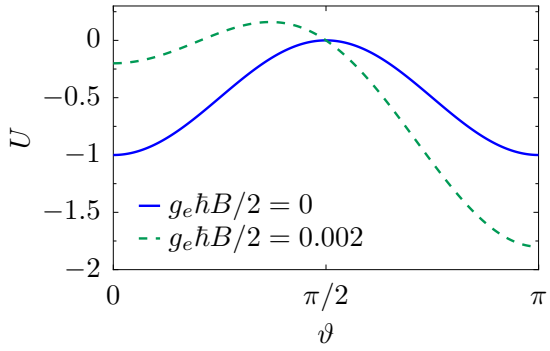


Figure 5.5. Potential experienced by the molecular spin in the absence of coupling to the electrons. $U(\vartheta)$ is shown with and without an external magnetic fields. All energies are measured in units of the barrier height without magnetic field $DM^2$.

## 5.5. Fluctuation-induced switching for unpolarized leads.

We now apply our results to discuss the switching dynamics for unpolarized leads. In the absence of coupling to the electrons the molecular spin moves in the potential $U = g_d B M_z - D M_z^2$. For sufficiently small magnetic fields, two minima are present, corresponding to parallel and antiparallel alignment of the spin to the magnetic field. This is shown in Fig. 5.5, where $U(\vartheta)$ is plotted for different magnetic fields and $\vartheta$ denotes the angle between $\boldsymbol{M}$ and the anisotropy-axis. Assume that the molecular spin is initially aligned parallel to the magnetic field. Due to the interaction with the electrons the molecular spin fluctuates about this initial state, causing spin flips at a certain rate which we calculate in this section. Clearly, these fluctuations depend on temperature and applied bias voltage. If the system is in thermal equilibrium, this is a standard problem [Brown, 1963]. Our approach allows us to extend these standard results to out-of-equilibrium situations in the presence of a bias voltage in addition to finite temperature. We also demonstrate that the orientation of the molecular spin can be read out by tracking the current through the molecule.

### 5.5.1. Fokker-Planck equation

Our approach is based on an equivalent Fokker-Planck formulation of the Langevin dynamics of the molecular spin. We first rewrite the Langevin equation (5.19) for unpolarized leads. Describing the orientation of the molecular spin in terms of a polar angle $\vartheta$ (measured relative to the applied magnetic field) and an azimuthal angle $\varphi$, and noting that $\dot{\boldsymbol{M}}/M = \dot{\vartheta}\hat{\mathbf{e}}_\vartheta + \dot{\varphi}\sin\vartheta\hat{\mathbf{e}}_\varphi$, we find the Langevin equation

$$\begin{aligned} \dot{\vartheta} &= \alpha\left[M\gamma^{s,1}\sin\vartheta\,\dot{\varphi} - \delta\mathcal{B}_\varphi\right] \\ \sin\vartheta\,\dot{\varphi} &= \alpha\left[-\partial_\vartheta U/M - Js_z\sin\vartheta + \delta\mathcal{B}_\vartheta - M\left(\gamma^{s,1} + \gamma^{s,2}\sin^2\vartheta\right)\dot{\vartheta}\right]. \end{aligned} \tag{5.37}$$

Here the noise correlator is given in polar coordinates by $\tilde{D}_{\varphi\varphi} = \tilde{D}_{\vartheta\varphi} = \tilde{D}^1$ and $\tilde{D}_{\vartheta\vartheta} = \tilde{D}^1 + [(g_e B/2)\cos\vartheta\sin\vartheta]^2\,\tilde{D}^2$, with $\tilde{D}^i$ defined in Eq. (5.35).

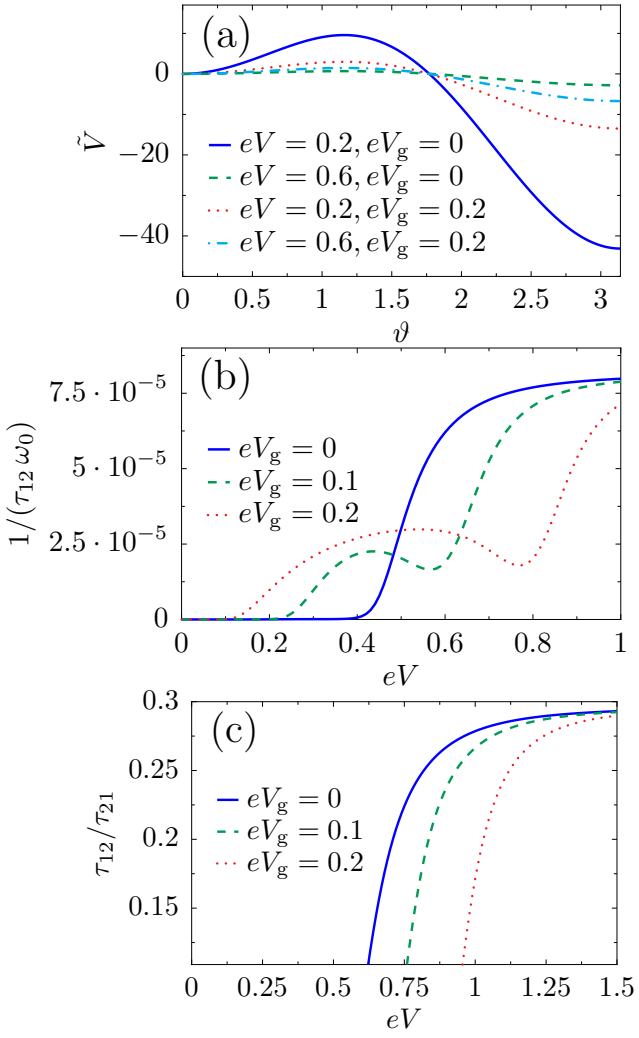


Figure 5.6. Switching dynamics for unpolarized leads. (a) $\tilde{V}$ is plotted for different bias and gate voltages. (b) The switching rate $1/\tau_{12}$ is plotted as a function of the applied bias voltage for different gate voltages. (c) The ratio between the switching rates $1/\tau_{21}$ and $1/\tau_{12}$ is shown. The plots are obtained with the same parameters as in Fig. 5.3. All energies are measured in units of the barrier height without magnetic field $DM^2$.

Following standard procedures [Zwanzig, 2001], we now derive the corresponding Fokker-Planck equation for the probability distribution $P(\boldsymbol{M},t)$ of the magnetization vector $\boldsymbol{M}$ at time $t$. We note that the probability distribution for the molecular spin is conserved for all $t$, $\int \mathrm{d}\boldsymbol{M}\, f(\boldsymbol{M},t) = 1$. Hence, we can write a continuity equation for the probability distribution,

$$\partial_t f(\boldsymbol{M},t) + \partial_{\boldsymbol{M}} \cdot \Big(\dot{\boldsymbol{M}}\, f(\boldsymbol{M},t)\Big) = 0. \tag{5.38}$$

Inserting Eq. (5.19) for $\dot{\boldsymbol{M}}$ we get

$$\partial_t f(\boldsymbol{M},t) = -L\, f(\boldsymbol{M},t) - \partial_{\boldsymbol{M}} \cdot (\alpha \boldsymbol{\xi}(t) f(\boldsymbol{M},t))\,, \tag{5.39}$$

where $\boldsymbol{\xi}(t) = \boldsymbol{M} \times \boldsymbol{\delta\mathcal{B}}$ and the differential operator $L$ is defined via its action on the function $f(\boldsymbol{M},t)$ as

$$L\, f = \partial_{\boldsymbol{M}} \cdot \Big(\alpha \boldsymbol{M} \times \Big[-\partial_{\boldsymbol{M}} U - J\boldsymbol{s}^0 - \gamma^s \dot{\boldsymbol{M}}\Big]\, f\Big)\,. \tag{5.40}$$

From this follows the implicit solution

$$f(\boldsymbol{M},t) = e^{-tL} f(\boldsymbol{M},0) - \int_0^t \mathrm{d}t'\, \mathrm{e}^{-(t-t')L} \partial_{\boldsymbol{M}} \cdot \big(\boldsymbol{\xi}(t')\, f(\boldsymbol{M},t')\big)\,. \tag{5.41}$$

Inserting this again in Eq. (5.39) and averaging over noise, denoted by $P(\boldsymbol{M},t) = \langle f(\boldsymbol{M},t)\rangle$, yields the Fokker-Planck equation

$$\partial_t P(\boldsymbol{M},t) = -L\, P(\boldsymbol{M},t) + \frac{1}{2}\partial_{\boldsymbol{M}} \cdot (\alpha^2 \tilde{\boldsymbol{D}}) \cdot \partial_{\boldsymbol{M}} P(\boldsymbol{M},t) = F\, P(\boldsymbol{M},t). \tag{5.42}$$

Here we use that the noise is Gaussian and delta-function correlated, $\langle \xi_k(t)\xi_l(t')\rangle = \tilde{D}_{kl}\delta(t-t')$ and introduce the Fokker-Planck operator $F$.

In the uniaxial situation under consideration, the probability distribution is independent of $\varphi$ and depends on the angle $\vartheta$ only. Therefore, the Fokker-Planck equation (5.42) takes the particularly simple form

$$\partial_t P(\vartheta,t) = \frac{1}{\sin\vartheta}\partial_\vartheta \sin\vartheta \mathrm{e}^{-\tilde{V}(\vartheta)} \partial_\vartheta \mathrm{e}^{\tilde{V}(\vartheta)} \tilde{\beta}(\vartheta)\, P(\vartheta,t). \tag{5.43}$$

This equation has the stationary solution $P(\vartheta)_{\mathrm{stat}} \propto \exp[-\tilde{V}(\vartheta)]/\tilde{\beta}$. Here we have introduced

$$\tilde{\beta}(\vartheta) = \frac{\alpha^2 \tilde{D}^1/2}{1 + \alpha^2 M^2 \gamma^{s,1}\left(\gamma^{s,1} + \gamma^{s,2}\sin^2\vartheta\right)}, \tag{5.44}$$

and

$$\tilde{V}(\vartheta) = \int^\vartheta \mathrm{d}\vartheta'\, \frac{\partial_{\vartheta'} U + M s_z J \sin\vartheta'}{\tilde{D}^1/(2\gamma^{s,1})}. \tag{5.45}$$

As long as the anisotropy is sufficiently large, $U(\vartheta)$ has a minimum $U_1$ at $\vartheta = \vartheta_1 = 0$, another minimum $U_2$ at $\vartheta = \vartheta_2 = \pi$, and a maximum $U_m$ at $\vartheta = \vartheta_\mathrm{m}$ with $0 < \vartheta_\mathrm{m} < \pi$. We assume that this holds also for $\tilde{V}(\vartheta)$ and visualize the dependence of $\tilde{V}(\vartheta)$ on gate and bias voltage in Fig. 5.6. One clearly sees that the difference between the values of $\tilde{V}$ at the minima and the maximum decreases with increasing bias voltage, as one expects from the behavior of fluctuations and damping, cp. Fig. 5.4.

Note that in equilibrium the ratio $\tilde{D}^1/(2\gamma^{s,1}) = T$, as dictated by the fluctuation-dissipation theorem. For zero temperature but finite bias voltages $V$ it is sometimes instructive to interpret this ratio as an effective temperature in each potential well, $T_\mathrm{eff} \simeq \tilde{D}^1/(2\gamma^{s,1})$ (as done for instance in the works by Mozyrsky *et al.* [2006], Pistolesi *et al.* [2008] and Núñez and Duine [2008]), see Fig. 5.4. Generally however, both coefficients, $\tilde{D}^1$ and $\gamma^{s,1}$ are angle dependent and non trivial functions of voltage, as we have seen explicitly above.

### 5.5.2. Switching rates

We calculate how long the molecular spin remains on one half of the Bloch sphere. The mean time $\tau_{ij}$ between passing the energy barrier (from the minimum $U_i$ to $U_j$) due to the interaction with the electrons is then found by a standard procedure [Zwanzig, 2001]. We consider the distribution $P(\boldsymbol{M}, t)$ of $\boldsymbol{M}$ which have been at $\boldsymbol{M}_0$ at time $t = 0$ and are inside a given volume at time $t$. The mean first passage time is then given by

$$\tau(\boldsymbol{M}_0) = \int \mathrm{d}t\, t \int \mathrm{d}\boldsymbol{M} \frac{-\mathrm{d}P(\boldsymbol{M}, t)}{\mathrm{d}t}, \tag{5.46}$$

where $-\int \mathrm{d}\boldsymbol{M}\mathrm{d}P(\boldsymbol{M}, t)/\mathrm{d}t$ is the distribution of first passage times and $\int \mathrm{d}\boldsymbol{M}P(\boldsymbol{M}, t)$ gives the number of $\boldsymbol{M}$ which are still in the volume of consideration at time $t$. The distribution of $\boldsymbol{M}$ is $P(\boldsymbol{M}, t) = \mathrm{e}^{tF}\delta(\boldsymbol{M} - \boldsymbol{M}_0)$ with $P(\boldsymbol{M}, t) = 0$ when $\boldsymbol{M}$ is at the boundary of the volume. Inserting this into Eq. (5.46) yields

$$\tau(\boldsymbol{M}_0) = \int \mathrm{d}t \int \mathrm{d}\boldsymbol{M} \mathrm{e}^{tF}\delta(\boldsymbol{M} - \boldsymbol{M}_0) = \int \mathrm{d}t \mathrm{e}^{tF^\dagger} 1, \tag{5.47}$$

where we have integrated by parts and $F^\dagger$ denotes the adjoint Fokker Planck operator. Hence we obtain the differential equation

$$F^\dagger \tau(\boldsymbol{M}) = -1 \tag{5.48}$$

for the mean first passage time with an absorbing boundary condition. Accordingly, we consider an adjoint equation to Eq. (5.43),

$$\frac{\tilde{\beta}(\vartheta)}{\sin\vartheta} \mathrm{e}^{\tilde{V}(\vartheta)} \partial_\vartheta \mathrm{e}^{-\tilde{V}(\vartheta)} \sin\vartheta \partial_\vartheta\, \tau_{ij}(\vartheta) = -1/2, \tag{5.49}$$

with an absorbing boundary condition $\tau_{ij}(\vartheta_m) = 0$. The factor $1/2$ takes into account that it is equally likely to go to $\vartheta \gtrless \vartheta_\mathrm{m}$ at $\vartheta = \vartheta_\mathrm{m}$. Solving the equation yields

$$\tau_{12}(\vartheta) = 2 \int_\vartheta^{\vartheta_m} \mathrm{d}\vartheta' \frac{\mathrm{e}^{\tilde{V}(\vartheta')}}{\sin\vartheta'} \int_{\vartheta_1}^{\vartheta'} \mathrm{d}\vartheta'' \frac{\sin\vartheta''}{\tilde{\beta}(\vartheta'')} \mathrm{e}^{-\tilde{V}(\vartheta'')} \tag{5.50}$$

for passing from $\vartheta < \vartheta_m$ to $\vartheta > \vartheta_m$ and an analogous expression for the opposite process.

When the potential minima are well separated and the fluctuations are small, we can give an analytical expression for the switching rate. In this limit, the integrals in (5.50) can be evaluated by saddle-point integration (see Brown [1963] for the situation in which the coefficients do not depend on $\vartheta$), yielding

$$\frac{1}{\tau_{ij}} \simeq \frac{1}{\sqrt{2\pi}} \sin\vartheta_m \sqrt{|\tilde{V}''(\vartheta_m)|}\tilde{\beta}(\vartheta_i)\tilde{V}''(\vartheta_i)\mathrm{e}^{-[\tilde{V}(\vartheta_m)-\tilde{V}(\vartheta_i)]}. \tag{5.51}$$

Hence, the rate depends exponentially on the difference between $\tilde{V}$ evaluated at its maximum and minimum, respectively, so that it can be tuned by varying bias voltage and gate potential. The general behavior of $1/\tau_{ij}$, as given by Eq. (5.50), is shown in Fig. 5.6 for typical values as a function of gate and bias voltages. We have discussed above that the fluctuations increase with the number of levels in the current window. This is also reflected in the fluctuation induced transition rates which increase with the bias voltage accordingly.

### 5.5.3. Current

The current through lead $\alpha$ is given by the change of the number of particles in the lead times the electronic charge, $I_\alpha = -\mathrm{i}e\langle\left[H, \sum_{k_\alpha,\sigma} c^\dagger_{k_\alpha,\sigma} c_{k_\alpha,\sigma}\right]\rangle$. In the adiabatic limit this is given by Eq. (3.55), as discussed in Section 3.4. We note that $I_L = -I_R = I/2$ and assume symmetric coupling to the leads, $\Gamma_L = \Gamma_R = \Gamma/2$. Then we obtain, by inserting the expressions for the Green's functions and the self-energies, see Appendix B.1, after straightforward algebra

$$I = \frac{e}{4\pi}\Gamma \sum_{\pm} \left[\arctan\left(\frac{\mu_L - \tilde{\epsilon} \mp b}{\Gamma/2}\right) - \arctan\left(\frac{\mu_R - \tilde{\epsilon} \mp b}{\Gamma/2}\right)\right], \tag{5.52}$$

which is valid at zero temperature. As discussed above, the electronic level splits due to the interaction with the effective magnetic field $\boldsymbol{b}$, defined in Eq. (5.8). When this level splitting is larger than the level broadening $\Gamma$, the current increases as the number of levels in the transport window increases, see Fig. 5.2. This is reflected in peaks of the differential conductance $\mathrm{d}I/\mathrm{d}V$ as a function of gate and bias voltage. Note that the splitting of the electronic levels and thus the number of levels in the transport window depends on the molecular spin orientation since $b = b(\vartheta)$. As a consequence, the current is also a function of $\vartheta$ and the corresponding current-voltage characteristics are shown in Fig. 5.7. In principle, this allows one to read out the molecular switch via current measurements.

## 5.6. Spin-torque-induced switching with polarized leads

The switching mechanism discussed in the previous section originates in fluctuations of the molecular magnetic moment, introduced by the coupling to the itinerant electrons.

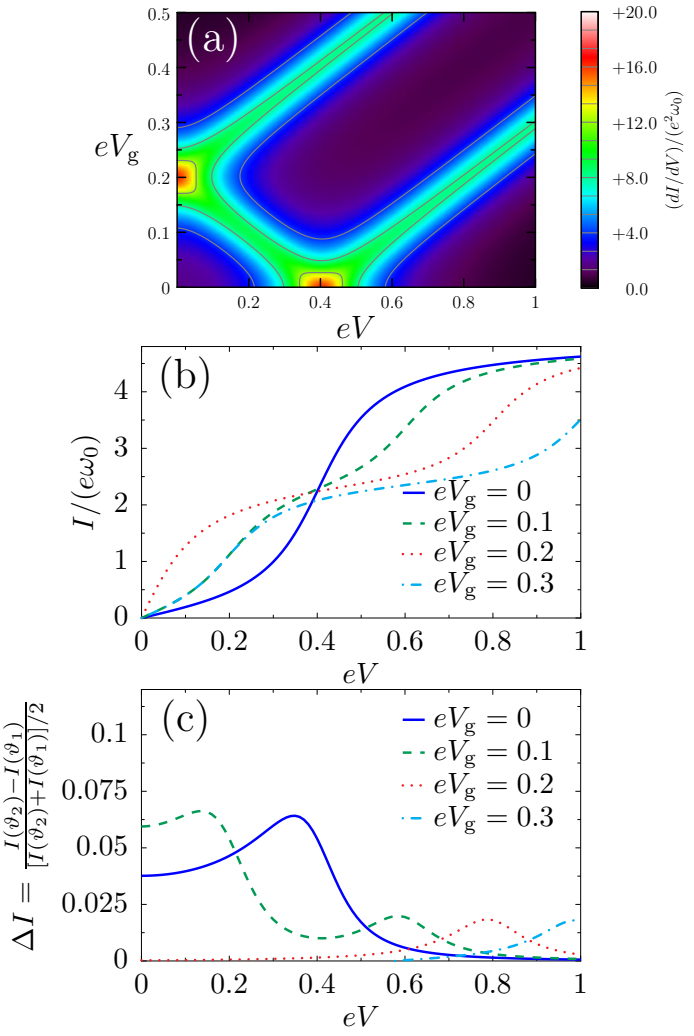


Figure 5.7. Current-voltage characteristics. (a) The differential conductance $\mathrm{d}I/\mathrm{d}V$ is peaked when the number of levels in the current window changes at $V_g \pm eV/2 = \pm b$. (b) Obviously, the current changes when the number of level with energy between the chemical potentials of the two leads changes. (c) The level splitting $2b(\vartheta)$ depends on the orientation of the molecular spin. The relative difference of the current evaluated at the two potential minima is plotted as a function of the bias voltage. [(a) and (b) are evaluated at $\vartheta = 0$. The plots are obtained with the same parameters as in Fig. 5.3 and all energies are measured in units of the barrier height without magnetic field $DM^2$.]

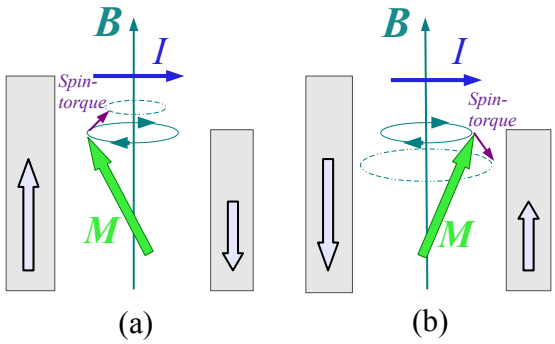


Figure 5.8. Sketch of the effect of polarized leads inducing spin-torque-transfer (indicated by the magenta arrow) on the molecular moment. Depending on the polarization and the current, the spin-torque tends to align the molecular moment either (a) along or (b) against the magnetic field.

In Section 5.3 we have seen that the presence of polarized leads opens the possibility of negative Gilbert damping which could favor the switching of the molecular spin. This mechanism strongly depends on the details of the system, like the value of the mean chemical potential $\mu$ and the applied bias voltage. However, for spin-polarized leads, switching of the molecular moment under general non-equilibrium conditions will typically be dominated by a different mechanism which is driven by the non-conservative (or spin-transfer) torque exerted by the coupling to the current carrying electrons. This term appears already in leading order of the Born-Oppenheimer approximation in which Gilbert damping and fluctuations can be neglected.

In this section we focus on this spin-torque $-Js_t(\hat{\mathbf{e}}_z \times \hat{\boldsymbol{M}})$, see Eq. (5.27), in the Landau-Lifshitz-Gilbert equation (5.19), where $s_t$ is given by Eq. (5.29). We analyze under which microscopic conditions it is expected to drive switching in our molecular setup. In the present case it is clear that it moves the vector $\boldsymbol{M}$ along the azimuthal direction, tending to align it along the magnetic field. Thus, given a tilted molecular magnetic moment $\boldsymbol{M}$ precessing around the magnetic field, for $s_t < 0$ the spin torque induces a spiral trajectory moving $\boldsymbol{M}$ toward orbits of smaller radius around the magnetic field. Instead, for $s_t > 0$ it induces orbits of larger radius enabling the switching to the opposite hemisphere, with $\boldsymbol{M}$ tending to align opposite to the external magnetic field.

In our model, the behavior of $s_t$ can be rather easily analyzed in the limit of completely polarized leads, *e.g.*, $\Gamma_L^{\uparrow} = \Gamma_R^{\downarrow} = \Gamma/2$. In this limit Eq. (5.29) simplifies to

$$s_t = -\frac{J\Gamma^2}{4\pi M} \int \mathrm{d}\epsilon \frac{f_L - f_R}{\prod_{\pm} [(\epsilon - \tilde{\epsilon} \pm b)^2 + (\Gamma/2)^2]}. \tag{5.53}$$

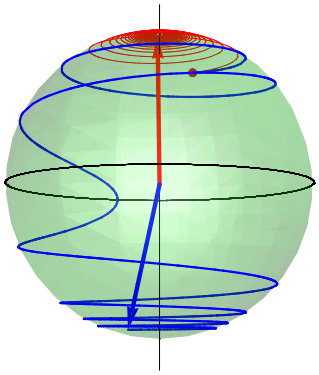

Figure 5.9. Motion of the molecular moment in the presence of spin-polarized leads. For negative bias voltage $eV = -0.4$, the magnetic moment is driven toward the positive $z$-axis (red curve) while inverting the voltage $eV \to -eV$ causes a flip of the magnetic moment (blue curve). (We consider $\Gamma_L^\uparrow = \Gamma_R^\downarrow = 0.1$, $\Gamma_L^\downarrow = \Gamma_R^\uparrow = 0$ and $eV_g = 0$; the other parameters are the same as in Fig. 5.3.)

More generally, the sign of $s_t$ is determined by the condition

$$\mathrm{sgn}[s_t] = \mathrm{sgn}\left[\left(\Gamma_L^\downarrow\Gamma_R^\uparrow - \Gamma_L^\uparrow\Gamma_R^\downarrow\right)(f_L - f_R)\right]. \tag{5.54}$$

This is sketched in Fig. 5.8. When we consider a left lead with spin-up polarized electrons and $\Gamma_L^\uparrow\Gamma_R^\downarrow > \Gamma_L^\downarrow\Gamma_R^\uparrow$, a current flowing from left to right ($\mu_L > \mu_R$) results in $s_t < 0$ and thus antialignment of magnetic moment and magnetic field. For the opposite spin-polarization, the spin-torque tends to align the magnetic moment with the magnetic field.

For a given spin-polarization, inverting the direction of the current can switch the orientation of the magnetic moment in the same way. This is studied by solving numerically the equation of motion for the molecular spin in the strictly adiabatic limit, hence neglecting Gilbert damping and fluctuations, in the presence of strongly polarized leads. In Fig. 5.9 we show the time evolution of the molecular spin initially slightly deviating from the magnetic field axis for two different voltages. Clearly, the motion of the molecular spin is determined by the direction of the current through the molecule, showing that inverting the bias voltage causes spin-flips in this setup.

## 5.7. Summary

We have applied the formalism of current-induced forces, discussed in Chapter 3, to an anisotropic magnetic molecule in a single-molecule junction in which conduction electrons couple via exchange to the localized magnetic moment.

The features of the current-induced torques allow us to use the anisotropic magnetic molecule in an external magnetic field as a molecular switch. The read-out of the latter can be accomplished via the backaction of the molecular spin on the transport current. When the molecule is attached to metallic leads in a uniaxial setup, we have transformed the Langevin equation into a Fokker-Planck equation allowing us to calculate the switching rates between the two stable spin orientations. Transitions between these states are driven by the fluctuations which we have analyzed – in addition to the mean torque, damping, and the current – as a function of the applied gate and bias voltages and the orientation of the molecular spin. In the presence of spin-polarized leads, the switching dynamics is dominated by the non-conservative (spin-transfer) part of the current-induced torque, which enables switching between the spin orientations by reversing the direction of the electronic current.

# 6. Cooling NEMS by current

In this chapter we investigate how the coupling of coherent electrons to vibrational modes can provide the functionality of a refrigerator. To this purpose, we analyze the phonon population in a nanomechanical resonator under the influence of an electronic current.

In the preceding chapters we have seen that when more than one electronic level is coupled to reservoirs, the interplay between collective degrees of freedom and conduction electrons can lead to an interesting exchange of energy between the subsystems. Here we focus on the situation sketched in Fig. 6.1, in which the electronic levels are tuned such that electron transport is preferentially accompanied by the absorption of phonons, yielding the possibility of refrigerating a NEMS by transport currents. We consider a generic model of a double quantum dot connected to electronic reservoirs and make several simplifying assumptions to allow for detailed analytical results. First, we assume that the hopping amplitude between the dots depends on the oscillator coordinate and that this is the only process in which phonons are involved. This situation might be realized in experiments on suspended carbon nanotubes, in which the suspended section remains far from the contacts to the leads. Second, we assume weak tunneling between the two dots.

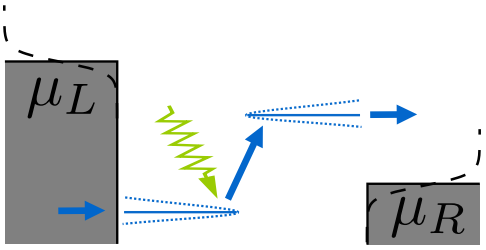


Figure 6.1. Alignment of electronic levels favoring the absorption of phonons.

With these simplifications, analytical expressions for the rates of emission and absorption of phonons can be obtained by perturbation theory. Specifically, this allows one to obtain the non-equilibrium phonon distribution from a simple rate equation. Our goal is to analyze the limitations on refrigeration imposed by the temperature of the electronic reservoirs as well as the heat bath to which the oscillator is coupled. We study how the phonon population can be tuned by external gate and bias voltages. We consider both the limit of weak and strong electron-phonon interaction. In the latter case, multi-phonon processes have to be considered which strongly affect the cooling dynamics. Here we focus on the regime in which the vibrational frequency is large compared to the coupling between quantum dots and leads. The opposite regime of a slow oscillator remains an interesting problem for future work. In fact, it is an interesting aspect of our model that it allows one to access the regimes of both fast and slow vibrations within the same analytical approach.

Utilizing electron-phonon coupling for the construction of a nanoscale refrigerator has already been studied in a number of works. In particular, cooling nanomechanical system

into the quantum ground state has attracted much attention, see [Clerk, 2012] for an overview of recent works. *Micrometer-scale refrigerators* have been reviewed by Muhonen *et al.* [2012]. It has been demonstrated experimentally that a 2DEG which is connected to two quantum dots can be cooled by a current when bias and gate voltages are tuned properly [Prance *et al.*, 2009]. Cooling nanomechanical systems which are coupled to superconducting single-electron transistors has been studied in [Naik *et al.*, 2006]. For the theoretical description of refrigerators rate equations have been used. For instance an adatom on a wire [McEniry *et al.*, 2009] or the generic model of a single electronic level coupled to an oscillator mode [Pistolesi, 2009] have been studied. More general situations have been considered in a number of model systems by Galperin *et al.* [2009], relying on non-trivial structures of the density of states to which the mechanical system is coupled. Cooling of a carbon nanotube, which hosts two quantum dots, has been studied by Zippilli *et al.* [2009, 2010].

The remainder of this chapter is organized as follows. The Hamiltonian and the description of cooling in terms of a rate equation is considered in Section 6.1. In Section 6.2 we calculate the transition rates for emission and absorption of phonons. Equipped with this knowledge we solve the rate equations in limiting cases and discuss the conditions for cooling in Section 6.3.

This chapter is based on unpublished results [Bode *et al.*, 2012b].

## 6.1. Model

We consider two quantum dots which are coupled to electronic reservoirs as depicted in Fig. 6.1. We describe this setup by the Hamiltonian

$$H = \sum_{\alpha=L,R} (H_\alpha + H_{c,\alpha} + E_\alpha d_\alpha^\dagger d_\alpha) + H_T, \tag{6.1}$$

which consists of two dots with energies $E_L$ and $E_R$ in contact to reservoirs modeled by free-electron Hamiltonians

$$H_\alpha = \sum_{k_\alpha} \epsilon_{k_\alpha} c_{k_\alpha}^\dagger c_{k_\alpha}. \tag{6.2}$$

Tunneling between leads and quantum dots is described by

$$H_{c,\alpha} = \sum_{k_\alpha} w_{k_\alpha} c_{k_\alpha}^\dagger d_\alpha + \text{h.c.}\,, \tag{6.3}$$

as we have discussed in Section 2.2.3. The two dots are connected through the tunnel Hamiltonian

$$H_T = t(\hat{x}) d_L^\dagger d_R + \text{h.c.}\,, \tag{6.4}$$

with a tunneling matrix element $t(\hat{x})$. We assume that this tunneling amplitude depends on the vibrational coordinate, providing the electron-vibron coupling to phonons with energy $\omega$. This electron-phonon coupling is represented by $t(\hat{x}) = t\mathrm{e}^{-\lambda\hat{x}}$. Here the

(dimensionless) oscillator coordinate is expressed in terms of phononic creation and annihilation operators, $\hat{x} = \hat{a} + \hat{a}^\dagger$, and $\lambda$ denotes the strength of the coupling between electrons and phonons.

Neglecting the coupling between the two dots, the levels of dot $\alpha$ are hybridized with the corresponding lead. This hybridization can be described along the same lines as we have outlined in Section 2.2.3, and the (retarded) Green's function of the dot becomes

$$G_\alpha^{0R}(\varepsilon) = \frac{1}{\varepsilon - E_\alpha - \Sigma_\alpha^{0R}(\varepsilon)}, \tag{6.5}$$

with the self-energy $\Sigma_\alpha^{0R}(\varepsilon) = \sum_{k_\alpha} |w_{k_\alpha}|^2 g_{k_\alpha}^R(\varepsilon)$. Here the free Green's function of lead $\alpha$ is given by $g_{k_\alpha}^R(\varepsilon) = 1/(\varepsilon - \varepsilon_{k_\alpha} + \mathrm{i}\eta)$, cp. Eq. (2.42). In the wide-band limit, the self-energy reads $\Sigma_\alpha^{0R}(\varepsilon) \simeq \mathrm{Re}[\Sigma_\alpha^0] - \mathrm{i}\Gamma_\alpha/2$, so that the local density of states, $\rho_\alpha(\varepsilon) = -\mathrm{Im}[G_\alpha^{0R}(\varepsilon)]/\pi$, becomes

$$\rho_\alpha(\varepsilon) = \frac{\Gamma_\alpha}{2\pi[(\varepsilon - \epsilon_\alpha)^2 + (\Gamma_\alpha/2)^2]}, \tag{6.6}$$

with the shorthand $\epsilon_\alpha = E_\alpha + \mathrm{Re}[\Sigma_\alpha^{0R}]$.

Now we can include the coupling between the dots. In the basis of the (hybridized) dots, the occupation of dot $\alpha$ changes as $\langle \dot{N}_\alpha \rangle = -\mathrm{i}\langle t(\hat{x})\, d_\alpha^\dagger(t) d_\beta(t)\rangle + \mathrm{h.c.}|_{\alpha\neq\beta}$, with $N_\alpha = d_\alpha^\dagger d_\alpha$. To lowest order in $t$ we obtain, analogous to Eq. (2.53),

$$\langle \dot{N}_\alpha \rangle = \sum_{nn'} P_n \left( W_{\beta\alpha}^{n\to n'} - W_{\alpha\beta}^{n\to n'} \right), \tag{6.7}$$

where $P_n$ is the probability for the oscillator to be in its $n$th excited state. Here we have identified the rates for transitions between dots $\alpha$ and $\beta$ accompanied by a change of the phonon population from $n$ to $n'$ as

$$W_{\alpha\beta}^{n\to n'} = |M_{n\to n'}|^2 |t|^2 I_{\alpha\beta}^{n\to n'}, \tag{6.8}$$

with the matrix elements $M_{n\to n'} = \langle n'|e^{-\lambda\hat{x}}|n\rangle$ and the abbreviations

$$I_{\alpha\beta}^{n\to n} = 2\pi \int \mathrm{d}\epsilon f_\alpha(\epsilon)\,[1 - f_\beta(\epsilon)]\,\rho_\alpha(\epsilon)\rho_\beta(\epsilon), \tag{6.9}$$

$$I_{\alpha\beta}^{n\to n\pm m} = 2\pi \int \mathrm{d}\epsilon f_\alpha(\epsilon)\,[1 - f_\beta(\epsilon \mp m\omega)]\,\rho_\alpha(\epsilon)\rho_\beta(\epsilon \mp m\omega). \tag{6.10}$$

Here the local density of states $\rho$ is given by Eq. (6.6), and $f_\alpha(\epsilon) = 1/\left(\mathrm{e}^{(\epsilon-\mu_\alpha)/T_\mathrm{e}} + 1\right)$ is the Fermi distribution of lead $\alpha$.

Our aim is the analysis of the phonon population. The temporal dynamics of the phonon population can be deduced from the rates which enter the expression for the current in Eq. (6.7). This results in the rate equation

$$\frac{\mathrm{d}P_n}{\mathrm{d}t} = -P_n \sum_{n'} W^{n\to n'} + \sum_{n'} P_{n'} W^{n'\to n} - \frac{1}{\tau}[P_n - P_n^{\mathrm{eq}}], \tag{6.11}$$

where $W^{n\to n'} = \sum_{\alpha\neq\beta} W^{n\to n'}_{\alpha\beta}$ are the rates for a transition from $n$ phonons to $n'$ phonons in the system. Note that to lowest order in the hopping amplitude $t$, within our model transitions always proceed between the two dots, $\beta \neq \alpha$. The last term in Eq. (6.11) is added on phenomenological grounds, describing the relaxation to the equilibrium distribution $P_n^{\mathrm{eq}} = \mathrm{e}^{-n\omega/T}(1-\mathrm{e}^{-\omega/T})$ [Koch *et al.*, 2006], with $T$ the temperature of an additional heat bath that the oscillator is coupled to. In the limit of fast relaxation, $1/\tau \to \infty$, the distribution is fixed to its equilibrium value while in the opposite limit $1/\tau \to 0$ the phonon dynamics is driven entirely by the electron-induced processes.[1]

In particular we are interested in the stationary state of the system so that we will have to solve the equation $\dot{P}_n = 0$.

## 6.2. Transition rates

In this section we analyze the rates $W^{n\to n'}_{\alpha\beta}$ in more detail.

### 6.2.1. Franck-Condon matrix elements

The transition rates given in Eq. (6.8) contain the vibrational Franck-Condon matrix elements for a phonon transition

$$M_{n\to n'} = [\mathrm{sgn}(n'-n)]^{n-n'}\,\lambda^{Q-q}\,\mathrm{e}^{-\lambda^2/2}\sqrt{\frac{q!}{Q!}}L_q^{Q-q}(\lambda^2), \tag{6.12}$$

with the abbreviations $q = \min(n,n')$ and $Q = \max(n,n')$, and $L_m^n(x)$ are generalized Laguerre polynomials. These matrix elements are calculated as the overlap of eigenfunctions belonging to two harmonic oscillators displaced relative to each other by a distance $\sqrt{2}\lambda l_{\mathrm{osc}}$ (with $l_{\mathrm{osc}} = \sqrt{\hbar M\omega}$ the oscillator length), see *e.g.* [Koch *et al.*, 2006].

In the limit of weak electron-phonon coupling, $\lambda \ll 1$, the matrix element is proportional to $\lambda^{Q-q}$, and accordingly single-phonon processes become dominant in changing the phonon population. Then the (square of the) corresponding matrix elements become

$$|M_{n\to n\pm1}|^2 \simeq \max(n, n\pm1)\,\lambda^2, \tag{6.13}$$

which we use particularly in the later discussion.

### 6.2.2. Zero temperature

At zero temperature we can easily evaluate the integrals in Eqs. (6.9) and (6.10) analytically, provided that both electronic levels lie within the current window, $\mu_L > \epsilon_L, \epsilon_R > \mu_R$. We assume that the level broadening $\Gamma$ is small compared to the applied bias voltage so that the electronic levels are not too smeared out.

[1] We note that in principle this description allows us to treat the electronic reservoirs to be at a different temperature $T_{\mathrm{e}}$ than the temperature $T$ of the additional bath coupled to the oscillator. Since we are interested in cooling through a charge current rather than due to coupling to a colder environment, we focus on $T = T_{\mathrm{e}}$.

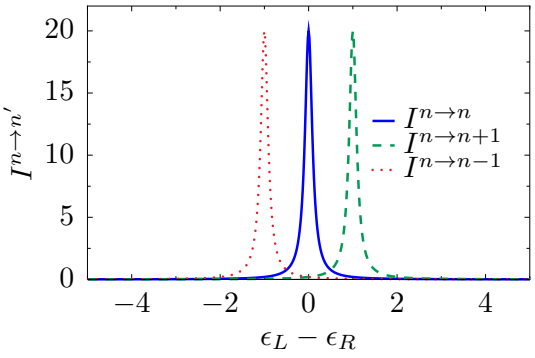


Figure 6.2. Contributions $I^{n\to n,n\pm1}$ to the rates as as function of difference between the electronic levels. Both electronic levels are in the transport window and the level broadening is small. When the levels are aligned one electrons tunnel through the junction without phonon emission or absorption (blue curve). Focusing on single-phonon processes, we see that phonons are preferentially emitted (absorbed) when the left level is $\omega$ above (below) the right level. We plot $I^{n\to n,n\pm1}$ in units of $\omega$ for $eV = 10$, $\epsilon_L$ is varied while $\epsilon_R = V/2$, and $\Gamma = 0.1$.

For processes that do not change the phonon state, we obtain

$$W^{n\to n} \simeq \frac{2\Gamma\,|t|^2}{(\epsilon_L - \epsilon_R)^2 + \Gamma^2}, \tag{6.14}$$

assuming symmetric coupling to the two leads, $\Gamma_L = \Gamma_R = \Gamma$. We also note that $W_{RL}^{n\to n} = 0$. This has been calculated by means of the relation

$$\int_{-\infty}^{\infty} \frac{\mathrm{d}\epsilon}{2\pi} \frac{\Gamma}{[(\epsilon-\epsilon_1)^2 + (\Gamma/2)^2][(\epsilon-\epsilon_2)^2 + (\Gamma/2)^2]} = \frac{2\Gamma}{(\epsilon_1-\epsilon_2)^2 + \Gamma^2}. \tag{6.15}$$

Next we consider rates for which $m\omega < eV$. We start with the process involving a transition from left to right dot while exciting $m$ vibrational quanta. Eq. (6.10) yields

$$\begin{aligned} W_{LR}^{n\to n+m} &= |t|^2 |M_{n\to n+m}|^2 \int \frac{\mathrm{d}\epsilon}{2\pi} \frac{f_L(\epsilon)\,[1 - f_R(\epsilon - m\omega)]\;\Gamma^2}{[(\epsilon-\epsilon_L)^2 + (\Gamma/2)^2]\,[(\epsilon-\epsilon_R-m\omega)^2 + (\Gamma/2)^2]} \\ &\simeq \frac{2\Gamma\,|t|^2 |M_{n\to n+m}|^2}{(\epsilon_L - \epsilon_R - m\omega)^2 + \Gamma^2}, \end{aligned} \tag{6.16}$$

while $W_{RL}^{n\to n+m} = 0$. Similarly we find for the processes with phonon absorption

$$W_{LR}^{n\to n-m} \simeq \frac{2\Gamma\,|t|^2 |M_{n\to n-m}|^2}{(\epsilon_L - \epsilon_R + m\omega)^2 + \Gamma^2}, \tag{6.17}$$

and $W_{RL}^{n\to n-m} = 0$. Typical plots are shown in Fig. 6.2, indicating that the electronic

levels can be tuned such that either emission or absorption of phonons dominates. Thus for $m\omega < eV$ we obtain the transition rates

$$W^{n\to n\pm m} \simeq \frac{2\Gamma\,|M_{n\to n\pm m}|^2|t|^2}{(\epsilon_L - \epsilon_R \mp m\omega)^2 + \Gamma^2}. \tag{6.18}$$

For our purpose of cooling it is optimal to tune the electronic levels such that $\epsilon_R = \epsilon_L + m_0\omega$. Then the expressions above simplify to

$$W^{n\to n\pm m} \simeq \frac{2\Gamma\,|M_{n\to n\pm m}|^2|t|^2}{[(m_0 \mp m)\omega]^2 + \Gamma^2}\,, \quad \text{for} \quad m \neq m_0\,, \tag{6.19}$$

$$W^{n\to n-m_0} \simeq \frac{2\,|M_{n\to n-m_0}|^2|t|^2}{\Gamma}\,, \tag{6.20}$$

for $eV > m\omega$. Cooling requires faster absorption than emission of phonons, $W^{n\to n-m} > W^{n\to n+m}$. Hence, for the resonant process $m = m_0$ at small level broadening, $\Gamma \ll 2m_0\omega$, the rate for absorption is much higher than the one for emission of phonons. Additionally, we note that the emission of phonons, described by the rate $W^{n\to n+m}$, is only possible for $m < eV/\omega$, see Eq. (6.10). In contrast, the number of phonons absorbed in a tunneling event is unlimited. The influence of all these phonon processes crucially depends on the coupling strength between electrons and phonons, encoded in the matrix element $|M_{n\to n\pm m}|^2$. This has to be studied by solving the rate equation, which is what we turn to do in the next section.

### 6.2.3. Finite temperature

The zero temperature results for the transition rates are the main ingredients for our investigation of refrigeration by means of a current. Nevertheless, for small voltages, $V < \omega$, in the limit of weak electron-phonon coupling, the dominant rate $W^{n\to n-1}$ is finite while $W^{n\to n+1} = 0$. Corrections to this are imposed by a finite temperature in the reservoirs which we consider now.

In order to calculate the corrections of the rates above due to a finite temperature in the electronic reservoirs, we introduce the shorthand

$$\Delta I_{\alpha\beta}^{n\to n\pm m}(T_\mathrm{e}) = I_{\alpha\beta}^{n\to n\pm m}(T_\mathrm{e}) - I_{\alpha\beta}^{n\to n\pm m}(0). \tag{6.21}$$

For the calculation of this correction we make use of the Sommerfeld expansion,

$$\int_\infty^{+\infty} \mathrm{d}\epsilon f_\alpha(\epsilon)\mathcal{F}(\epsilon) \simeq \int_\infty^{\mu_\alpha} \mathrm{d}\epsilon\mathcal{F}(\epsilon) + \frac{\pi^2}{6}T_\mathrm{e}^2\partial_\epsilon\mathcal{F}(\epsilon)|_{\epsilon=\mu_\alpha}\,, \tag{6.22}$$

in the limit $\mu_\alpha \ll T_\mathrm{e}$ for a function $\mathcal{F}(\epsilon)$ which vanishes sufficiently fast for $\epsilon \to \pm\infty$. Applying this prescription to Eq. (6.10) yields

$$\begin{aligned}
&\Delta I_{\alpha\beta}^{n\to n\pm m}(T_\mathrm{e}) \\
&\simeq +2\pi\frac{\pi^2}{6}T_\mathrm{e}^2\Big\{\partial_\epsilon[\rho_\alpha(\epsilon)\rho_\beta(\epsilon\mp m\omega)]|_{\mu_\alpha} - f_\alpha(\mu_\beta \pm m\omega)\partial_\epsilon[\rho_\alpha(\epsilon)\rho_\beta(\epsilon\mp m\omega)]|_{\mu_\beta\pm m\omega} \\
&\quad - \partial_\epsilon f_\alpha(\epsilon)|_{\mu_\beta\pm m\omega}\rho_\alpha(\mu_\beta \pm m\omega)\rho_\beta(\mu_\beta)\Big\},
\end{aligned} \tag{6.23}$$

using the relation $f_\alpha(\epsilon)[1-f_\alpha(\epsilon)] = -T_\mathrm{e}\partial_\epsilon f_\alpha(\epsilon)$.

As stated above, for weak electron-phonon coupling we obtain for small voltages, $V < m\omega$, that the rates for absorption of single phonons are finite while heating is completely absent, $I^{n\to n+1}(0) = 0$, see Eqs. (6.10) and (6.20). Accordingly, here the influence of temperature corrections should be most important. We restrict the following discussion of finite temperatures to single-phonon processes. In particular, we assume the two levels $\epsilon_L < \mu_L$ and $\epsilon_R > \mu_R$ are at resonance, $\epsilon_R = \epsilon_L + \omega$. Thus it is sufficient to focus on the two resonant processes $I_{RL}^{n\to n+1}$ and $I_{LR}^{n\to n-1}$. We obtain in the limit $|\mu_\alpha - \epsilon_\alpha| \gg \Gamma/2$

$$\Delta I_{RL}^{n\to n+1}(T_\mathrm{e}) \simeq \frac{\pi\Gamma^2 T_\mathrm{e}^2}{12}\Big\{\frac{4}{(\epsilon_R-\mu_R)^5} + \frac{4f_R(\mu_L+\omega)}{(\mu_L-\epsilon_L)^5} + \frac{f_R(1-f_R)|_{\mu_L+\omega}}{T_\mathrm{e}(\mu_L-\epsilon_L)^4}\Big\}. \tag{6.24}$$

Assuming small temperatures, $T_\mathrm{e} < eV + \omega$, this simplifies to

$$\Delta I_{RL}^{n\to n+1}(T_\mathrm{e}) \simeq +\frac{\pi}{3}\frac{\Gamma^2 T_\mathrm{e}^2}{(\epsilon_R-\mu_R)^5}. \tag{6.25}$$

In the same limit, the correction to the cooling rates becomes similarly

$$\Delta I_{LR}^{n\to n-1}(T_\mathrm{e}) \simeq -\frac{\pi}{3}\left(\frac{\Gamma^2 T_\mathrm{e}^2}{(\mu_L-\epsilon_L)^5} + \frac{\Gamma^2 T_\mathrm{e}^2}{(\epsilon_R-\mu_R)^5}\right), \tag{6.26}$$

which is also quadratic in the temperature. We discuss these results below, after solving the rate equation.

## 6.3. Solving the rate equation

In the limit of small electron-phonon coupling, $\lambda \ll 1$, we can focus on single phonon processes, $W^{n\to n\pm1}$, and the rate equation can be easily solved analytically. In this limit electrons and phonons couple linearly and the rates for emission and absorption of phonons, see Eqs. (6.8) and (6.13), are given by

$$W^{n\to n\pm1} \simeq \max(n, n\pm1)\,\lambda^2|t|^2 I^\pm, \tag{6.27}$$

using the abbreviation $I^\pm = I^{n\to n\pm1}$. With this restriction the rate equation (6.11) simplifies considerably and becomes

$$\begin{aligned}\frac{\mathrm{d}P_n}{\mathrm{d}t} =& -\left(W^{n\to n+1} + W^{n\to n-1}\right)P_n + W^{n+1\to n}P_{n+1} \\ &+ W^{n-1\to n}P_{n-1} - \frac{1}{\tau}\left(P_n - P_n^\mathrm{eq}\right).\end{aligned} \tag{6.28}$$

Here we note that only the rates involving phonon processes, $W^{n\to(n'\neq n)}$, enter.

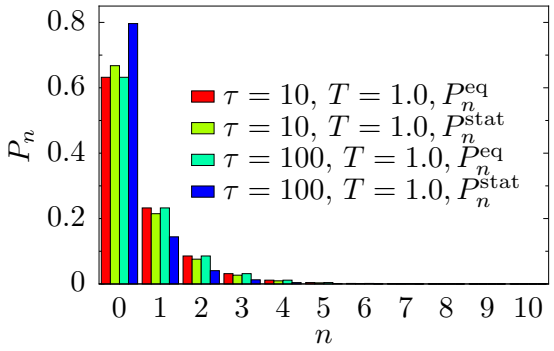


Figure 6.3. Population of the states $P_n^{\rm stat}$ in comparison with $P_n^{\rm eq}$. For large $\tau$ the population of the ground state $P_0$ increases. We consider different temperatures (of the uncoupled oscillator) $T$ and equilibration rates $1/\tau$ (in units of $\omega$), for $I^+/I^- = 0.1$ and $\lambda = 0.1$ (justifying that only transitions $n \to n \pm 1$ are considered). The states $P_0, P_1, ..., P_{10}$ are included in the simulation. We approximate that only the rates $W^{n\to n\pm1}$ are non-vanishing.

### 6.3.1. Analytical solution

From this rate equation we obtain for the average phonon number, $\overline{n} = \sum_n nP_n$, that

$$\dot{\overline{n}} = -\left[\lambda^2|t|^2(I^- - I^+) + 1/\tau\right]\overline{n} + \lambda^2|t|^2 I^+ + \overline{n}^{\rm eq}/\tau, \tag{6.29}$$

where $\overline{n}^{\rm eq} = \left(\mathrm{e}^{\beta\omega} - 1\right)^{-1}$. Far from equilibrium, $1/\tau \to 0$, the stationary solution of this equation is given by

$$\overline{n}_0 = \frac{I^+}{I^- - I^+}, \tag{6.30}$$

provided that $I^- > I^+$. Generally, for a positive cooling rate (meaning that $\lambda^2|t|^2[I^- - I^+] + 1/\tau > 0$), the stationary solution is given by

$$\overline{n}^{\rm stat} = \frac{\lambda^2|t|^2 I^+ + \overline{n}^{\rm eq}/\tau}{\lambda^2|t|^2(I^- - I^+) + 1/\tau} \simeq \overline{n}_0 + \frac{\overline{n}^{\rm eq} - \overline{n}_0}{\tau\lambda^2|t|^2\,(I^- - I^+)}, \tag{6.31}$$

cp. for instance [Zippilli *et al.*, 2009]. Here the last approximation holds when the electron-induced cooling dominates over the relaxation to equilibrium, $\lambda^2|t|^2\,(I^- - I^+) \gg 1/\tau$. In order to cool the system, *i.e.* $\overline{n}^{\rm stat} < \overline{n}^{\rm eq}$, it is necessary that $\overline{n}_0 < \overline{n}^{\rm eq}$. From this condition one can conclude at what temperatures (of the electrons in the leads and the oscillator) cooling is possible. A system with general $\lambda$ can be studied by searching numerically for the stationary solution of the rate equation Eq. (6.11). Results are shown in Fig. 6.3: depending on the initial temperature of the oscillator and the relaxation rate it is possible to remove phonons from the system, so that the occupation of the vibrational ground state becomes more likely.

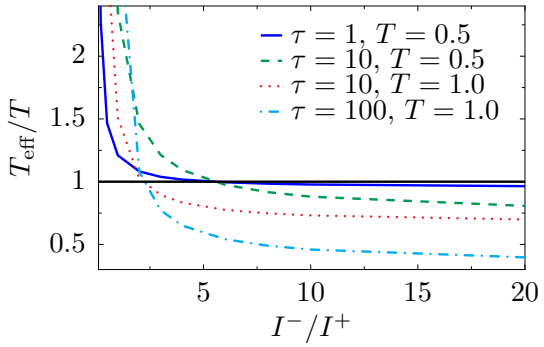


Figure 6.4. Effective temperature as a function of the ratio between the rates for absorption and emission of a phonon, see Eq. (6.8). We consider different temperatures (of the uncoupled oscillator) $T$ and equilibration rates $1/\tau$ and $I^{n\to n-1} = 1$ (in units of $\omega$), and $\lambda = 0.1$ (note that only transitions $n \to n \pm 1$ are considered). The states $P_0, P_1, ..., P_{10}$ are included in the simulation.

In order quantify this cooling it is useful to define an effective temperature of the electromechanical refrigerator. We note that the average phonon energy is always, also out-of equilibrium, a well-defined quantity, given by $E_{\rm av} = \omega \sum_n n P_n$. In equilibrium one has $E_{\rm av} = \omega/(\mathrm{e}^{\beta\omega} - 1)$ with $1/\beta = T$. Accordingly, the effective temperature of a non-equilibrium system can be defined as

$$T_{\rm eff} = \omega/\ln(1 + 1/\overline{n}^{\rm stat}), \tag{6.32}$$

see, *e.g.*, [Pistolesi, 2009]. In Fig. 6.4 we show at which cooling rates it is possible to obtain temperature $T_{\rm eff} < T$, depending on the relaxation towards equilibrium.

### 6.3.2. Small voltages

At small voltages, $eV < \omega$, heating processes are strongly suppressed[2] which is optimal for a refrigerator. We consider $\lambda \ll 1$, so that only the rates $W^{n\to n\pm1}$ have to be included and we focus on the resonant situation, $\epsilon_L = \epsilon_R - \omega$. For $eV < \omega$, we have seen above that $W^{n\to n-1}$ is finite while the heating rate is absent, $W^{n\to n+1} = 0$, for zero electronic temperature in the reservoirs. Then the average phonon population becomes

$$\overline{n}^{\rm stat} \simeq \frac{\Gamma}{2\tau\lambda^2|t|^2}\overline{n}^{\rm eq}, \tag{6.33}$$

as given by Eq. (6.31), with $\overline{n}_0 = 0$. Note that, since we consider the limit of small $\lambda$, this equation indicates that the level broadenig $\Gamma$ and the equilibrium towards equilbrium, given by $1/\tau$, have to be small compared to the hopping amplitude in order to achieve a phonon population which is smaller than $\overline{n}^{\rm eq}$. Note that our approach requires a current

[2] Electronic heating rates are suppressed in powers of $\Gamma/\omega$ so that we assume that they are slow compared to the phonon absorption processes.

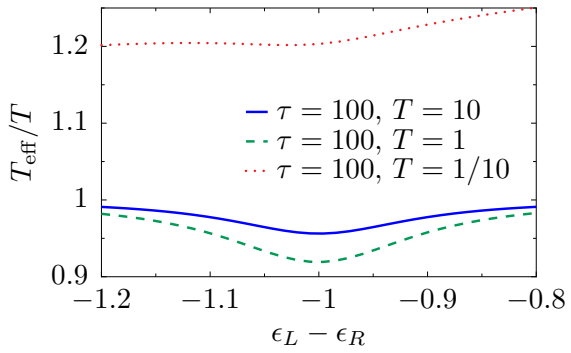


Figure 6.5. Effective temperature as a function of the difference between the electronic levels for different temperatures and relaxation rates. When the levels are tuned such that the absorption of phonons is favored, $\epsilon_R = \epsilon_L + \omega$, the effective temperature of the oscillator decreases, provided that $\omega < T$. We consider that both levels are in the transport window and the level broadening is small. $\epsilon_L$ is varied while $\epsilon_R = V/2$, $eV = 10$ (in units of $\omega$), $\lambda = 0.1$, $t = 0.1$, and $\Gamma = 0.1$.

through the device in order to achieve cooling, hence implying that the operational principle terminates for $V \to 0$.

Including the effect of a finite temperatures $T_{\rm e}$ in the reservoirs, where the corrections to the zero temperature result are given by Eq. (6.25) and Eq. (6.26), we find that cooling is possible as long as $\xi^2\sqrt{2\xi/(\pi\Gamma)} > \Gamma T_{\rm e}$, abbreviating $\xi \approx |\mu_\alpha - \epsilon_\alpha|$. Then we obtain

$$\overline{n}_0 \simeq \frac{\pi}{6}\frac{\Gamma^3\, T_{\rm e}^2}{\xi^5}\frac{1}{1-(\pi/3)\Gamma^3\, T_{\rm e}^2/\xi^5}, \tag{6.34}$$

within the approximation $\Gamma \ll \xi$. This is the stationary solution for the phonon population in the limit of vanishing relaxation to the equilibrium, $1/\tau \to 0$, see Eqs. (6.30) and (6.31), and can clearly be smaller than $\overline{n}^{\rm eq}$. Cooling by current in the presence of a larger applied voltage is considered next.

### 6.3.3. Large voltages

At high voltages, $eV > \omega$, when both levels are in the conduction window, there are always processes which contribute to heating. The competition between the latter and the absorption of phonons sets the temperature to which the system can be cooled. We still consider the limit of small electron-phonon coupling when the levels are tuned to be at resonance, $\epsilon_L = \epsilon_R - \omega$. With the results obtained above, Eqs. (6.19) and (6.20), we obtain $I^- = 2/\Gamma$ and $I^+ = 2\Gamma/[(2\omega)^2 + \Gamma^2]$, here neglecting the corrections due to temperature. Thus we obtain

$$\overline{n}_0 = \frac{\Gamma^2}{(2\omega)^2}, \tag{6.35}$$

which, as outlined above, is the stationary solution in the limit far away from equilibrium, $1/\tau \to 0$, see Eq. (6.30). We note that $\overline{n}_0$ can be well below the equilibrium value $\overline{n}^{\rm eq}$, when temperatures are comparable or larger than $\omega$ allowing one to cool the oscillator. For temperatures small compared to $\omega$ one effectively heats the phonon system. This is illustrated in Fig. 6.5. There we also show that due to the finite width of the electronic levels cooling (or heating) is also possible slightly away from resonance.

## 6.4. Summary

In this chapter we have studied how one can use a charge current in order to cool a nanomechanical system. We have considered a double quantum dot in which the two dots are coupled to leads and weak tunneling between the dots can be accompanied by emission and absorption of phonons. It is a general feature of our model that the electronic levels can be tuned such that emission of phonons happens more often than absorption, allowing one to remove energy from the mechanical system.

We have studied the phonon population by means of a rate equation and have written down the general expressions for the rates. These have been evaluated analytically in some limiting cases, mainly focusing on the regime of weak electron-phonon coupling. Here the resonance situation $\epsilon_R = \epsilon_L + \omega$ is favorable, as well as small temperatures and small $\Gamma$, in order to achieve efficient cooling. When only a few phonons are left in the system, even a small probability of emitting phonons might prevent to cool down the system further. We have commented on the effect of a finite (electronic) temperature in the reservoirs and the temperature of the heat bath coupled to the oscillator which limit the operational principle of the refrigerator. At the end of this chapter we have focused on weak electron-phonon coupling; the analysis of strong interactions is a promising topic for further research. Furthermore it will be interesting to understand cooling mechanisms in the opposite limit of slow vibrational dynamics, connecting with our results obtained in Chapter 3.

# 7. Molecular switches on graphene

In the preceding chapters we have considered single molecule switches which can be both switched and read out through the electronic current through the junction. In this chapter we consider a different scenario in which many switches affect the conductance of a layer of graphene. This substrate is particularly appealing for this functionalization due to its two-dimensionality and its good transport properties.

Here the switching is triggered externally and we focus on the read-out of the switching state by current measurements, providing a theory of the electronic transport properties of a graphene layer decorated with molecular switches (as sketched in Fig. 7.1). In particular, our considerations are motivated by photochromic molecular switches, in which the reversible switching between two conformations affects the carriers in graphene through the associated change in the molecular dipole moment. We provide model calculations of how this modifies the conductance of graphene both in the quasiclassical (Boltzmann) and in the quantum-coherent regimes of transport. In the former the scattering on the single impurities are independent of each other while in the latter interference between multiple scattering trajectories can increase the sensitivity to the precise impurity configuration.

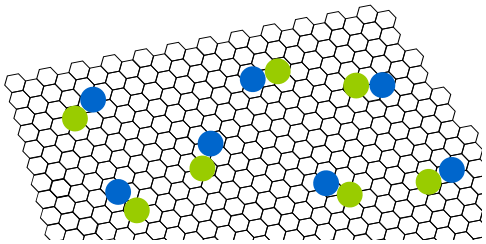

Figure 7.1. Sketch of graphene functionalized with dipolar molecules.

This chapter is organized as follows. We give a brief introduction to the electronic properties of graphene in Section 7.2 and comment on its quasiclassical transport properties in Section 7.3. The influence of the dipoles on the conductivity is studied in Section 7.4. Coherent processes are considered in Section 7.5. Some technical details of the calculations are relegated to an appendix.

The results presented here have been published in [Bode *et al.*, 2012c].

## 7.1. Introduction

The very first measurements in graphene on a substrate gave rise to to a linear dependence of the conductivity on the carrier concentration and thus a – remarkably high – density-independent mobility [Novoselov *et al.*, 2004, 2005]. This indicates that charged impurities are the main source for scattering and thus limit the conductivity predominantly while short range scatterers cause only smaller corrections which become more important for

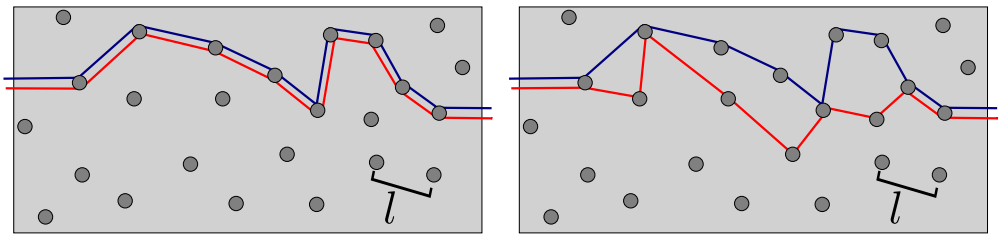


Figure 7.2. Illustration of the two transport regimes considered in this chapter. Consecutive scattering events are considered to be independent in the Boltzmann limit (left) while interference effects (right) change the transport properties in the mesoscopic regime.

larger carrier concentrations [Ando, 2006; Nomura and MacDonald, 2006; Hwang *et al.*, 2007].

Graphene provides a particularly attractive substrate for decoration with molecular switches due to its unique conduction properties, such as the absence of backscattering and an easily tunable carrier concentration [Novoselov *et al.*, 2004, 2005], as well as its strictly two-dimensional nature. Especially this last fact suggests that the conduction properties of graphene could serve as a sensitive detector for the conformational state of the molecular switches, cp. also the work by Schedin *et al.* [2007].

In this chapter, we consider the electronic transport properties of graphene layers functionalized by spiropyran which we briefly described in the introduction, Section 1.2.3. Specifically, we consider how the conductance of the graphene layer differs between the switching states which are characterized by very different electric dipole moments. For isolated molecules, it is estimated [Malic *et al.*, 2011] that the dipole moment is of order of 6.2D in the ring-closed spiropyran form, while it is 13.9D in the zwitterionic merocyanine.[1]

Our calculations of the conductance of the graphene layer consider both the Boltzmann regime and the mesoscopic regime of coherent quantum transport, see Fig. 7.2. When the electronic mean free path is much larger than the Fermi wavelength and the system is sufficiently large, electronic transport is characterized by the quasiclassical Boltzmann conductivity. In contrast, in the mesoscopic regime, the sample size is no longer large compared to the phase coherence length, so that quantum interference effects become important and the conductance becomes sensitive to the particular impurity configuration. The average magnitude of these fluctuations around their mean value is universal and of order of the conductance quantum $e^2/h$ [Lee and Stone, 1985; Al'tshuler, 1985; Lee *et al.*, 1987; Kane *et al.*, 1988], and rather small changes in the precise configuration of the impurities cause significant changes in the conductance due to interference of multiple scattering trajectories [Al'tshuler and Spivak, 1985; Feng *et al.*, 1986]. Besides the dependence on the conformational state of the decorating molecules, we also consider the influence of the densities of charge carriers and impurities, as well as the density and orientation of the dipolar switches.

[1] One Debye corresponds to: $1\mathrm{D} \approx 0.2082 e\text{Å} \approx 3.336 \times 10^{-30}\mathrm{Cm}$.

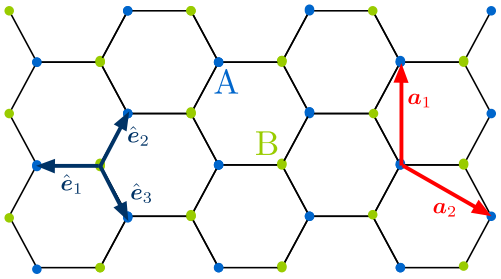


Figure 7.3. Honeycomb lattice of graphene.

## 7.2. Electronic properties of graphene

From the theoretical point of view, the electronic properties of single 2d graphene sheets had been studied several decades ago, in connection to the investigation of 3d graphite [Wallace, 1947]. Due to the honeycomb symmetry of the lattice, electrons in graphene behave as massless charged Dirac particles with a constant group velocity approximately 300 times smaller than the velocity of light. Although the linear dispersion stems from an expansion of the electronic spectrum in the vicinity of two points where valence and conductance band touch, due to the peculiar bandstructure it holds true over a wide bandwidth of several electron-Volts. This yields the important consequence that the low energy massless Dirac description of electrons in graphene remains relevant up to very large temperatures (much larger than room temperature) and doping levels. Indeed, similarly to conventional semiconductor structures, both electron and hole doping can be induced in the sheet through adatoms and/or by applying an external gate voltage.

Starting from a tight-binding description we derive the low-energy Hamiltonian and the dispersion relation for the charge carriers in graphene. Then we introduce the (impurity-averaged) Green's functions, which we need for the description of the transport properties in the remainder of this chapter. We refer to the reviews by Neto *et al.* [2009] and Das Sarma *et al.* [2011] for a detailed discussion of the electronic properties of graphene.

### 7.2.1. Tight-binding description

Graphene has been studied in terms of the tight-binding model, stating that electrons hop between nearest-neighbor lattice sites, by Wallace [1947] more than half a century ago. Further details on the underlying atomic structure of graphene can be found, for example, in [Saito *et al.*, 1998].

The honeycomb lattice of graphene is formed by two inequivalent sublattices on which the electrons are described by the Hamiltonian

$$H = -\sum_{<i,j>} t\left(c_i^\dagger c_j + c_j^\dagger c_i\right), \tag{7.1}$$

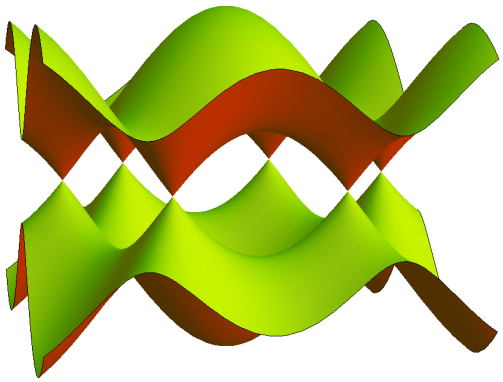

Figure 7.4. Sketch of the dispersion relation $\epsilon_{\boldsymbol{k}}$ over the $k_x$, $k_y$ plane. We focus on the low-energy physics close to the points where the conduction and the valence band touch.

where $t \approx 2.8\text{eV}$ is the hopping energy between nearest neighbors, $c_i^\dagger$ ($c_i$) creates (annihilates) an electron on lattice site $i$ and the sum is restricted to nearest neighbors. As depicted in Fig. 7.3, the honeycomb lattice of graphene consists of two triangular sublattices A and B. Each lattice site has three neighboring ions from the other sublattice separated by $a \approx 1.42\text{Å}$. Thus we can write the tight-binding Hamiltonian as

$$H = -t \sum_{\boldsymbol{R}_B} \sum_i \big|\boldsymbol{R}_B\big\rangle\big\langle \boldsymbol{R}_B + \hat{\boldsymbol{e}}_i\big| + \text{h.c.}\,, \tag{7.2}$$

where we have choose a coordinate system in which a B-site is connected with its neighbors via the three vectors $\hat{\boldsymbol{e}}_1 = (-a, 0)$, $\hat{\boldsymbol{e}}_2 = (a/2, \sqrt{3}a/2)$ and $\hat{\boldsymbol{e}}_3 = (a/2, -\sqrt{3}a/2)$. Electrons in the lattice can be described by Bloch states involving a superposition of the wave functions of the two sublattices,

$$\big|\psi_{\boldsymbol{k}}\big\rangle = \sum_{\boldsymbol{R}_A} u_A(\boldsymbol{k}) \mathrm{e}^{\mathrm{i}\boldsymbol{k}\cdot\boldsymbol{R}_A} \big|\boldsymbol{R}_A\big\rangle + \sum_{\boldsymbol{R}_B} u_B(\boldsymbol{k}) \mathrm{e}^{\mathrm{i}\boldsymbol{k}\cdot\boldsymbol{R}_B} \big|\boldsymbol{R}_B\big\rangle, \tag{7.3}$$

where $u_A(\boldsymbol{k})$ [$u_B(\boldsymbol{k})$] give the amplitudes for the occupation of lattice site A (B), and the sums are over all sites of the particular sublattice. Projecting onto the Schrödinger equation, $H\big|\psi_{\boldsymbol{k}}\big\rangle = \epsilon_{\boldsymbol{k}}\big|\psi_{\boldsymbol{k}}\big\rangle$, with $\big\langle \boldsymbol{R}_A\big|$ and $\big\langle \boldsymbol{R}_B\big|$, respectively, one obtains

$$\begin{pmatrix} 0 & -t\sum_i \mathrm{e}^{-\mathrm{i}\boldsymbol{k}\cdot\hat{\boldsymbol{e}}_i} \\ -t\sum_i \mathrm{e}^{\mathrm{i}\boldsymbol{k}\cdot\hat{\boldsymbol{e}}_i} & 0 \end{pmatrix} \begin{pmatrix} u_A \\ u_B \end{pmatrix} = \epsilon_{\boldsymbol{k}} \begin{pmatrix} u_A \\ u_B \end{pmatrix}.$$

Inserting the vectors $\hat{\boldsymbol{e}}_i$ in this expression yields straightforwardly the spectrum

$$\epsilon_{\boldsymbol{k}} = \pm t\sqrt{1 + 4\cos(\tfrac{3ak_x}{2})\cos(\tfrac{\sqrt{3}ak_y}{2}) + 4\cos^2(\tfrac{\sqrt{3}ak_y}{2})}\,, \tag{7.4}$$

which is schematically depicted in Fig. 7.4. Neutral graphene has just one electron per lattice site and one concludes that the Fermi energy is at $\epsilon_{\boldsymbol{k}} = 0$ around which the

spectrum is symmetric. Solving for $\boldsymbol{k}$ one sees that in graphene there is no Fermi line as in usual 2d systems but rather isolated Fermi points. In order to identify the first Brillouin zone we introduce a minimal set of lattice vectors $\boldsymbol{a}_1 = \hat{\boldsymbol{e}}_3 - \hat{\boldsymbol{e}}_2$ and $\boldsymbol{a}_2 = \hat{\boldsymbol{e}}_2 - \hat{\boldsymbol{e}}_3$ as depicted in Fig. 7.3, generating the two inequivalent sublattices. The basis vectors in the reciprocal lattice are thus $\boldsymbol{b}_1 = 2\pi/(3a)(2,0)$ and $\boldsymbol{b}_2 = 2\pi/(3a)(1,\sqrt{3})$. Only the two Fermi points at position

$$\pm\boldsymbol{k}_{\mathrm{D}} = \pm\frac{3\pi}{3\sqrt{3}a}\begin{pmatrix}\sqrt{3}\\1\end{pmatrix} \tag{7.5}$$

lie inside the first Brillouin zone of the reciprocal lattice. These are the so-called *Dirac points*.

### 7.2.2. Low-energy physics close to the Dirac points

In order to describe the low-energy physics of electrons close to the Dirac points we expand the Hamiltonian (7.2) around the Dirac points $\boldsymbol{k}_{\mathrm{D}}$ as a function of the deviation (which we denote from now on with $\boldsymbol{k}$) from these points. After some calculations this yields

$$\sum_j \mathrm{e}^{\mathrm{i}(\boldsymbol{k}_{\mathrm{D}}+\boldsymbol{k})\cdot\hat{\boldsymbol{e}}_j} = \sum_j \mathrm{e}^{\pm\mathrm{i}\boldsymbol{k}_{\mathrm{D}}\cdot\hat{\boldsymbol{e}}_j}\mathrm{e}^{\mathrm{i}\boldsymbol{k}\cdot\hat{\boldsymbol{e}}_j} \simeq -\mathrm{i}\tfrac{3a}{2}\mathrm{e}^{\mp\mathrm{i}\frac{2\pi}{3}}(k_x \pm \mathrm{i}k_y), \tag{7.6}$$

where the $\pm$ refers to the two distinct Dirac points. In order to simplify the notation we introduce an additional phase factor in the amplitudes of the Bloch waves.[2] Accordingly, the relevant low-energy bandstructure is captured by the Dirac Hamiltonian

$$H = \Pi^z \otimes H_0\ , \tag{7.7}$$

describing the two inequivalent Dirac cones inside the first Brillouin zone. This Hamiltonian acts on the 4-component spinor $(u_A^+, u_B^+, u_B^-, u_A^-)$ with Bloch amplitudes $u$ where $(+,-)$ labels the Dirac cone and $(A,B)$ the sublattice. Here $\Pi^z$ denotes a Pauli matrix[3] in the space of Dirac points and $H_0$ is the Hamiltonian of a single Dirac cone,

$$H_0 = \hbar v\boldsymbol{\sigma}\cdot\boldsymbol{k}, \tag{7.8}$$

where $v = 3at/(2\hbar)$ and $\sigma^\mu$ ($\mu = x, y$) are Pauli matrices acting in the space of the two sublattices. One finds the effective dispersion

$$\epsilon_{s,\boldsymbol{k}} = s\hbar vk, \tag{7.9}$$

which is linear in $k = |\boldsymbol{k}|$, and $s = \pm 1$ labels the conduction and valence bands, respectively. Obviously, this dispersion can be also obtained from Eq. (7.4) by expanding in the vicinity

[2] The redefinition of the Bloch amplitudes is explicitly $u_B \to \mathrm{e}^{\mp i\varphi}u_B$, where $\mathrm{e}^{\mp i\varphi} = -i\mathrm{e}^{\frac{2\pi}{3}}$, while $u_A$ remain unchanged, $u_A \to u_A$

[3] See the footnote on page 44 for the definition of the Pauli matrices.

of $\boldsymbol{k}_\mathrm{D}$. Note that the Fermi velocity $v$ is roughly 300 times smaller than the velocity of light and does not depend on the energy [in contrast to the usual case of massive electrons with $\epsilon_{\boldsymbol{k}} = (\hbar k)^2/(2m)$]. The corresponding eigenfunctions of $H_0$ are

$$\boldsymbol{\psi}_{s,\boldsymbol{k}}(\boldsymbol{r}) = \langle \boldsymbol{r}|\boldsymbol{k}\rangle = \frac{1}{\sqrt{2\Omega}} \exp(\mathrm{i}\boldsymbol{k}\cdot\boldsymbol{r}) \begin{pmatrix} s \\ \mathrm{e}^{\mathrm{i}\varphi(\boldsymbol{k})} \end{pmatrix}, \tag{7.10}$$

where $\cos\varphi(\boldsymbol{k}) = k_x/k$ and $\Omega$ is the sample area.

In summary, we obtained that, due to the honeycomb lattice structure, low energy electronic quasiparticles in graphene are described by a Dirac Hamiltonian resembling the behavior of relativistic massless particles as in quantum electrodynamics. In the following we consider the two Dirac cones (valleys) to be completely decoupled as is the case in the absence of short-range scatterers. Consequently, we account for the two valleys simply through the appropriate degeneracy factor.

The concentration of charge carriers in graphene can be tuned via external gate voltages which allows one to vary the Fermi wavenumber $k_\mathrm{F}$. The density $n$ of conduction electrons is related to $k_\mathrm{F}$ through

$$n = g\int_0^{\epsilon_\mathrm{F}} \mathrm{d}\epsilon\, \nu(\epsilon) = \frac{k_\mathrm{F}^2}{\pi}, \tag{7.11}$$

where $\nu(\epsilon) = \epsilon/2\pi(\hbar v)^2$ is the density of states per spin and valley, $\epsilon_\mathrm{F}$ is the Fermi energy, and $g = 4$ accounts for the spin and valley degeneracy. We refer to the article by Neto *et al.* [2009] for a detailed review of the electronic properties of graphene.

### 7.2.3. Green's functions

Our discussion of the transport properties is based on a Green's function approach. The free retarded (advanced) Green's function for electrons (focusing on one Dirac cone) is

$$G_0^{R(A)}(\epsilon, \boldsymbol{k}) = \frac{1}{2}\sum_{s=\pm1} \frac{1 + s\,\boldsymbol{\sigma}\cdot\boldsymbol{k}/k}{\epsilon - \epsilon_{s,\boldsymbol{k}} \pm \mathrm{i}0^+}. \tag{7.12}$$

The numerators in these expressions act as projectors onto states in the conduction ($s = +1$) and valence ($s = -1$) band, respectively. In the following we consider only electron-doped systems with a sufficiently high Fermi energy, such that all relevant processes occur in the conduction band. This allows us to restrict attention to $s = +1$ only. In fact, both our quasiclassical and our diagrammatic approaches are valid only when the system is sufficiently far from the Dirac point (characterized by electron and hole puddles in real samples [Das Sarma *et al.*, 2011]).

Scattering on impurities broadens the electronic spectral function, so that the impurity averaged (indicated by the overbar) matrix elements of the retarded (advanced) electronic Green's function become

$$\overline{\langle \boldsymbol{k}'|G_\epsilon^{R(A)}|\boldsymbol{k}\rangle} = \frac{\delta_{\boldsymbol{k},\boldsymbol{k}'}}{\epsilon - \epsilon_{\boldsymbol{k}} \pm \mathrm{i}\hbar/2\tau(\epsilon_{\boldsymbol{k}})} \equiv \delta_{\boldsymbol{k},\boldsymbol{k}'}\overline{G}_\epsilon^{R/A}(\boldsymbol{k}). \tag{7.13}$$

Here, the elastic scattering time, evaluated in the Born approximation, is

$$\frac{1}{\tau(\epsilon_{\boldsymbol{k}})} = \frac{2\pi}{\hbar} \sum_{\boldsymbol{k}'} \overline{|\langle \boldsymbol{k}|V_{\mathrm{i}}|\boldsymbol{k}'\rangle|^2}\, \delta(\epsilon_{\boldsymbol{k}} - \epsilon_{\boldsymbol{k}'}), \tag{7.14}$$

in accordance with Fermi's golden rule. The electronic mean free path is related to the scattering time through $l = v\tau$. The impurity potential $V_{\mathrm{i}}(\boldsymbol{r}) = \sum_{j=1}^{N_{\mathrm{i}}} V(\boldsymbol{r} - \boldsymbol{r}_j)$ is a sum over the individual potentials $V$ of the $N_{\mathrm{i}}$ impurities which we take to be randomly distributed. Because the precise impurity configuration is unknown only quantities which are averaged over all possible impurity configurations are accessible. This impurity averaging is denoted by

$$\overline{(...)} = \int \Pi_{j=1}^{N_{\mathrm{i}}} \mathrm{d}(\boldsymbol{r}_j/\Omega)\,(...). \tag{7.15}$$

Note that we restrict our discussion to potentials which do neither flip the spin nor transfer momenta large enough to couple the two Dirac cones. Averaging over the impurity configurations yields

$$\overline{|\langle \boldsymbol{k}|V_{\mathrm{i}}|\boldsymbol{k}'\rangle|^2} = \frac{n_{\mathrm{i}}}{\Omega} |V_{\boldsymbol{k}-\boldsymbol{k}'}|^2 \frac{1+\cos\vartheta}{2}, \tag{7.16}$$

with $\vartheta$ the angle between $\boldsymbol{k}$ and $\boldsymbol{k}'$, $V_{\boldsymbol{k}-\boldsymbol{k}'}$ the Fourier transform of $V(\mathbf{r})$, and $n_{\mathrm{i}} = N_{\mathrm{i}}/\Omega$ the impurity density. The factor $(1 + \cos\vartheta)$ reflects the absence of backscattering in graphene, even for isotropic scattering potentials.

## 7.3. Quasiclassical transport properties

Before discussing the influence of molecular switches on the conductivity, we briefly review the conductivity of doped graphene within a Boltzmann approach [Novoselov *et al.*, 2004, 2005; Ando, 2006; Nomura and MacDonald, 2006; McCann *et al.*, 2006; Adam *et al.*, 2007; Auslender and Katsnelson, 2007].

For zero temperature, the longitudinal conductivity is given by the Kubo formula

$$\sigma = g\frac{\hbar}{\pi\Omega} \mathrm{Tr}\left[\hat{j}_x \mathrm{Im} G^R_{\epsilon_{\mathrm{F}}}\, \hat{j}_x \mathrm{Im} G^R_{\epsilon_{\mathrm{F}}}\right], \tag{7.17}$$

where the Green's functions are evaluated at the Fermi energy. The current operator is $\hat{j}_x = (-\mathrm{e})\frac{\mathrm{i}}{\hbar}[H_0, x] = (-\mathrm{e})v\sigma^x$, with matrix elements

$$(j_x)_{\boldsymbol{k},\boldsymbol{k}'} = (-\mathrm{e})v\langle \boldsymbol{k}'|\sigma^x|\boldsymbol{k}\rangle = (-\mathrm{e})v\cos\vartheta. \tag{7.18}$$

To lowest order, the diagram for the impurity-averaged conductivity is depicted in Fig. 7.5. It involves the diffuson, describing diffusive motion of the electrons in the sample, which we will encounter and discuss in some detail in Section 7.5. Following standard procedures [Akkermans and Montambaux, 2007] we obtain

$$\overline{\sigma} = g e^2 \nu_0 D, \tag{7.19}$$

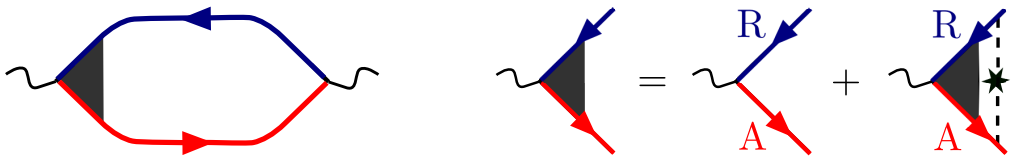


Figure 7.5. (left) Diagram for the conductivity. The conductivity loop consists of a retarded (blue) and an advanced (red) impurity averaged Green's function meeting at two current vertices. (right) Vertex corrections. The star denotes impurity scattering. Note that one only has to include diagrams with a retarded and an advanced Green's function meeting at a current vertex [Al'tshuler and Shklovskii, 1986; Kane *et al.*, 1988; Baranger and Stone, 1989].

with $D = v^2\tau_{\rm tr}/2$ the diffusion constant. The movement of an electron through a conductor is hindered by the scattering on the impurities. Hence in the regime under consideration, the typical time between these collisions limits the conductivity. In fact, in Eq. (7.19) enters the rate at which the memory of the $\boldsymbol{k}$-direction of the incoming electron is lost. This transport scattering rate is given by

$$\begin{aligned}\frac{1}{\tau_{\rm tr}(\epsilon_{\boldsymbol{k}})} &= \frac{2\pi}{\hbar}\sum_{\boldsymbol{k}'}\overline{|\langle \boldsymbol{k}|V_{\rm i}|\boldsymbol{k}'\rangle|^2}(1-\cos\vartheta)\,\delta(\epsilon_{\boldsymbol{k}}-\epsilon_{\boldsymbol{k}'}) \\ &= \frac{\pi}{\hbar}n_{\rm i}\nu(\epsilon_{\boldsymbol{k}})\left\langle |V_{\boldsymbol{k}-\boldsymbol{k}'}|^2\sin^2\vartheta\right\rangle_\vartheta. \end{aligned} \tag{7.20}$$

Here, $\langle ...\rangle_\vartheta = \int_0^{2\pi}{\rm d}\vartheta\,(...)/(2\pi)$ denotes an angular average over the Fermi circle. From now on, $\tau$ and $\tau_{\rm tr}$ without explicit momentum labels are calculated at the Fermi energy. We also use the notation $\nu_0 \equiv \nu(\epsilon_{\rm F})$. We close this section with a brief discussion of the transport scattering time for two common sources of scattering, namely short-range and Coulomb scatterers.

### Short-range scatterers

Scatterers with a short-range potential, *e.g.*, point defects or neutral impurities, have a Fourier transform which is (approximately) independent of momentum, $V_{\boldsymbol{k}-\boldsymbol{k}'} = V$. Thus, due to the density-of-states factor, Eq. (7.20) yields a transport scattering rate which is proportional to $k$ and the conductivity becomes independent of the electron density. (We assume that the potential still varies smoothly enough that the two Dirac cones remain uncoupled.) Note that in a conventional 2d system (with the quadratic dispersion $\epsilon_{\boldsymbol{k}} = (\hbar k)^2/(2m)$ and thus a constant density of states) the scattering rate for pointlike scatterers is independent of the electron concentration yielding a conductivity $\sigma_{\rm 2d} \propto n/n_{\rm i}$, in contrast to the situation in graphene.

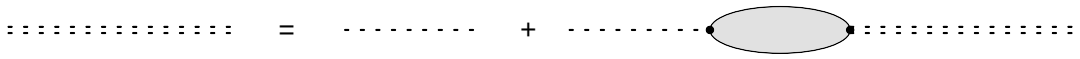

Figure 7.6. The Dyson equation connects the full Coulomb interaction (double line) with the unscreened interaction (single line). The screening of the other conduction electrons is contained in the full polarization bubble.

### Coulomb scatterers

Another frequent source of scattering in graphene samples are charged impurities, located at a distance $z$ above the graphene sheet. The Fourier transform of the corresponding single-impurity potential is

$$V_{\boldsymbol{q}}^{\mathrm{c}} = \frac{2\pi\alpha\hbar v}{q}\mathrm{e}^{-zq}, \tag{7.21}$$

where $q = |\boldsymbol{k} - \boldsymbol{k}'| = 2k\sin(\vartheta/2)$ for elastic scattering processes. Here, $\alpha = e^2/(\hbar v\kappa)$ denotes the effective fine structure constant which involves the average dielectric constants of the neighboring media, $\kappa = (\kappa_1 + \kappa_2)/2$ [Adam *et al.*, 2007; Das Sarma *et al.*, 2011].

In a solid the conduction electrons screen the Coulomb interaction. The exact screened Coulomb interaction can be obtained via the Dyson equation depicted in Fig. 7.6. The dominant long wavelength screened interaction has been shown [Gell-Mann and Brueckner, 1957; Schrieffer, 1964] to be given by approximating the exact polarization bubble with the free one. This procedure is called *random phase approximation* (RPA). It yields

$$\tilde{V}_{\boldsymbol{q}}^{\mathrm{c}} = V_{\boldsymbol{q}}^{\mathrm{c}} + V_{\boldsymbol{q}}^{\mathrm{c}}\Pi^0 V_{\boldsymbol{q}}^{\mathrm{c}} + V_{\boldsymbol{q}}^{\mathrm{c}}\Pi^0 V_{\boldsymbol{q}}^{\mathrm{c}}\Pi^0 V_{\boldsymbol{q}}^{\mathrm{c}} + ... = V_{\boldsymbol{q}}^{\mathrm{c}} + V_{\boldsymbol{q}}^{\mathrm{c}}\Pi^0\tilde{V}_{\boldsymbol{q}}^{\mathrm{c}}, \tag{7.22}$$

which can be easily solved for $\tilde{V}_{\boldsymbol{q}}^{\mathrm{c}}$. The bare polarization bubble, $\Pi^0 = \Pi^0(\boldsymbol{q}, \epsilon)$, is given by

$$\mathrm{i}\,\Pi^0(\boldsymbol{q}, \epsilon) = g\int\frac{\mathrm{d}\epsilon'}{2\pi}\,\mathrm{Tr}\left[G_0^R(\boldsymbol{k}, \epsilon')\,G_0^A(\boldsymbol{k}+\boldsymbol{q}, \epsilon'+\epsilon)\right], \tag{7.23}$$

where we restrict ourselves to the upper half of one Dirac cone. This is justified as long as the doping is sufficiently large and the wavenumber small, preventing scattering between the two different Dirac cones. We are interested in the long wavelength limit $q \ll k_{\mathrm{F}}$ so that one finds

$$\Pi^0(q \ll k_{\mathrm{F}}, \epsilon \to 0) \simeq -g\nu_0. \tag{7.24}$$

Thus the polarizability is given by the density of states evaluated at the Fermi energy $\nu_0$. To summarize, in this Thomas-Fermi approximation one obtains the effective potential $\tilde{V}_{\boldsymbol{q}}^{\mathrm{c}} = V_{\boldsymbol{q}}^{\mathrm{c}}/\varepsilon(\boldsymbol{q})$. The dielectric function, in the limit of zero temperature, can be approximated by

$$\varepsilon(\boldsymbol{q}) = 1 - V_{\boldsymbol{q}}^{\mathrm{c}}\Pi^0 \simeq 1 + q_{\mathrm{TF}}/q, \tag{7.25}$$

involving the characteristic wave vector $q_{\mathrm{TF}} = 2\pi\alpha\hbar v g\nu_0$ [Ando, 2006; Nomura and MacDonald, 2006]. Note that accordingly also the screened Coulomb interaction scales as $\propto 1/q$.

In graphene, the average conductivity is found to be

$$\overline{\sigma}^{\mathrm{c}} = \frac{ge^2}{h}\,\frac{1}{\pi\alpha^2 I_0}\,\frac{n}{n_{\mathrm{i}}^{\mathrm{c}}}, \tag{7.26}$$

which is valid at zero temperature, showing that the conductivity increases linearly with the density of charge carriers $n$ participating in the transport. This result follows from inserting the transport scattering time $\tau_{\mathrm{tr}}^{\mathrm{c}}$ into Eq. (7.19). The scattering rates evaluated at the Fermi level, see Eqs. (7.20) and (7.14), are

$$\left.\begin{matrix} 1/\tau_{\mathrm{tr}}^{\mathrm{c}} \\ 1/\tau^{\mathrm{c}} \end{matrix}\right\} = \frac{n_{\mathrm{i}}^{\mathrm{c}}\,\pi^2\alpha^2 v}{2k_{\mathrm{F}}} \left\{\begin{matrix} I_0 \\ J_0 \end{matrix}\right. , \tag{7.27}$$

with $n_{\mathrm{i}}^{\mathrm{c}}$ the density of charged impurities and the abbreviations

$$\left.\begin{matrix} I_m \\ J_m \end{matrix}\right\} = \int_0^{2\pi} \frac{\mathrm{d}\vartheta}{2\pi}\,\frac{\sin^m(\vartheta/2)\mathrm{e}^{-4zk_{\mathrm{F}}\sin(\vartheta/2)}}{\left[\sin(\vartheta/2)+g\alpha/2\right]^2} \left\{\begin{matrix} \sin^2\vartheta \\ 1+\cos\vartheta \end{matrix}\right. . \tag{7.28}$$

For $q_{\mathrm{TF}}/(2k_{\mathrm{F}}) = g\alpha/2 \approx 2$ (corresponding to graphene on a $SiO_2$ substrate [Adam *et al.*, 2007]) and $4zk_{\mathrm{F}} \ll 1$ we have $I_0 \approx 0.071$, $I_1 \approx 0.046$, $I_2 \approx 0.033$, $J_0 \approx 0.18$, $J_1 \approx 0.065$, and $J_2 \approx 0.035$.

In summary, the conductivity of graphene is independent of the electron density $n$ for short-range scatterers and linear in the density for Coulomb scatterers [Ando, 2006; Nomura and MacDonald, 2006; Adam *et al.*, 2007]. Combining both contributions, one obtains a linear rise of the conductivity which saturates at higher $n$. At low temperatures this behavior is in agreement with many experiments [Novoselov *et al.*, 2004, 2005; Chen *et al.*, 2008].

## 7.4. Effect of switches on the conductivity – Boltzmann theory

After these preparations we can now focus on the effect of switches decorating a graphene monolayer. We consider graphene samples with a dilute and random covering by molecular switches whose switching states are characterized by different electric dipole moments.[4] In this section, we will assume that the electronic scattering is adequately described within a Boltzmann approach which treats consecutive scattering events as independent. We will also assume that the switching is only effected externally, *e.g.*, by irradiation of the sample, and that all molecules are switched so that we need only discuss the conductivity for the static dipole moments associated with the two different conformations.

[4] In the spiropyran-merocyanine system, the switching states differ most significantly in their corresponding dipole moments and thus higher order terms in a multipole expansion of the charge distribution can presumably be neglected.

Consider a molecule with a nonzero electric dipole moment $\boldsymbol{d}$ attached to graphene. We assume that the electric dipole is located at a distance $z$ above the graphene sheet with the dipolar potential

$$V^{\mathrm{d}}(\boldsymbol{r}, z) = (-e)\frac{\boldsymbol{d}_{\parallel} \cdot \boldsymbol{r} + d_{\perp} z}{(r^2 + z^2)^{3/2}}. \tag{7.29}$$

Here, $\boldsymbol{d}_{\parallel}$ and $d_{\perp}$ are the components of the dipole moment parallel and perpendicular to the substrate, respectively, and $\boldsymbol{r}$ is a two-dimensional vector in the surface. The two dimensional Fourier transform of the dipolar potential follows readily from Gauss's law $\nabla^2 V^{\mathrm{d}} = 4\pi e\rho$, where $\rho$ is the charge density of the dipoles. (Note that $V^{\mathrm{d}}$ is defined as the potential energy of an electron in the field of the dipole.) Fourier transforming Gauss's law and integrating over the out-of-plane component of the wave vector, one obtains

$$V^{\mathrm{d}}_{\boldsymbol{q}} = 4\pi \mathrm{i} e \int \frac{\mathrm{d}q_{\perp}}{2\pi} \frac{\boldsymbol{d}_{\parallel} \cdot \boldsymbol{q} + d_{\perp} q_{\perp}}{q^2 + q_{\perp}^2} \mathrm{e}^{\mathrm{i}q_{\perp} z}, \tag{7.30}$$

and therefore

$$V^{\mathrm{d}}_{\boldsymbol{q}} = V^{\mathrm{d}_{\parallel}}_{\boldsymbol{q}} + V^{\mathrm{d}_{\perp}}_{\boldsymbol{q}}, \tag{7.31}$$

$$V^{\mathrm{d}_{\parallel}}_{\boldsymbol{q}} = 2\pi \mathrm{i} \alpha \hbar v (d_{\parallel}/e) \cos\phi \, \mathrm{e}^{-qz}, \tag{7.32}$$

$$V^{\mathrm{d}_{\perp}}_{\boldsymbol{q}} = -2\pi \alpha \hbar v (d_{\perp}/e) \mathrm{e}^{-qz}, \tag{7.33}$$

where $\phi$ denotes the angle between the wave vector $\boldsymbol{q}$ and $\boldsymbol{d}_{\parallel}$. Note that $V^{\mathrm{d}_{\perp}}_{\boldsymbol{q}}$ is real, while $V^{\mathrm{d}_{\parallel}}_{\boldsymbol{q}}$ is imaginary, reflecting their symmetry properties. The resulting screened potential is given by $\tilde{V}^{\mathrm{d}}_{\boldsymbol{q}} = V^{\mathrm{d}}_{\boldsymbol{q}}/\varepsilon(q)$, with the dielectric function in Eq. (7.25).

We first consider a clean graphene sample where the scattering is entirely due to the decorating molecular switches with dipolar impurity potential. In such a system, the electrons are scattered at impurities with a dipole moment (but without monopole potential), and the averaged matrix elements of the impurity potential read

$$\overline{|\langle \boldsymbol{k} | V^{\mathrm{d}}_{\mathrm{i}} | \boldsymbol{k'} \rangle|^2} = \frac{n^{\mathrm{d}}_{\mathrm{i}}}{\Omega} \frac{(\alpha \hbar v \tilde{d}/e)^2}{1 + q_{\mathrm{TF}}/q} \frac{1 + \cos\vartheta}{2}, \tag{7.34}$$

with $n^{\mathrm{d}}_{\mathrm{i}}$ the density of dipoles. We use $\tilde{d}^2 = d^2 \left(1 + \cos^2\xi\right)/2$, where the angle $\xi$ measures the orientation of the dipole moment with respect to the plane such that $d_{\perp} = d\cos\xi$. To be specific, we assume that $\boldsymbol{d}_{\parallel}$ is oriented along an arbitrary direction within the graphene layer while the perpendicular component is (approximately) the same for all dipolar switches. Inserting Eq. (7.34) into Eqs. (7.20) and (7.14) yields the scattering rates

$$\left.\begin{matrix} 1/\tau^{\mathrm{d}}_{\mathrm{tr}} \\ 1/\tau^{\mathrm{d}} \end{matrix}\right\} = 2(\pi\alpha)^2 n^{\mathrm{d}}_{\mathrm{i}} \, v k_{\mathrm{F}} \, (\tilde{d}/\mathrm{e})^2 \left\{ \begin{matrix} I_2 \\ J_2 \end{matrix} \right. , \tag{7.35}$$

where $I_2$ and $J_2$ are given by Eq. (7.28). In the absence of other types of scatterers, Eq. (7.19) yields the conductivity

$$\overline{\sigma}^{\mathrm{d}} = \frac{ge^2}{h}\frac{1}{(2\pi\alpha)^2 I_2}\frac{1}{n_{\mathrm{i}}^{\mathrm{d}}(\tilde{d}/e)^2}. \tag{7.36}$$

Note that this result for the conductivity is independent of the electron concentration.

If the graphene sample is disordered even in the absence of the molecular switches, it is natural to consider a situation in which the dominant source of scattering is due to $N_{\mathrm{i}}^{\mathrm{c}}$ charged impurities, supplemented by $N_{\mathrm{i}}^{\mathrm{d}}$ additional dipolar scatterers. For the moment, we assume that these latter scatterers are not associated with a monopolar potential. If the distributions of these two different types of scatterers are statistically independent, the total transport scattering rate is obtained by Matthiessen's rule through adding the two individual scattering rates, $1/\tau_{\mathrm{tr}}^{\mathrm{c,d}} = 1/\tau_{\mathrm{tr}}^{\mathrm{c}} + 1/\tau_{\mathrm{tr}}^{\mathrm{d}}$. Hence, switching the dipole moments causes a relative change of the conductivity

$$\frac{\delta\sigma}{\overline{\sigma}^{\mathrm{c}}} \simeq -2(\pi\alpha)^2\frac{J_0 I_2}{I_0}\delta n_{\mathrm{i}}\, k_{\mathrm{F}} l_{\mathrm{c}}\,(\tilde{d}/e)^2, \tag{7.37}$$

reflecting the fact that the conductivity decreases when scatterers are added to the system. We have used $\overline{\sigma}^{\mathrm{d}} \ll \overline{\sigma}^{\mathrm{c}}$ which holds for $k_{\mathrm{F}}d/e \ll 1$. This limit is relevant for typical electron densities in graphene, $n \approx 10^{12}\mathrm{cm}^{-2}$, and even rather large dipole moments $d \approx 10\mathrm{D}$ (yielding $k_{\mathrm{F}}d/e \approx 0.03$). The prefactor in Eq. (7.37) is given by $2(\pi\alpha)^2 J_0 I_2/I_0 \approx 1.7$ for impurities close to the graphene sheet, $zk_{\mathrm{F}} \ll 1$, see Eq. (7.28). Note that the mean free path $l_{\mathrm{c}} = v\tau_{\mathrm{c}}$ is proportional to $k_{\mathrm{F}}$, see Eq. (7.27). Thus, the influence of the dipoles on the conductivity is quadratic in $(k_{\mathrm{F}}d/e)$, which increases linearly with the electron density $n$.

Frequently, an attached molecular switch will affect electronic transport not only through its dipole moment, but may also be associated with a monopolar scattering potential, *e.g.*, due to some degree of charge transfer between graphene and the molecular switch. For this reason, we generalize our results to situations with $N_{\mathrm{i}}$ charged impurities (with screened potential $\tilde{V}_{\boldsymbol{q}}^{\mathrm{c}}$) and $\delta N_{\mathrm{i}}$ impurities with an additional dipole moment, where the latter also transfer an amount $\delta e = \zeta e$ of charge to the graphene. Then, the scattering potential for the latter takes the form $\tilde{V}_{\boldsymbol{q}}^{\mathrm{c+d}} = \tilde{V}_{\boldsymbol{q}}^{\mathrm{c}} + \tilde{V}_{\boldsymbol{q}}^{\mathrm{d}}$. The corresponding transport scattering rate, Eq. (7.20), is

$$\frac{1}{\tau_{\mathrm{tr}}^{\mathrm{c+d}}} = \frac{1}{\tau_{\mathrm{tr}}^{\mathrm{c}}} + \frac{1}{\tau_{\mathrm{tr}}^{\mathrm{d}}} + \frac{1}{\tau_{\mathrm{tr}}^{\mathrm{c,d}_\perp}}, \tag{7.38}$$

where $\tau_{\mathrm{tr}}^{\mathrm{c}}$ and $\tau_{\mathrm{tr}}^{\mathrm{d}}$ are given by Eqs. (7.27) and (7.35), and we introduce the shorthand

$$\left.\begin{matrix} 1/\tau_{\mathrm{tr}}^{\mathrm{c,d}_\perp} \\ 1/\tau^{\mathrm{c,d}_\perp} \end{matrix}\right\} = -2\delta n_{\mathrm{i}}\pi^2\zeta\alpha v\frac{d_\perp}{e}\left\{\begin{matrix} I_1 \\ J_1 \end{matrix}\right. , \tag{7.39}$$

with $\delta n_{\mathrm{i}}$ the density of switched molecules. This latter contribution involves interference between monopole and dipole scattering. Interestingly, $d_\perp$ enters linearly into this

contribution while the in-plane component of the individual dipoles cancels out. This cancellation follows from the fact that $V_{\boldsymbol{q}}^{\mathrm{d}\parallel}$ in Eq. (7.32) is purely imaginary, while the Coulomb potential is real. $I_1$ and $J_1$ follow from Eq. (7.28) and we have used the (impurity averaged) matrix element of the total impurity potential

$$\overline{|\langle \boldsymbol{k}|V_{\mathrm{i}}^{\mathrm{c+d}}|\boldsymbol{k'}\rangle|^2} = \frac{1+\cos\vartheta}{2\Omega}\Big[(n_{\mathrm{i}}+\delta n_{\mathrm{i}}\zeta^2)|\tilde{V}_{\boldsymbol{q}}^{\mathrm{c}}|^2 + 2\delta n_{\mathrm{i}}\zeta\tilde{V}_{\boldsymbol{q}}^{\mathrm{c}}\tilde{V}_{\boldsymbol{q}}^{\mathrm{d}\perp} + \delta n_{\mathrm{i}}|\tilde{V}_{\boldsymbol{q}}^{\mathrm{d}\perp}|^2 + \frac{1}{2}\delta n_{\mathrm{i}}|\tilde{V}_{\boldsymbol{q}}^{\mathrm{d}\parallel}|^2\Big]. \tag{7.40}$$

The relative change of the conductivity due to switching of the dipole moments is then

$$\frac{\delta\sigma}{\overline{\sigma}^{\mathrm{c}}} \simeq \delta n_{\mathrm{i}}\,\frac{2J_0(\pi\alpha)^2}{I_0}\,\Big[I_1\zeta\, l_{\mathrm{c}} d_\perp/e - I_2\, k_{\mathrm{F}} l_{\mathrm{c}}\,(\tilde{d}/e)^2\Big], \tag{7.41}$$

with $\delta\sigma = \left(\overline{\sigma}^{\mathrm{c+d}} - \overline{\sigma}^{\mathrm{c}}\right)$ and again assuming that the switching induced change in the conductivity is small. The prefactors can be approximated by $2(\pi\alpha)^2 J_0 I_1/I_0 \approx 2.3$ and $2(\pi\alpha)^2 J_0 I_2/I_0 \approx 1.7$ for $q_{\mathrm{TF}}/(2k_{\mathrm{F}}) = g\alpha/2 \approx 2$ and $4zk_{\mathrm{F}} \ll 1$, see Eq. (7.28).

In the Boltzmann limit scattering events are independent and thus interference can only appear for scattering channels (such as monopole and dipole contributions) associated with the same scatterer. Nevertheless, our result (7.41) indicates that such interference contributions can significantly increase the sensitivity of the conductivity to changes of the molecular switching state. Indeed, while the change in conductivity due to switching is quadratic in the molecular dipole moment in the absence of interference, see Eqs. (7.36) and (7.37), interference gives rise to a contribution which is *linear* in $d_\perp$, and thus dominant in the relevant limit $k_{\mathrm{F}} d/e \ll 1$.

Assuming a perpendicular dipole moment and charge transfer to the graphene, we estimate that a density of switches $\delta n_{\mathrm{i}} \approx 5\times 10^{10}\mathrm{cm}^{-2}$ is required for changing the conductivity by 1%, see Eq. (7.41). (Here we assume $n \approx 10^{12}\mathrm{cm}^{-2}$, $l \approx 50\mathrm{nm}$ and $d \approx 10\mathrm{D}$.)

## 7.5. Effect of switches on the conductance – quantum coherent transport

In the previous section we have seen that interference between charge and dipole scattering originating from the same scatterer can be favorable for the read-out of the switching state. Now we consider quantum coherent transport, implying that interference between partial waves scattered at different impurities becomes relevant such that one might again expect an enhanced sensitivity to the switching state of the molecules.

### 7.5.1. Mesoscopic fluctuations

Because a macroscopic sample can be viewed as built of a number of mesoscopic phase coherent subsystems, which are quantum mechanically independent of each other, the macroscopic measurement effectively averages over these subsystems. The system becomes

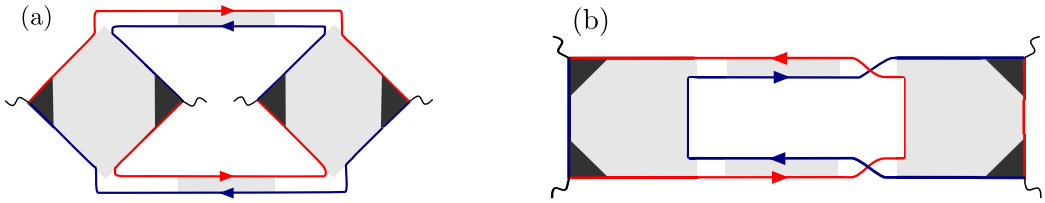


Figure 7.7. Diagrams involved in the UCF. The building blocks of these diagrams are shown in Figs. 7.8 and 7.9.

*self-averaging* and is characterized by intensive quantities, such as the impurity-averaged electric conductivity $\overline{\sigma}$. At this level, the conductivity can be obtained from the Boltzmann equation, as we did in the previous section.

In contrast, in the mesoscopic regime (*i.e.*, at sufficiently low temperatures and small system sizes where the phase coherence length becomes larger than the sample dimensions), interference between multiple scattering trajectories is important and a change in the microscopic impurity configuration or a continuous system parameter, such as the Fermi energy or an applied magnetic field, yields reproducible variations of the conductance. It is well known that the typical magnitude of these fluctuations around the mean value of the conductance is universal in the sense that it depends only on the sample geometry but is independent of the microscopic details of disorder [Lee and Stone, 1985; Al'tshuler, 1985; Lee *et al.*, 1987; Kane *et al.*, 1988]. Importantly, such changes in the conductance are already effected by rather small changes in the impurity potential [Al'tshuler and Spivak, 1985; Feng *et al.*, 1986]. This suggests that indeed, interference terms involving different scatterers may make a graphene sheet, in the regime of quantum coherent transport, a particularly accurate sensor of the switching state of the attached molecules. The general concepts of mesoscopic fluctuations have been introduced by Lee and Stone [1985], Al'tshuler [1985], Lee *et al.* [1987], and Kane *et al.* [1988] (see the book by Akkermans and Montambaux [2007] for a pedagogical account). For the peculiarities of universal conductance fluctuations in graphene, we refer to [Kechedzhi *et al.*, 2009; Kharitonov and Efetov, 2008; Rycerz *et al.*, 2007; Berezovsky *et al.*, 2010].

### 7.5.2. Diagrammatic calculation

We consider charged impurities as the dominant source of scattering and an impurity potential $V_\mathrm{i}$, which is formed by $N_\mathrm{i}$ of these Coulomb scatterers. We are interested in the change of the conductance when the impurity potential changes, $V_\mathrm{i} \to V_\mathrm{i}'$. To be specific, we assume that $\delta N_\mathrm{i}$ charged impurities acquire an additional dipole moment causing the change in the impurity potential. (We note that the derivation would follow the same lines, and leave our results unaffected, when dipolar impurities were added to a background of charged impurities.) For generality, we consider the correlation function of the conductance evaluated not only for different impurity potentials, but also at different Fermi energies $\epsilon_\mathrm{F}$ and $\epsilon_\mathrm{F}'$.

A measure for the effect of the microscopic modifications is the conductivity-conductivity correlation function,

$$\overline{\Delta\sigma(\xi)\Delta\sigma(\xi')} = \overline{[\sigma(\xi) - \overline{\sigma}(\xi)]\,[\sigma(\xi') - \overline{\sigma}(\xi')]}, \tag{7.42}$$

where $\xi$ is the quantity which is modified (*e.g.* $\xi = \{\epsilon_\mathrm{F}, V_\mathrm{i}\}$), and the conductivity $\sigma$ is given by Eq. (7.17). The diagrams representing $\overline{\Delta\sigma\Delta\sigma}$ consist of two conductivity loops (one evaluated for Fermi energy $\epsilon_\mathrm{F}$ and impurity potential $V_\mathrm{i}$, the other for $\epsilon'_\mathrm{F} = \epsilon_\mathrm{F} + \omega$ and impurity potential $V'_\mathrm{i}$) which are connected by impurity lines. There are two distinct possibilities to connect the two loops, $\overline{\Delta\sigma\Delta\sigma} = \overline{\Delta\sigma\Delta\sigma}^{(a)} + \overline{\Delta\sigma\Delta\sigma}^{(b)}$, as shown in Figs. 7.7 (a) and (b), respectively. Note that unconnected loops correspond to $\overline{\sigma}^2$ and hence do not enter into the variance.

Based on the standard Feynman rules for disordered systems [Akkermans and Montambaux, 2007], Fig. 7.7 (a) and (b) translate into the analytical expressions

$$\overline{\Delta\sigma(\xi)\Delta\sigma(\xi')}^{(a)} = \left(\frac{g\hbar}{4\pi\Omega}\right)^2 4\beta \sum_{\boldsymbol{q}} (H_1)^2 \left|\tilde{D}_\omega(\boldsymbol{q})\right|^2, \tag{7.43}$$

and

$$\overline{\Delta\sigma(\xi)\Delta\sigma(\xi')}^{(b)} = \left(\frac{g\hbar}{4\pi\Omega}\right)^2 8\beta \sum_{\boldsymbol{q}} (H_2)^2 \,\mathrm{Re}\left[\left(\tilde{D}_\omega(\boldsymbol{q})\right)^2\right], \tag{7.44}$$

which are valid in the diffusive limit, $k_\mathrm{F} l \gg 1$ and $\omega\tau \ll 1$. The building blocks of the diagrams, the short ranged Hikami boxes $H_{1(2)}$ and the long ranged diffuson $\tilde{D}_\omega(\boldsymbol{q})$, are depicted in Figs. 7.8 and 7.9. The corresponding analytical expressions are given below in Eqs. (7.50) and (7.54). The expressions for $\overline{\Delta\sigma\Delta\sigma}^{(a)}$ and $\overline{\Delta\sigma\Delta\sigma}^{(b)}$ also involve a combinatorial factor of 4, which reflects that the diagrams in Fig. 7.7 (a) and (b) are invariant under interchange of retarded and advanced Green's functions as well as of momentum labels. In a time reversal invariant system, additional contributions stem from replacing the diffusons by Cooperons [Akkermans and Montambaux, 2007]. This is taken care of by the symmetry factor $\beta = 2\,(1)$ for a system with (without) time reversal invariance.

We now turn to a brief discussion of the constituents of these fluctuation diagrams, namely the diffusons $\tilde{D}_\omega$ and the Hikami boxes $H_{1(2)}$. We follow standard procedures [Akkermans and Montambaux, 2007], which have been also applied to the study of graphene [Kechedzhi *et al.*, 2008, 2009; Kharitonov and Efetov, 2008; Rycerz *et al.*, 2007; Berezovsky *et al.*, 2010].

### Diffusons

The diffusons $\tilde{D}_\omega$ describe the diffusive motion of electrons across the sample. As depicted in Fig. 7.8, they are represented diagrammatically by ladder diagrams in which the two Green's functions are connected by any number of parallel impurity lines. Analytically,

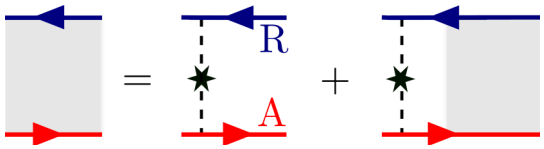


Figure 7.8. Ladder series for the diffuson. The retarded (advanced) Green's function, shown in blue (red), is given by $\overline{G}^{\mathrm{R}}_{\epsilon_\mathrm{F}}(\boldsymbol{k})$ [$\overline{G}^{\mathrm{A}}_{\epsilon_\mathrm{F}-\omega}(\boldsymbol{k}-\boldsymbol{q})$].

this series of ladder diagrams satisfies the integral equation

$$\begin{aligned}\tilde{D}_\omega(\hat{\boldsymbol{k}},\hat{\boldsymbol{k}}',\boldsymbol{q}) =& U_2(\hat{\boldsymbol{k}}-\hat{\boldsymbol{k}}') \\ &+ \frac{1}{\Omega}\sum_{\hat{\boldsymbol{k}}''}\tilde{D}_\omega(\hat{\boldsymbol{k}},\hat{\boldsymbol{k}}'',\boldsymbol{q})\overline{G}^{\mathrm{R}}_{\epsilon_\mathrm{F}}(\boldsymbol{k})\overline{G}^{\mathrm{A}}_{\epsilon_\mathrm{F}-\omega}(\boldsymbol{k}-\boldsymbol{q})U_2(\hat{\boldsymbol{k}}''-\hat{\boldsymbol{k}}'),\end{aligned} \tag{7.45}$$

where we leave implicit that the two Green's functions are evaluated for the impurity potentials $V_\mathrm{i}$ and $V_\mathrm{i}'$, respectively, while impurity lines connecting them represent the correlators $\overline{V_\mathrm{i}V_\mathrm{i}'}$. For convenience, we use the shorthand notation

$$U_1(\hat{\boldsymbol{k}}-\hat{\boldsymbol{k}}') = \frac{\Omega}{2}\Big(\overline{|\langle\boldsymbol{k}|V_\mathrm{i}|\boldsymbol{k}'\rangle|^2} + \overline{|\langle\boldsymbol{k}|V_\mathrm{i}'|\boldsymbol{k}'\rangle|^2}\Big), \tag{7.46}$$

$$U_2(\hat{\boldsymbol{k}}-\hat{\boldsymbol{k}}') = \Omega\,\overline{\langle\boldsymbol{k}|V_\mathrm{i}|\boldsymbol{k}'\rangle\langle\boldsymbol{k}'|V_\mathrm{i}'|\boldsymbol{k}\rangle}. \tag{7.47}$$

In particular, we will need the quantities

$$\langle U_1\rangle = \frac{\hbar}{2\pi\nu_0}\left(\frac{1}{\tau^\mathrm{c}} + \frac{1}{2\tau^\mathrm{d}} + \frac{1}{2\tau^{\mathrm{c,d}_\perp}}\right), \tag{7.48}$$

$$\langle U_2\rangle = \frac{\hbar}{2\pi\nu_0}\left(\frac{1}{\tau^\mathrm{c}} + \frac{1}{2\tau^{\mathrm{c,d}_\perp}}\right), \tag{7.49}$$

where we have used the notation $\langle U_i\rangle \equiv \langle U_i(\hat{\boldsymbol{k}}-\hat{\boldsymbol{k}}')\rangle_{\hat{\boldsymbol{k}}'}$ for the angular average, evaluated at $k = k_\mathrm{F}$. Solving the integral equation (7.45) results in

$$\tilde{D}_\omega(\boldsymbol{q}) \simeq \frac{\hbar/(2\pi\nu_0\tau^2)}{Dq^2 - \mathrm{i}\omega + \big(\langle U_1\rangle/\langle U_2\rangle - 1\big)/\tau}, \tag{7.50}$$

which is valid for small changes $\langle U_1\rangle - \langle U_2\rangle$ in the impurity configuration, see App. C for a more detailed description. Here, we also introduced the scattering rate $1/\tau = (2\pi/\hbar)\nu_0\langle U_1\rangle$.

### Hikami boxes

In the fluctuation diagrams, see Fig. 7.7, the diffusons are connected by Hikami boxes, labeled $H_1$ and $H_2$, respectively, which are depicted in Fig. 7.9. Approximating $k_\mathrm{F}l \gg 1$ and $\omega\tau \ll 1$, three diagrams contribute to leading order to the Hikami boxes $H_i = H_i^{(a)} + H_i^{(b)} + H_i^{(c)}$, with $i = 1, 2$.

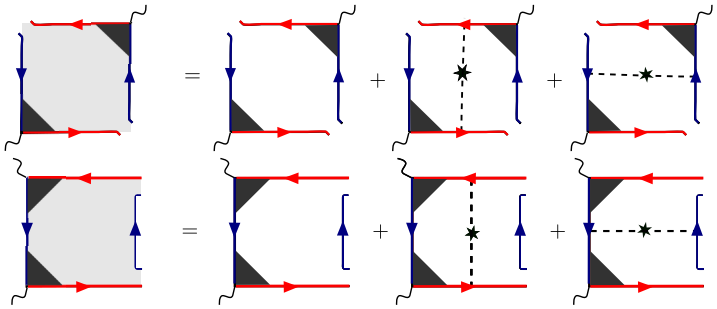

Figure 7.9. Hikami boxes $H_1$ (top) and $H_2$ (bottom).

The diagram $H_2^{(a)}$ consists of two retarded and two advanced Green's functions with momentum $\boldsymbol{k}$. In contrast to the evaluation of the diffuson, the Hikami boxes are rather short-ranged and we can neglect the $\boldsymbol{q}$-dependences. Because of the vertex corrections a factor $\tau_{\rm tr}/\tau$ comes with each of the current vertices so that we obtain

$$H_2^{(a)} = \left(ev\frac{\tau_{\rm tr}}{\tau}\right)^2 \sum_{\boldsymbol{k}} \cos^2\vartheta \left(\overline{G}^R_{\epsilon_{\rm F}}(\boldsymbol{k})\overline{G}^A_{\epsilon_{\rm F}}(\boldsymbol{k})\right)^2 = 2\pi\left(ev\frac{\tau_{\rm tr}}{\tau}\right)^2 \nu_0\tau^3, \tag{7.51}$$

assuming $(U_1 - U_2)$ to be small. The diagram $H_2^{(b)}$ consists of twice two retarded and one advanced Green's function with the same wave vector, respectively, and an additional impurity cross, so that

$$\begin{aligned} H_2^{(b)} &= \left(ev\frac{\tau_{\rm tr}}{\tau}\right)^2 \sum_{\boldsymbol{k}} \cos^2\vartheta \left(\overline{G}^R_{\epsilon_{\rm F}}(\boldsymbol{k})\right)^2 \overline{G}^A_{\epsilon_{\rm F}}(\boldsymbol{k}) \sum_{\boldsymbol{k}'} n_{\rm i}|V_{\boldsymbol{q}}|^2 \frac{1+\cos\vartheta'}{2} \left(\overline{G}^R_{\epsilon_{\rm F}}(\boldsymbol{k}')\right)^2 \overline{G}^A_{\epsilon_{\rm F}}(\boldsymbol{k}') \\ &= -\frac{1}{2}H_2^{(a)}. \end{aligned} \tag{7.52}$$

Here we have replaced the sum by an integral and used that the integration over two retarded and one advanced Green's function yields a factor $(\tau)^2/\mathrm{i}$ while the extra factor $|V_{\boldsymbol{q}}|^2$ contributes a factor $1/\tau$. The calculation of $H_2^{(c)}$ follows similar lines, but here the two current vertices are evaluated at different wave vectors with the consequence that the extra $|V_{\boldsymbol{q}}|^2$ yields a factor $(1/\tau - 1/\tau_{\rm tr})$, resulting in

$$H_2^{(c)} = \left(\frac{\tau_{\rm tr}}{\tau} - 1\right) H_2^{(a)}. \tag{7.53}$$

In a similar manner the other type of Hikami boxes, $H_1$, is evaluated. One finds $H_1^{(a)} = H_2^{(a)}$ and $H_1^{(b)} = H_1^{(c)} = H_2^{(c)}$. Combining these contributions yields

$$H_1 = 2H_2 = \frac{4\pi}{\hbar^3} D\nu_0\tau^2. \tag{7.54}$$

#### Conductance-Conductance correlation

We can now combine these building blocks and obtain the correlation function of the conductance. Relating conductivity and conductance through Ohm's law, $G = (L_y/L_x)\sigma$, we obtain from inserting the expressions for diffusons and the Hikami boxes, Eqs. (7.50) and (7.54), into Eqs. (7.43) and (7.44) that

$$\overline{\Delta G(\xi)\,\Delta G(\xi')} = \frac{2\beta g^2}{\pi^4}\Big(\frac{e^2}{h}\Big)^2 \sum_m \left\{ \mathrm{Re}\left(\frac{1}{\lambda_m + \Delta\lambda}\right)^2 + 2\left|\frac{1}{\lambda_m + \Delta\lambda}\right|^2 \right\}. \tag{7.55}$$

Here, we use the abbreviations $m = \{m_x, m_y\}$, and

$$\lambda_m = (m_x)^2 + (m_y\, L_x/L_y)^2\,, \tag{7.56}$$

$$\Delta\lambda = -\frac{L_x^2}{D\pi^2}\left[\mathrm{i}\omega + \frac{1}{\tau}\left(1 - \langle U_1\rangle/\langle U_2\rangle\right)\right]. \tag{7.57}$$

The boundary conditions of the system, namely perfect leads and hard walls at the transverse boundaries, imply the quantization $q_\alpha = m_\alpha \pi/L_\alpha$ ($\alpha = x, y$) with $m_x = \{1, ..., \infty\}$ and $m_y = \{0, 1, ..., \infty\}$. We note that both the Hikami boxes and the diffusons depend separately on the microscopic details of the sample, as encapsulated in the scattering rates and the density of states. Nevertheless, in the conductance-conductance correlation function, Eq. (7.55), these quantities cancel against each other such that all microscopic details enter only through $\Delta\lambda$.

### 7.5.3. Results

In order to see the influence of the quantum coherent processes, we first review [Akkermans and Montambaux, 2007; Kechedzhi *et al.*, 2008, 2009; Kharitonov and Efetov, 2008; Rycerz *et al.*, 2007; Berezovsky *et al.*, 2010] the variance of the conductance, $\overline{(\Delta G)^2} = \overline{\left[G - \overline{G}\right]^2}$, describing the average magnitude of the universal conductance fluctuations. From Eq. (7.55) (with $\Delta\lambda = 0$) we obtain

$$\overline{(\Delta G)^2} = \frac{6\beta}{\pi^4}\left(\frac{ge^2}{h}\right)^2 \sum_m \frac{1}{(\lambda_m)^2} = \beta\eta\left(\frac{g\mathrm{e}^2}{h}\right)^2, \tag{7.58}$$

where $\eta \simeq 1/15$ for $L_x \gg L_y$, and $\eta \approx 0.1$ for a square device. Hence the amplitude of the fluctuations depends on the sample geometry but is universal in the sense, that it is independent of the electron concentration and the microscopic type or configuration of disorder. Comparing the amplitude of the fluctuations with the average conductance yields

$$\frac{\sqrt{\overline{(\Delta G)^2}}}{\overline{G}} = \frac{2\sqrt{\beta\eta}}{I_0 J_0 \pi^2 \alpha^4}\frac{L_x}{L_y}\frac{1}{k_\mathrm{F} l_\mathrm{c}}, \tag{7.59}$$

again assuming that charged scatterers, cp. Eq. (7.26), predominantly limit the conductance. For a square device this yields $\sqrt{\overline{(\Delta G)^2}}/\overline{G} \approx 7.1/(k_\mathrm{F} l_\mathrm{c})$. This indicates that

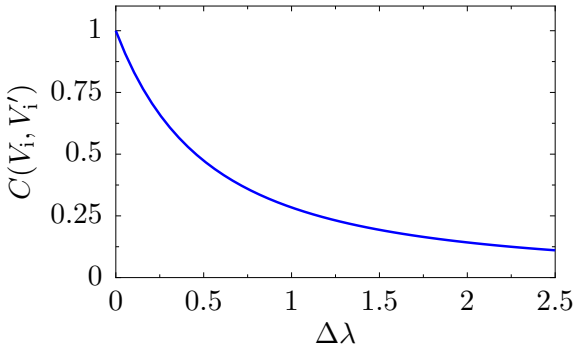


Figure 7.10. The normalized correlation function $C(V_\mathrm{i}, V_\mathrm{i}') = \overline{\Delta G(V_\mathrm{i})\Delta G(V_\mathrm{i}')}/\overline{(\Delta G)^2}$, plotted as a function of $\Delta\lambda$.

for charged impurities, the quantum coherent processes are more important at large Fermi wavelengths and high impurity concentrations (albeit such that our underlying assumption of $k_\mathrm{F} l_\mathrm{c} \gg 1$ still holds).

Switching the decorating molecules affects the correlation function $\overline{\Delta G(V_\mathrm{i})\,\Delta G(V_\mathrm{i}')}$, see Eq. (7.55), via a change of the diffuson pole,

$$\begin{aligned}\Delta\lambda &= \frac{L_x^2}{D\pi^2}\,\frac{\langle U_1\rangle - \langle U_2\rangle}{\langle U_2\rangle}\,\frac{1}{\tau} \simeq \frac{L_x^2}{D\pi^2}\,\frac{1}{2\tau^\mathrm{d}} \\ &\simeq (2\alpha^2 I_0 J_2/J_0)\,(L_x/L_y)\delta N_\mathrm{i}\,(k_\mathrm{F}/l_\mathrm{c})\,(\tilde{d}/e)^2, \end{aligned} \tag{7.60}$$

see Eq. (7.57). Note that this depends linearly on the number of switches $\delta N_\mathrm{i}$ and is independent of the electron concentration. Again, we assume that the monopole contribution of the charged impurities predominantly limits the conductivity, and thus $\left(\langle U_1\rangle - \langle U_2\rangle\right)/\langle U_2\rangle$ is a small quantity. The prefactor can be approximated by $(2\alpha^2 I_0 J_2/J_0) \approx 0.028$, see Eq. (7.28). The dependence of $\overline{\Delta G(V_\mathrm{i})\,\Delta G(V_\mathrm{i}')}$ on $\Delta\lambda$ can be easily evaluated numerically and is depicted in Fig. 7.10. One finds that the correlation function varies linearly with $\Delta\lambda$ for small modifications of the microscopic impurity configuration. We thus conclude that the typical variation of the conductance with switching state is given by

$$\frac{\sqrt{\overline{\left[G(V_\mathrm{i}) - G(V_\mathrm{i}')\right]^2}}}{\sqrt{\overline{(\Delta G)^2}}} \simeq \chi\,\frac{\sqrt{\delta N_\mathrm{i}}}{\sqrt{k_\mathrm{F} l_\mathrm{c}}}\,(k_\mathrm{F}\tilde{d}/e), \tag{7.61}$$

where we lumped the numerical prefactors into $\chi = 2\alpha\sqrt{(I_0 J_2/J_0)L_x/L_y}$ which is $\chi \approx 0.23$ for a square device. Note that Eq. (7.61) depends linearly on the dipole moment $d$. In contrast to the Boltzmann interference result, this also holds for dipoles which are oriented parallel to the graphene sheet, $d = d_\parallel$, as well as for molecular switches which are pure dipole scatterers. We also note that in the Boltzmann limit, the changes of the conductance scale with $\delta n_\mathrm{i}$ and are larger for clean devices and large electron densities,

see Eq. (7.41). In contrast, in the mesoscopic regime the changes are proportional to $\sqrt{\delta N_\mathrm{i}}$, cf. Eq. (7.61), and larger impurity concentrations $n_\mathrm{i}$ and large Fermi wavelengths are favorable for the effect of interference.

Our result Eq. (7.61) indicates that the conductance of mesoscopic samples (here assuming $L_x = L_y \approx 5\mu$m) would be modified by 10% of the UCF even for moderately low densities of switches $\delta n_\mathrm{i} \approx 10^9 \mathrm{cm}^{-2}$. (Again we assume $n \approx 10^{12}\mathrm{cm}^{-2}$, $l \approx 50$nm and $d \approx 10$D.)

## 7.6. Summary

Due to its two-dimensional nature, graphene layers are attractive substrates for functionalization by molecular switches. In this chapter, we have analyzed how the conductance of a graphene layer may serve as an all-electrical read-out of the molecular switching state. Specifically, we have investigated theoretically the spiropyran-merocyanine system where the two switching states affect the charge carriers via large changes in the electric dipole moment.

Within a quasiclassical approach, quantum interference has to emerge from scattering on a single impurity. In this case, we find a strong sensitivity to the switching state when the molecular switches cause scattering of carriers both through a monopolar contribution (*e.g.*, due to charge transfer between graphene and the molecular switches) as well as a dipolar contribution. Specifically, the interference contribution involving the corresponding scattering amplitudes is nonzero whenever the molecular dipole moment has a component perpendicular to the graphene layer. In this quasiclassical regime, high densities of electrons and switches, but otherwise clean samples, are favorable for the use in molecular electronics.

In the regime of quantum coherent transport, the quantum interference contributions result in a switching-induced change of the conductance which is linear in the change of the molecular dipole moment, albeit with a random sign. This mesoscopic contribution becomes particularly important in samples with low carrier density for the read-out of the switching-state. In the regime of quantum coherent transport, larger impurity concentrations and smaller electron densities are favorable for the effect of interference.

# 8. Conclusions and Outlook

In this thesis we have discussed how the transport properties of coherent conductors are affected by collective modes. We have paid particular attention to the regime in which the latter, *e.g.*, vibrations or localized spin degrees of freedom, are moving slowly so that the conduction electrons are subject to a quasistatic configuration. In this limit, we can work within a non-equilibrium Born-Oppenheimer (NEBO) approximation, in which the collective modes obey a Langevin dynamics subject to forces exerted by the conduction electrons. Within the NEBO approximation, we can derive the full dependences of these forces and of the current on the bias voltage and the collective mode coordinates. In a central part of this thesis we have expressed these forces in terms of the scattering matrix of the system, extending the celebrated Landauer-Büttiker approach to the study of current-induced forces in general out-of-equilibrium situations, and providing a general theory of the interplay of coherent electronic transport and local collective modes.

In the simplest case of one collective degree of freedom, the Langevin equation contains an average force, a friction force, as well as a fluctuating Langevin force. The average force depends only on the mode coordinate and is thus necessarily conservative. The friction force is linear in the mode velocity, although the friction coefficient will in general still depend on the mode coordinate. In thermal equilibrium situations, thermodynamic stability requires that the friction coefficient is positive. This is no longer the case in general non-equilibrium situations where energy can be transferred from the electronic degrees of freedom to the collective degree of freedom. As a result, the friction coefficient can become negative in the presence of a bias voltage. Finally, in thermal equilibrium, the variance of the fluctuating force is related to the friction coefficient by the fluctuation-dissipation theorem. Again, this relation no longer holds in out-of-equilibrium situations but the NEBO approximation allows one to obtain the fluctuating force beyond the fluctuation-dissipation theorem.

When more than one collective degrees of freedom couples to the current flowing through the device, several new effects appear. First, the average force can become non-conservative. Second, the contribution to the force that is linear in the velocity not only contains a frictional contribution but also an effective Lorentz force. We can again write these contributions in terms of the scattering matrix of the phase coherent conductor. This allows one to make general statements about the current-induced forces from symmetry considerations. For instance, in thermal equilibrium the Lorentz-like force can appear only in the absence of time-reversal invariance. In out-of-equilibrium situations, on the other hand, it can be present even in time-reversal invariant systems. In this thesis, we have carried out this general program both for nanoelectromechanical systems where the collective modes correspond to localized mechanical degrees of freedom and for single-molecule junctions containing magnetic molecules.

Applying our formalism to the study of NEMS, we have considered the influence of the applied voltages on the current-induced forces. Here a non-conservative force or a negative damping coefficient in the Langevin equation might be important in order to overcome or compensate for other damping mechanisms, generating dynamical instabilities of the collective mode. We have shown that that this can drive a nanoelectromechanical system into interesting dynamically stable regimes. Specifically, in a limit-cycle the vibrational modes vary periodically in time, providing an operating principle for devices such as sensors or molecular motors. Under certain conditions the average force exerted by the current can be described by a bistable potential giving rise to electronically controlled switches.

We have explored this option of switching also in the context of transport through molecular magnets. Here the resulting current-induced torques have also been analyzed by means of the NEBO approximation, giving rise to Langevin dynamics of the magnetic moment. This has been described by a generalized Landau-Lifshitz-Gilbert (LLG) equation, involving necessarily more than one collective mode degree of freedom. Unlike previous works, our approach does not follow a perturbative route either in the tunneling between leads and the molecule or in the coupling between the electronic spin and the molecular magnetic moment. Accordingly, we obtain the full dependence of the parameters of the LLG equation on the state of the molecular moment as well as on the applied bias and gate voltages. In the presence of spin-polarized leads, due to the analog of a non-conservative force, the orientation of the localized magnetic moment can be controlled by the direction of the current through the device – a notably useful effect for switches. We also express the various torques entering into the LLG equation in terms of the scattering matrix, generalizing previous results in the literature to non-equilibrium situations.

It is also interesting to consider the backaction of the collective modes on the electronic transport. For the slow mechanical modes under study, the current can be obtained from the Landauer-Büttiker formula in the strictly adiabatic limit. When including the first adiabatic correction in thermal equilibrium situations, the problem becomes equivalent to adiabatic quantum pumping, which has been studied extensively in the literature. Within the NEBO approximation, we can generalize these results to out-of-equilibrium situations. Generally, transport measurements encode information about the collective modes which can serve, *e.g.*, as a detector of the collective mode dynamics or the read-out of the switching dynamics.

Starting from a microscopic model we have calculated the current-induced forces in terms of non-equilibrium Green's functions and have expressed the results in the language of scattering theory. In order to express all current-induced forces in terms of the scattering matrix, we have realized that it is necessary to expand the latter beyond the strictly adiabatic approximation. This introduces a new fundamental quantity into the problem, the A-matrix, which needs to be calculated together with the frozen S-matrix for a given system. The average as well as the fluctuating force can be expressed solely in terms of the adiabatic S-matrix. In equilibrium, the frictional force reduces to an expression in terms of the adiabatic S-matrix, in accordance with the fluctuation-dissipation theorem. Out of equilibrium, however, an important new contribution involving the A-matrix

appears. In order to express the Lorentz-like force, the A-matrix is always required, even in thermal equilibrium.

One of the fascinating possibilities opened by systems which couple nanoscale electronic transport to localized collective modes is the realization of new functional devices. We have explored this possibility in two specific systems. In one of these, the idea is to modify the conductance of graphene sheets through attached molecular switches. Due to its two dimensional nature, graphene is a particularly attractive substrate for this purpose. Indeed, this two dimensionality suggests that the conduction properties of graphene will be strongly affected when switching the attached molecules. Specifically, we have considered the spiropyran-merocyanine system which is characterized by a large difference in the electric dipole moment between the two switching states. Our theory suggests that the sensitivity to the switching state is particularly pronounced in the regime of coherent electronic transport where quantum interference causes universal conductance fluctuations.

In another device application, we have discussed a setup which allows one to cool a NEMS. We have investigated the interaction between a vibrational mode and electrons tunneling through a double quantum dot for general coupling strengths. When the electronic levels are tuned in an appropriate way, we have shown that the transport through the device is accompanied more frequently by absorption than by emission of phonons, providing the functionality of a refrigerator. This may be helpful in achieving the ultimate goal of reaching the quantum mechanical ground state of the vibrational mode.

A fascinating topic of recent research is the construction of machines at the nanoscale. Indeed, several recent experiments suggest that the coupling between electronic transport and collective degrees of freedom can generate directed (rotational or translational) motion, such as propelling molecules [Tierney *et al.*, 2011] or so-called nano-cars [Kudernac *et al.*, 2011]. We believe that our general theory of current-induced forces will have interesting applications in this context and will thus contribute to the understanding and the fabrication of these intriguing devices.

# Appendix

# A. Current-induced forces

In this appendix we provide some concrete expressions for the various current-induced forces of the model systems which we study in Chapter 4.

## A.1. Current-induced forces for the two-level model

The mean force is given by

$$F(X) = -\lambda_1 \Gamma \int \frac{\mathrm{d}\epsilon}{2\pi} \Big[ (f_L + f_R) \frac{2\lambda_1 X(\epsilon - \epsilon_0)}{|\Delta|^2} + (f_L - f_R) \frac{(\epsilon - \epsilon_0)^2 + (\lambda_1 X)^2 - t^2 + (\Gamma/2)^2}{|\Delta|^2} \Big], \tag{A.1}$$

with $\Delta(X) = (\epsilon - \tilde{\epsilon}_- + \mathrm{i}\Gamma_L)(\epsilon - \tilde{\epsilon}_+ + \mathrm{i}\Gamma_R) - t^2$ as stated in the main text. The friction coefficient reads $\gamma^s = \gamma^{s,eq} + \gamma^{s,ne}$, with

$$\begin{aligned} \gamma^{s,eq} =& \frac{\lambda_1^2 \Gamma^2}{4\pi} \int \mathrm{d}\epsilon \Bigg\{ -\frac{\partial_\epsilon f_L + \partial_\epsilon f_R}{|\Delta|^4} \Big[ \big( (\epsilon - \epsilon_0)^2 + (\Gamma/2)^2 + (\lambda_1 X)^2 + t^2 \big)^2 \\ &+ \big(2(\epsilon - \epsilon_0)\lambda_1 X\big)^2 - \big(2(\epsilon - \epsilon_0) t\big)^2 \Big] \\ &+ + \frac{\partial_\epsilon f_R - \partial_\epsilon f_L}{|\Delta|^4} \left[ 4(\epsilon - \epsilon_0)\lambda_1 X \left( (\epsilon - \epsilon_0)^2 + (\Gamma/2)^2 + (\lambda_1 X)^2 - t^2 \right) \right] \Bigg\}, \end{aligned} \tag{A.2}$$

$$\begin{aligned} \gamma^{s,ne} =& \frac{2\lambda_1^2 \Gamma^2 t^2 \lambda_1 X}{\pi} \int \mathrm{d}\epsilon \, \frac{f_R - f_L}{|\Delta|^6} \Big[ \big( (\epsilon - \epsilon_0)^2 - (\lambda_1 X)^2 - t^2 \big)^2 \\ &+ 2(\Gamma/2)^2 \left( (\epsilon - \epsilon_0)^2 + (\lambda_1 X)^2 + t^2 \right) + (\Gamma/2)^4 \Big]. \end{aligned} \tag{A.3}$$

## A.2. Current-induced forces for the two vibrational modes model

Here we list the current-induced forces quantities, calculated from Eqs. (3.37), (3.39), (3.49), and (3.53) for the two-modes example discussed in the main text. For convenience,

we define the following quantities:

$$g_{\alpha 0}(\epsilon) = \frac{(\epsilon-\tilde{\epsilon})^2+\tilde{t}^2+\Gamma_{1-\alpha}^2}{|\Delta|^2}, \tag{A.4}$$

$$g_{\alpha 1}(\epsilon) = \frac{2\tilde{t}\,(\epsilon-\tilde{\epsilon})}{|\Delta|^2}, \tag{A.5}$$

$$g_{\alpha 2}(\epsilon) = \pm\,\frac{-2\tilde{t}\,\Gamma_{1-\alpha}}{|\Delta|^2}, \tag{A.6}$$

$$g_{\alpha 3}(\epsilon) = \pm\,\frac{(\epsilon-\tilde{\epsilon})^2+\Gamma_{1-\alpha}^2-\tilde{t}^2}{|\Delta|^2}, \tag{A.7}$$

where the $+(-)$ refers to $\alpha = L(R)$ and with $1-\alpha = R(L)$ for $\alpha = L(R)$, and $\Delta(X_1,X_2) = (\epsilon-\tilde{\epsilon}+\mathrm{i}\Gamma_L)(\epsilon-\tilde{\epsilon}+\mathrm{i}\Gamma_R)-\tilde{t}^2$.

### A.2.1. Mean force

$$F_1 = -2\int\frac{\mathrm{d}\epsilon}{2\pi}\,\lambda_1\sum_\alpha \frac{f_\alpha(\epsilon)\Gamma_\alpha\left((\epsilon-\tilde{\epsilon})^2+\tilde{t}^2+\Gamma_{1-\alpha}^2\right)}{\left[(\epsilon-\tilde{\epsilon})^2-\tilde{t}^2-\Gamma_L\Gamma_R\right]^2+\left[(\Gamma_L+\Gamma_R)(\epsilon-\tilde{\epsilon})\right]^2} \tag{A.8}$$

$$F_2 = -4\int\frac{\mathrm{d}\epsilon}{2\pi}\,\lambda_2\frac{\tilde{t}\,(\epsilon-\tilde{\epsilon})\;(f_L(\epsilon)\Gamma_L+f_R(\epsilon)\Gamma_R)}{\left[(\epsilon-\tilde{\epsilon})^2-\tilde{t}^2-\Gamma_L\Gamma_R\right]^2+\left[(\Gamma_L+\Gamma_R)(\epsilon-\tilde{\epsilon})\right]^2} \tag{A.9}$$

### A.2.2. Fluctuating force

$$D_{11} = 2\,(\lambda_1)^2\int\frac{\mathrm{d}\epsilon}{2\pi}\sum_{\alpha\beta} f_\alpha(\epsilon)\Gamma_\alpha\,(1-f_\beta(\epsilon))\,\Gamma_\beta\sum_\mu g_{\alpha\mu}g_{\beta\mu} \tag{A.10}$$

$$D_{12} = 2\lambda_1\lambda_2\int\frac{\mathrm{d}\epsilon}{2\pi}\sum_{\alpha\beta} f_\alpha(\epsilon)\Gamma_\alpha\,(1-f_\beta(\epsilon))\,\Gamma_\beta\,(g_{\alpha 0}g_{\beta 1}+g_{\alpha 1}g_{\beta 0}) \tag{A.11}$$

$$D_{22} = 2\,(\lambda_2)^2\int\frac{\mathrm{d}\epsilon}{2\pi}\sum_{\alpha\beta} f_\alpha(\epsilon)\Gamma_\alpha\,(1-f_\beta(\epsilon))\,\Gamma_\beta\times \\ \times\,(g_{\alpha 0}g_{\beta 0}+g_{\alpha 1}g_{\beta 1}-g_{\alpha 2}g_{\beta 2}-g_{\alpha 3}g_{\beta 3}) \tag{A.12}$$

### A.2.3. Damping coefficients

$$\gamma_{11}^{s} = \frac{(\lambda_1)^2}{2\pi} \int \mathrm{d}\epsilon \sum_{\alpha\beta} \left(-\partial_\epsilon f_\alpha(\epsilon)\right) \Gamma_\alpha \Gamma_\beta \sum_{\mu} g_{\alpha\mu} g_{\beta\mu} \tag{A.13}$$

$$\gamma_{12}^{s} = 2\lambda_1\lambda_2 \int \frac{\mathrm{d}\epsilon}{2\pi} \sum_{\alpha\beta} f_\alpha(\epsilon)\Gamma_\alpha \left(-\partial_\epsilon f_\beta(\epsilon)\right) \Gamma_\beta \left(g_{\alpha 0} g_{\beta 1} + g_{\alpha 1} g_{\beta 0}\right) \tag{A.14}$$

$$\gamma_{22}^{s} = 2\left(\lambda_2\right)^2 \int \frac{\mathrm{d}\epsilon}{2\pi} \sum_{\alpha\beta} f_\alpha(\epsilon)\Gamma_\alpha \left(-\partial_\epsilon f_\beta(\epsilon)\right) \Gamma_\beta \left(g_{\alpha 0} g_{\beta 0} + g_{\alpha 1} g_{\beta 1} - g_{\alpha 2} g_{\beta 2} - g_{\alpha 3} g_{\beta 3}\right) \tag{A.15}$$

### A.2.4. "Lorentz" term

$$\gamma_{12}^{a} = -2\tilde{t}\, \frac{\lambda_1\lambda_2}{\pi} \Gamma_L \Gamma_R (\Gamma_L^2 - \Gamma_R^2) \int \mathrm{d}\epsilon \left[\partial_\epsilon \frac{\epsilon - \tilde{\epsilon}}{|\Delta|^2}\right] \left[\frac{f_L - f_R}{|\Delta|^2}\right] \tag{A.16}$$

# B. Magnetic molecules

In this appendix we provide explicit expressions for the self-energies, the Green's functions, the expressions $s_l^0(\boldsymbol{M})$ and $\gamma_{lk}^s(\boldsymbol{M})$, and the noise correlator, which are considered in Chapter 5.

## B.1. Green's functions

The coupling of molecular electronic leveles with leads has been discussed in Section 2.2.3. In the wide band limit for the retarded self-energy we obtain

$$\Sigma_{\alpha,\sigma}^R(\epsilon) \simeq \mathrm{Re}\left(\Sigma_{\alpha,\sigma}^R\right) - \pi \mathrm{i}\, \nu_{\alpha,\sigma} \left|w_\alpha\right|^2, \tag{B.1}$$

with the approximately constant density of states $\nu_{\alpha,\sigma}(\epsilon) \simeq \nu_\sigma$ and $|w|^2 = (|w_L|^2 + |w_R|^2)/2$. We take into account possibly spin-polarized leads through $\Sigma_{c,s}^R = [\Sigma_\uparrow^R \pm \Sigma_\downarrow^R]/2$ as well as $\Gamma_{c,s} = \sum_\alpha \Gamma_{\alpha,c(s)}$, where $\Gamma_{\alpha,c(s)} = (\Gamma_{\alpha,\uparrow} \pm \Gamma_{\alpha,\downarrow})/2$. We also introduce the abbreviation $\Gamma_\sigma/2 = -\mathrm{Im}\left[\Sigma_{L,\sigma}^R(\epsilon) + \Sigma_{R,\sigma}^R(\epsilon)\right] \simeq \pi\, \nu_\sigma\, |w|^2$.

From Eq. (5.7) we find for the frozen retarded Green's function

$$G^R(\epsilon, \boldsymbol{M}) = \frac{1}{\tilde{\epsilon}^2 - \tilde{b}^2}\left[\tilde{\epsilon}\, 1 + \tilde{\boldsymbol{b}}\cdot\boldsymbol{\sigma}\right] = \frac{1}{2}\frac{1 + \boldsymbol{\sigma}\cdot\tilde{\boldsymbol{b}}/\tilde{b}}{\tilde{\epsilon} - \tilde{b}} + \frac{1}{2}\frac{1 - \boldsymbol{\sigma}\cdot\tilde{\boldsymbol{b}}/\tilde{b}}{\tilde{\epsilon} + \tilde{b}}, \tag{B.2}$$

with $\tilde{\epsilon} = \left(\epsilon - \epsilon_0 - \Sigma_c^R\right) \simeq \epsilon - \tilde{\epsilon} + \mathrm{i}\Gamma_c/2$. Here, we include the antisymmetric part of the self-energy in the effective magnetic field,

$$\tilde{\boldsymbol{b}}(t) = \frac{1}{2}(J\boldsymbol{M}(t) + g_e\boldsymbol{B}) + \Sigma_s^R \hat{\mathbf{e}}_z. \tag{B.3}$$

After some algebra we find the following expression for the lesser Green's function, see Eq. (5.10),

$$G^<(\epsilon, \boldsymbol{M}) = G_I^<(\epsilon, \boldsymbol{M}) + G_b^<(\epsilon, \boldsymbol{M})\boldsymbol{b}\cdot\boldsymbol{\sigma} + G_z^<(\epsilon, \boldsymbol{M})\sigma^z + G_t^<(\epsilon, \boldsymbol{M})\boldsymbol{\sigma}\cdot(\hat{\mathbf{e}}_z \times \boldsymbol{b}), \tag{B.4}$$

where the coefficients are given by

$$\begin{aligned}
G_I^<(\epsilon, \boldsymbol{M}) =& \frac{1}{|\Delta(\epsilon, \boldsymbol{M})|^2}\{\Sigma_c^<(\epsilon)[|\tilde{\epsilon}|^2 + |\tilde{\boldsymbol{b}}|^2] + \Sigma_s^<(\epsilon)\, 2[\mathrm{Re}[\tilde{\epsilon}]b_z - \frac{\Gamma_c\Gamma_s}{4}]\},\\
G_b^<(\epsilon, \boldsymbol{M}) =& \frac{2}{|\Delta(\epsilon, \boldsymbol{M})|^2}\{\Sigma_c^<(\epsilon)\mathrm{Re}[\tilde{\epsilon}] + \Sigma_s^<(\epsilon)b_z\},\\
G_z^<(\epsilon, \boldsymbol{M}) =& \frac{1}{|\Delta(\epsilon, \boldsymbol{M})|^2}\{-\Sigma_c^<(\epsilon)\frac{\Gamma_c\Gamma_s}{2} + \Sigma_s^<(\epsilon)[|\tilde{\epsilon}|^2 - |\tilde{\boldsymbol{b}}|^2 + \frac{\Gamma_s^2}{2}]\},\\
G_t^<(\epsilon, \boldsymbol{M}) =& \frac{1}{|\Delta(\epsilon, \boldsymbol{M})|^2}\{\Sigma_c^<(\epsilon)\Gamma_s - \Sigma_s^<(\epsilon)\Gamma_c\}.
\end{aligned} \tag{B.5}$$

Here we use $\Delta(\epsilon, \boldsymbol{M}) = \tilde{\epsilon}^2 - \tilde{b}^2$ and $\tilde{\boldsymbol{b}} \simeq \boldsymbol{b} - \mathrm{i}(\Gamma_s/2)\hat{\mathbf{e}}_z$. Substituting the above expressions for $\Gamma_{c,s}$, it can be seen that $G_t^<(\boldsymbol{M}, \epsilon) = 0$, for $\Gamma_{L,\sigma} = \Gamma_{R,\sigma}$, implying that this component of the Green's function contributes only for polarized leads. The corresponding expressions for the larger Green's function $G_0^>(\epsilon, \boldsymbol{M})$ are obtained by replacing $\Sigma_{c,s}^< = \mathrm{i}\sum_\alpha f_\alpha(\epsilon)\Gamma_{\alpha,c(s)}$ by $\Sigma_{c,s}^> = -\mathrm{i}\sum_\alpha (1 - f_\alpha(\epsilon))\,\Gamma_{\alpha,c(s)}$ in the expressions above.

## B.2. Electronic spin and damping coefficient

Using the Green's functions expressions, we find for the mean value of the electronic spin at the molecule

$$\boldsymbol{s}^0(\boldsymbol{M}) = \int \frac{\mathrm{d}\epsilon}{2\pi\mathrm{i}}\{G_b^<\boldsymbol{b} + G_z^<\hat{\mathbf{e}}_z + G_t^<(\hat{\mathbf{e}}_z \times \boldsymbol{b})\}, \tag{B.6}$$

resulting in Eq. (5.26) in the case of axial symmetry. The explicit expression for the component parallel to $\boldsymbol{M}$ reads

$$s_M(\boldsymbol{M}) = -\frac{\mathrm{i}J}{M}\int \frac{\mathrm{d}\epsilon}{2\pi} G_b^<(\epsilon, \boldsymbol{M}). \tag{B.7}$$

Considering a setup with unpolarized leads and the external magnetic field pointing along the anisotropy axis, hence $\boldsymbol{b} = (J\boldsymbol{M} + g_e B\hat{\mathbf{e}}_z)/2$, Eq. (5.13) becomes

$$\begin{aligned}\gamma_{kl}^s(\boldsymbol{M}) =& \frac{J^2}{4}\int \frac{\mathrm{d}\epsilon}{2\pi}\sum_{\alpha\beta}\frac{\Gamma_\alpha\Gamma_\beta(-\partial_\epsilon f_\beta)}{[(\epsilon - \tilde{\epsilon} + b)^2 + (\Gamma/2)^2]\,[(\epsilon - \tilde{\epsilon} - b)^2 + (\Gamma/2)^2]}\delta_{kl} \\ &+ \frac{J^2}{2}\int \frac{\mathrm{d}\epsilon}{2\pi}\sum_{\alpha\beta}\frac{\Gamma_\alpha\Gamma_\beta(-\partial_\epsilon f_\beta)\,(\epsilon - \tilde{\epsilon})^2}{[(\epsilon - \tilde{\epsilon} + b)^2 + (\Gamma/2)^2]^2\,[(\epsilon - \tilde{\epsilon} - b)^2 + (\Gamma/2)^2]^2} b_k b_l. \end{aligned} \tag{B.8}$$

This can be decomposed into a term proportional to the unit matrix and a projector onto the $z$-axis, as described in Sec. 5.4. Note that the sign of the eigenvalues of $\gamma_{kl}^s$ is fixed, corresponding to *damping* both in and out-of equilibrium.

# C. Molecular switches on graphene

In this appendix we sketch the derivations of the diffuson, which is used in Sec. 7.5. We follow standard procedures [Akkermans and Montambaux, 2007], which have been also applied to the study of graphene [Kechedzhi *et al.*, 2008, 2009; Kharitonov and Efetov, 2008; Rycerz *et al.*, 2007; Berezovsky *et al.*, 2010].

The ladder series for the diffuson, Eq. (7.45), is depicted in Fig. 7.8. For low temperatures we consider only processes at the Fermi energy, yielding

$$\int \mathrm{d}\epsilon_k \nu(\epsilon_k) \overline{G}^{\mathrm{R}}_{\epsilon_\mathrm{F}}(\boldsymbol{k}) \overline{G}^{\mathrm{A}}_{\epsilon_\mathrm{F}-\omega}(\boldsymbol{k}-\boldsymbol{q}) \simeq \frac{f_\omega(\hat{\boldsymbol{k}},\boldsymbol{q})}{\langle U_1 \rangle}. \tag{C.1}$$

Here we use the abbreviation

$$f_\omega(\hat{\boldsymbol{k}},\boldsymbol{q}) = 1 + \mathrm{i}\omega\tau - (v\tau)^2(\boldsymbol{q}\cdot\hat{\boldsymbol{k}})^2 - \mathrm{i}v\tau\boldsymbol{q}\cdot\hat{\boldsymbol{k}}, \tag{C.2}$$

where the approximation holds in the limit of small $\omega$ and $\boldsymbol{q}$. Hence, the ladder series for the diffuson, Eq. (7.45), becomes

$$\tilde{D}_\omega(\hat{\boldsymbol{k}},\hat{\boldsymbol{k}}',\boldsymbol{q}) = U_2(\hat{\boldsymbol{k}}-\hat{\boldsymbol{k}}') + \frac{1}{\langle U_1\rangle}\big\langle \tilde{D}_\omega(\hat{\boldsymbol{k}},\hat{\boldsymbol{k}}'',\boldsymbol{q}) f_\omega(\hat{\boldsymbol{k}}'',\boldsymbol{q}) U_2(\hat{\boldsymbol{k}}''-\hat{\boldsymbol{k}}')\big\rangle_{\hat{\boldsymbol{k}}''}, \tag{C.3}$$

*cf.* for example the derivation in [Akkermans and Montambaux, 2007]. First we average over $\hat{\boldsymbol{k}}$ in order to obtain $\tilde{D}_\omega(\hat{\boldsymbol{k}}',\boldsymbol{q}) \equiv \big\langle \tilde{D}_\omega(\hat{\boldsymbol{k}},\hat{\boldsymbol{k}}',\boldsymbol{q})\big\rangle_{\hat{\boldsymbol{k}}}$ which satisfies the integral equation

$$\tilde{D}_\omega(\hat{\boldsymbol{k}}',\boldsymbol{q}) = \langle U_2\rangle + \frac{1}{\langle U_1\rangle}\big\langle \tilde{D}_\omega(\hat{\boldsymbol{k}}'',\boldsymbol{q}) f_\omega(\hat{\boldsymbol{k}}'',\boldsymbol{q}) U_2(\hat{\boldsymbol{k}}''-\hat{\boldsymbol{k}}')\big\rangle_{\hat{\boldsymbol{k}}''}. \tag{C.4}$$

We approximate

$$\tilde{D}_\omega(\hat{\boldsymbol{k}}',\boldsymbol{q}) \simeq \tilde{D}_\omega(\boldsymbol{q}) + 2\hat{\boldsymbol{k}}'\cdot\big\langle \hat{\boldsymbol{k}}'\tilde{D}_\omega(\hat{\boldsymbol{k}}',\boldsymbol{q})\big\rangle_{\hat{\boldsymbol{k}}'}, \tag{C.5}$$

and introduce the shorthand $\tilde{D}_\omega(\boldsymbol{q}) \equiv \big\langle \tilde{D}_\omega(\hat{\boldsymbol{k}}',\boldsymbol{q})\big\rangle_{\hat{\boldsymbol{k}}'}$. Then, averaging over $\hat{\boldsymbol{k}}'$ results in

$$\tilde{D}_\omega(\boldsymbol{q}) = \langle U_2\rangle + \tilde{D}_\omega(\boldsymbol{q})\frac{\langle U_2\rangle}{\langle U_1\rangle}\Big(1 + \mathrm{i}\omega\tau - \frac{(v\tau q)^2}{2}\Big) - \mathrm{i}v\tau\boldsymbol{q}\cdot\big\langle \hat{\boldsymbol{k}}'\tilde{D}_\omega(\hat{\boldsymbol{k}}',\boldsymbol{q})\big\rangle_{\hat{\boldsymbol{k}}'}. \tag{C.6}$$

Multiplying Eq. (C.5) with $\hat{\boldsymbol{k}}'$ and then averaging over $\hat{\boldsymbol{k}}'$ yields

$$\big\langle \hat{\boldsymbol{k}}'\tilde{D}_\omega(\hat{\boldsymbol{k}}',\boldsymbol{q})\big\rangle_{\hat{\boldsymbol{k}}'} = \gamma\big(\big\langle \hat{\boldsymbol{k}}'\tilde{D}_\omega(\hat{\boldsymbol{k}}',\boldsymbol{q})\big\rangle_{\hat{\boldsymbol{k}}'} - \mathrm{i}\boldsymbol{q}(v\tau/2)\tilde{D}_\omega(\boldsymbol{q})\big), \tag{C.7}$$

with $\gamma = \big\langle \hat{\boldsymbol{k}}\cdot\hat{\boldsymbol{k}}' U_2(\hat{\boldsymbol{k}}-\hat{\boldsymbol{k}}')\big\rangle_{\hat{\boldsymbol{k}}'}/\langle U_1\rangle$. Multiplication of the last line with $\boldsymbol{q}$ yields

$$\boldsymbol{q}\cdot\big\langle \hat{\boldsymbol{k}}'\tilde{D}_\omega(\hat{\boldsymbol{k}}',\boldsymbol{q})\big\rangle_{\hat{\boldsymbol{k}}'} = -\mathrm{i}\frac{v\tau q^2}{2}\frac{\gamma}{1-\gamma}\tilde{D}_\omega(\boldsymbol{q}). \tag{C.8}$$

Plugging this result into Eq. (C.6) brings after straightforward algebra Eq. (7.50) for the diffuson $\tilde{D}_\omega(\boldsymbol{q})$, as stated in the main text.

# Acknowledgements

First of all I would like to thank Felix von Oppen for supervising this PhD thesis and introducing me to the fascinating field of condensed matter physics. I would like to thank Piet W. Brouwer, not only for co-refereeing this thesis, but also for valuable comments and questions. Additionally I would like to thank both of them for creating the beautiful research environment in the Dahlem Center for Complex Quantum Systems at the Freie Universität Berlin.

I have greatly benefited from and I am grateful for the collaborations with Silvia Viola Kusminskiy (Berlin), Reinhold Egger (Düsseldorf), Liliana Arrachea (Buenos Aires), Gustavo S. Lozano (Buenos Aires), Tamara S. Nunner (Berlin), and Eros Mariani (Exeter). Furthermore I would like to thank the members of the DCCQS for various discussions and providing such a friendly and inspiring atmosphere.

Finally, I gratefully acknowledge financial support by the Alexander-von-Humboldt foundation and by the Deutsche Forschungsgemeinschaft through Sonderforschungsbereich 658.

# Curriculum Vitae

For reasons of data protection,
the *curriculum vitae* is not included in the online version of this thesis.

# Publications

- *Scattering theory of current-induced forces in mesoscopic systems.*
  Phys. Rev. Lett. **107**, 036804 (2011).
  N. Bode, S. Viola Kusminskiy, R. Egger, and F. von Oppen.

- *Current-induced forces in mesoscopic systems: a scattering matrix approach.*
  Beilstein J. Nanotechnol. **3**, 144 (2012).
  N. Bode, S. Viola Kusminskiy, R. Egger, and F. von Oppen.

- *Current-induced switching in transport through anisotropic magnetic molecules.*
  Phys. Rev. B **85**, 115440 (2012).
  N. Bode, L. Arrachea, G. S. Lozano, T. S. Nunner, and F. von Oppen.

- *Transport properties of graphene functionalized with molecular switches.*
  accepted for publication, J.Phys.: Condens. Matter (2012).
  N. Bode, E. Mariani, and F. von Oppen.

# Bibliography


S. Adam, E. H. Hwang, V. Galitski, and S. Das Sarma, *A self-consistent theory for graphene transport.* Proc. Natl. Acad. Sci. **104**, 18392 (2007).

E. Akkermans and G. Montambaux, *Mesoscopic physics of electrons and photons.* Cambridge University Press (2007).

I. L. Aleiner, P. W. Brouwer, and L. I. Glazman, *Quantum effects in Coulomb blockade.* Physics Reports **358**, 309 (2002).

B. Al'tshuler, *Fluctuations in the extrinsic conductivity of disordered conductors.* JETP Lett. **41**, 648 (1985).

B. L. Al'tshuler and B. I. Shklovskii, *Repulsion of energy levels and conductivity of small metal samples.* JETP **64**, 127 (1986).

B. L. Al'tshuler and B. Z. Spivak, *Variation of the random potential and the conductivity of samples of small dimensions.* JETP Lett. **42**, 447 (1985).

T. Ando, *Screening effect and impurity scattering in monolayer graphene.* J. Phys. Soc. Jap. **75**, 074716 (2006).

L. Arrachea and M. Moskalets, *Relation between scattering-matrix and Keldysh formalisms for quantum transport driven by time-periodic fields.* Phys. Rev. B **74**, 245322 (2006).

M. Auslender and M. I. Katsnelson, *Generalized kinetic equations for charge carriers in graphene.* Phys. Rev. B **76**, 235425 (2007).

J. E. Avron, A. Elgart, G. M. Graf, and L. Sadun, *Optimal quantum pumps.* Phys. Rev. Lett. **87**, 236601 (2001).

H. U. Baranger and A. D. Stone, *Electrical linear-response theory in an arbitrary magnetic field: A new fermi-surface formation.* Phys. Rev. B **40**, 8169 (1989).

D. M. Basko and M. G. Vavilov, *Stochastic dynamics of magnetization in a ferromagnetic nanoparticle out of equilibrium.* Physical Review B **79**, 064418 (2009).

S. D. Bennett, J. Maassen, and A. A. Clerk, *Scattering approach to backaction in coherent nanoelectromechanical systems.* Phys. Rev. Lett. **105**, 217206 (2010).

S. D. Bennett, J. Maassen, and A. A. Clerk, *Erratum: Scattering approach to backaction in coherent nanoelectromechanical systems [Phys. Rev. Lett. 105, 217206 (2010)].* Phys. Rev. Lett. **106**, 199902 (2011).

J. Berezovsky, M. Borunda, E. Heller, and R. Westervelt, *Imaging coherent transport in graphene (part i): Mapping universal conductance fluctuations.* Nanotechnology **21**, 274013 (2010).

L. Berger, *Emission of spin waves by a magnetic multilayer traversed by a current.* Phys. Rev. B **54**, 9353 (1996).

M. V. Berry and J. M. Robbins, *Chaotic classical and half-classical adiabatic reactions: Geometric magnetism and deterministic friction.* Proc. R. Soc. Lond. A **442**, 659 (1993).

N. Bode, L. Arrachea, G. S. Lozano, T. S. Nunner, and F. von Oppen, *Current-induced switching in transport through anisotropic magnetic molecules.* Phys. Rev. B **85**, 115440 (2012a).

N. Bode, L. Arrachea, and F. von Oppen, *Cooling a nanomechanical systems with a charge current.* to be published (2012b).

N. Bode, E. Mariani, and F. von Oppen, *Transport properties of graphene functionalized with molecular switches.* accepted for publication, J.Phys.: Condens. Matter (2012c).

N. Bode, S. Viola Kusminskiy, R. Egger, and F. von Oppen, *Scattering theory of current-induced forces in mesoscopic systems.* Phys. Rev. Lett. **107**, 036804 (2011).

N. Bode, S. Viola Kusminskiy, R. Egger, and F. von Oppen, *Current-induced forces in mesoscopic systems: a scattering matrix approach.* Beilstein J. Nanotechnol. **3**, 144 (2012d).

A. Brataas, Y. Tserkovnyak, and G. E. W. Bauer, *Scattering theory of Gilbert damping.* Phys. Rev. Lett. **101**, 037207 (2008).

A. Brataas, Y. Tserkovnyak, and G. E. W. Bauer, *Magnetization dissipation in ferromagnets from scattering theory.* Phys. Rev. B **84**, 054416 (2011).

C. Bronner, G. Schulze, K. J. Franke, J. I. Pascual, and P. Tegeder, *Switching ability of nitro-spiropyran on Au(111): electronic structure changes as a sensitive probe during a ring-opening reaction.* J. Phys.: Condens. Matter **23**, 484005 (2011).

P. W. Brouwer, *Scattering approach to parametric pumping.* Phys. Rev. B **58**, R10135 (1998).

W. F. Brown, *Thermal fluctuations of a single-domain particle.* Phys. Rev. **130**, 1677 (1963).

J. Brüggemann, G. Weick, F. Pistolesi, and F. von Oppen, *Large current noise in nanoelectromechanical systems close to continuous mechanical instabilities.* Phys. Rev. B **85**, 125441 (2012).

M. Büttiker, *Four-terminal phase-coherent conductance.* Phys. Rev. Lett. **57**, 1761 (1986).

M. Büttiker, *Scattering theory of current and intensity noise correlations in conductors and wave guides.* Phys. Rev. B **46**, 12485 (1992).

M. Büttiker, Y. Imry, R. Landauer, and S. Pinhas, *Generalized many-channel conductance formula with application to small rings.* Phys. Rev. B **31**, 6207 (1985).

J. H. Chen, C. Jang, M. S. Fuhrer, E. D. Williams, and M. Ishigami, *Charged impurity scattering in graphene.* Nature Phys. **4**, 377 (2008).

A. Clerk, *Seeing the "quantum" in quantum zero-point fluctuations.* Physics **5**, 8 (2012).

A. A. Clerk and S. Bennett, *Quantum nanoelectromechanics with electrons, quasi-particles and Cooper pairs: effective bath descriptions and strong feedback effects.* New Journal of Physics **7**, 238 (2005).

S. Das Sarma, S. Adam, E. H. Hwang, and E. Rossi, *Electronic transport in two-dimensional graphene.* Rev. Mod. Phys. **83**, 407 (2011).

S. Datta, *Electronic Transport in Mesoscopic Systems.* Cambridge University Press (1995).

D. Djukic, K. S. Thygesen, C. Untiedt, R. H. M. Smit, K. W. Jacobsen, and J. M. van Ruitenbeek, *Stretching dependence of the vibration modes of a single-molecule Pt-$H_2$-Pt bridge.* Phys. Rev. B **71**, 161402 (2005).

D. Dundas, E. J. McEniry, and T. N. Todorov, *Current-driven atomic waterwheels.* Nat. Nano. **4**, 99 (2009).

T. Dunn and A. Kamenev, *Optimization of the current pulse for spin-torque switches.* Applied Physics Letters **98** (2011).

O. Entin-Wohlman, A. Aharony, and Y. Levinson, *Adiabatic transport in nanostructures.* Phys. Rev. B **65**, 195411 (2002).

S. Feng, P. A. Lee, and A. D. Stone, *Sensitivity of the conductance of a disordered metal to the motion of a single atom: Implications for* $1/f$ *noise.* Phys. Rev. Lett. **56**, 1960 (1986).

A. Fert, *Nobel lecture: Origin, development, and future of spintronics.* Rev. Mod. Phys. **80**, 1517 (2008).

S. Florens, A. Freyn, N. Roch, W. Wernsdorfer, F. Balestro, P. Roura-Bas, and A. A. Aligia, *Universal transport signatures in two-electron molecular quantum dots: gate-tunable Hund's rule, underscreened Kondo effect and quantum phase transitions.* J. Phys. Condens. Matter **23**, 243202 (2011).

K. J. Franke, G. Schulze, and J. I. Pascual, *Competition of superconducting phenomena and Kondo screening at the nanoscale.* Science **332**, 940 (2011).

J. Fransson, *Subnanosecond switching of local spin-exchange coupled to ferromagnets.* Phys. Rev. B **77**, 205316 (2008).

J. R. Friedman and M. P. Sarachik, *Single-molecule nanomagnets.* Annu. Rev. Cond. Mat. **1**, 109 (2010).

J. R. Friedman, M. P. Sarachik, J. Tejada, and R. Ziolo, *Macroscopic measurement of resonant magnetization tunneling in high-spin molecules.* Phys. Rev. Lett. **76**, 3830 (1996).

M. Galperin, K. Saito, A. V. Balatsky, and A. Nitzan, *Cooling mechanisms in molecular conduction junctions.* Phys. Rev. B **80**, 115427 (2009).

M. Gell-Mann and K. A. Brueckner, *Correlation energy of an electron gas at high density.* Phys. Rev. **106**, 364 (1957).

K. M. D. Hals, A. Brataas, and Y. Tserkovnyak, *Scattering theory of charge-current-induced magnetization dynamics.* Europhys. Lett. **90**, 47002 (2010).

P. Hanggi and P. Riseborough, *Dynamics of nonlinear dissipative oscillators.* Am. J. Phys. **51**, 347 (1983).

H. Haug and A.-P. Jauho, *Quantum Kinetics in Transport and Optics of Semiconductors.* Springer Berlin, Heidelberg, New York (2008).

H. B. Heersche, Z. de Groot, J. A. Folk, H. S. J. van der Zant, C. Romeike, M. R. Wegewijs, L. Zobbi, D. Barreca, E. Tondello, and A. Cornia, *Electron transport through single $Mn_{12}$ molecular magnets.* Phys. Rev. Lett. **96**, 206801 (2006).

R. Hussein, A. Metelmann, P. Zedler, and T. Brandes, *Semiclassical dynamics of nano-electromechanical systems.* Phys. Rev. B **82**, 165406 (2010).

E. H. Hwang, S. Adam, and S. Das Sarma, *Carrier transport in 2d graphene layers.* Phys. Rev. Lett. **98**, 186806 (2007).

P. Hyldgaard, *Control of molecular excitations in nanotube-heterostructure transistors.* Materials Science and Engineering: C **23**, 243 (2003).

Y. Imry and Landauer, *Conductance viewed as transmission.* Rev. Mod. Phys. **71** (1999).

M.-H. Jo, J. E. Grose, K. Baheti, M. M. Deshmukh, J. J. Sokol, E. M. Rumberger, D. N. Hendrickson, J. Long, H. Park, and D. C. Ralph, *Signatures of molecular magnetism in single-molecule transport spectroscopy.* Nano Lett. **6**, 2014 (2006).

A. Kamenev and A. Levchenko, *Keldysh technique and non-linear $\sigma$-model: basic principles and applications.* Advances in Physics **58**, 197 (2009).

C. L. Kane, R. A. Serota, and P. A. Lee, *Long-range correlations in disordered metals.* Phys. Rev. B **37**, 6701 (1988).

H. Katsura, A. V. Balatsky, Z. Nussinov, and N. Nagaosa, *Voltage dependence of Landau-Lifshitz-Gilbert damping of spin in a current-driven tunnel junction.* Phys. Rev. B **73** (2006).

K. Kechedzhi, D. W. Horsell, F. V. Tikhonenko, A. K. Savchenko, R. V. Gorbachev, I. V. Lerner, and V. I. Fal'ko, *Quantum transport thermometry for electrons in graphene.* Phys. Rev. Lett. **102**, 066801 (2009).

K. Kechedzhi, O. Kashuba, and V. I. Fal'ko, *Quantum kinetic equation and universal conductance fluctuations in graphene.* Phys. Rev. B **77**, 193403 (2008).

L. Keldysh, *Diagram technique for nonequilibrium processes.* Sov. Phys. JETP **20**, 1018 (1965).

M. Y. Kharitonov and K. B. Efetov, *Universal conductance fluctuations in graphene.* Phys. Rev. B **78**, 033404 (2008).

M. Kindermann and C. W. J. Beenakker, *Quantum theory of electromechanical noise and momentum transfer statistics.* Phys. Rev. B **66**, 224106 (2002).

J. Koch and F. von Oppen, *Franck-Condon blockade and giant Fano factors in transport through single molecules.* Phys. Rev. Lett. **94**, 206804 (2005).

J. Koch, F. von Oppen, and A. V. Andreev, *Theory of the Franck-Condon blockade regime.* Phys. Rev. B **74**, 205438 (2006).

T. Kudernac, N. Ruangsupapichat, M. Parschau, B. Macia, N. Katsonis, S. R. Harutyunyan, K.-H. Ernst, and B. L. Feringa, *Electrically driven directional motion of a four-wheeled molecule on a metal surface.* Nature **479**, 208 (2011).

J. N. Kupferschmidt, S. Adam, and P. W. Brouwer, *Ferromagnetic resonance in a current driven nanopillar.* Phys. Rev. B **74**, 134416 (2006).

R. Landauer, *Spatial variation of currents and fields due to localized scatterers in metallic conduction.* IBM J. Res. Dev. **1**, 223 (1957).

R. Landauer, *Electrical resistance of disordered one-dimensional lattices.* Philos. Mag. **21**, 863 (1970).

A. Larkin and Y. Ovchinnikov, *Nonlinear conductivity of superconductors in the mixed state.* Sov. Phys. JETP **41**, 960 (1975).

B. Lassagne, Y. Tarakanov, J. Kinaret, D. Garcia-Sanchez, and A. Bachtold, *Coupling mechanics to charge transport in carbon nanotube mechanical resonators.* Science **325**, 1107 (2009).

P. A. Lee and A. D. Stone, *Universal conductance fluctuations in metals.* Phys. Rev. Lett. **55**, 1622 (1985).

P. A. Lee, A. D. Stone, and H. Fukuyama, *Universal conductance fluctuations in metals: Effects of finite temperature, interactions, and magnetic field.* Phys. Rev. B **35**, 1039 (1987).

R. Leturcq, C. Stampfer, K. Inderbitzin, L. Durrer, C. Hierold, E. Mariani, M. Schultz, F. von Oppen, and K. Ensslin, *Franck-Condon blockade in suspended carbon nanotube quantum dots.* Nature Physics **5**, 327 (2009).

W. Liang, M. Shores, M. Bockrath, J. Long, and H. Park, *Kondo resonance in a single-molecule transistor.* Nature **417**, 725 (2002).

C. López-Monís, C. Emary, G. Kiesslich, G. Platero, and T. Brandes, *Limit cycles and chaos in the current through a quantum dot.* Phys. Rev. B **85**, 045301 (2012).

J.-T. Lü, M. Brandbyge, and P. Hedegåard, *Blowing the fuse: Berry's phase and runaway vibrations in molecular conductors.* Nano Letters **10**, 1657 (2010).

J.-T. Lü, P. Hedegård, and M. Brandbyge, *Laserlike vibrational instability in rectifying molecular conductors.* Phys. Rev. Let **107**, 046801 (2011).

E. Malic, C. Weber, M. Richter, V. Atalla, T. Klamroth, P. Saalfrank, S. Reich, and A. Knorr, *Microscopic model of the optical absorption of carbon nanotubes functionalized with molecular spiropyran photoswitches.* Phys. Rev. Lett. **106**, 097401 (2011).

E. McCann, K. Kechedzhi, V. I. Fal'ko, H. Suzuura, T. Ando, and B. L. Altshuler, *Weak-localization magnetoresistance and valley symmetry in graphene.* Phys. Rev. Lett. **97**, 146805 (2006).

E. J. McEniry, T. N. Todorov, and D. Dundas, *Current-assisted cooling in atomic wires.* J.Phys.: Condens. Matter **21**, 195304 (2009).

A. Metelmann and T. Brandes, *Adiabaticity in semiclassical nanoelectromechanical systems.* Phys. Rev. B **84**, 155455 (2011).

M. Misiorny and J. Barnas, *Switching of molecular magnets.* Phys. Status Solidi B 246 **246**, 695 (2009).

M. Moskalets and M. Büttiker, *Adiabatic quantum pump in the presence of external ac voltages.* Phys. Rev. B **69**, 20531 (2004).

M. Moskalets and M. Büttiker, *Magnetic-field symmetry of pump currents of adiabatically driven mesoscopic structures.* Phys. Rev. B **72**, 035324 (2005).

D. Mozyrsky, M. B. Hastings, and I. Martin, *Intermittent polaron dynamics: Born-Oppenheimer approximation out of equilibrium.* Phys. Rev. B **73**, 035104 (2006).

J. T. Muhonen, M. Meschke, and J. P. Pekola, *Micrometre-scale refrigerators.* Reports on Progress in Physics **75**, 046501 (2012).

A. Naik, O. Buu, M. D. LaHaye, A. D. Armour, A. A. Clerk, M. P. Blencowe, and K. C. Schwab, *Cooling a nanomechanical resonator with quantum back-action.* Nature **443**, 193 (2006).

Y. Nazarov and Y. Blanter, *Quantum Transport.* Cambridge University Press, Cambridge (2010).

A. H. C. Neto, F. Guinea, N. M. R. Peres, K. S. Novoselov, and A. K. Geim, *The electronic properties of graphene.* Rev. Mod. Phys. **81**, 109 (2009).

K. Nomura and A. H. MacDonald, *Quantum Hall ferromagnetism in graphene.* Phys. Rev. Lett. **96**, 256602 (2006).

K. S. Novoselov, A. K. Geim, S. V. Morozov, D. Jiang, M. I. Katsnelson, I. V. Grigorieva, S. V. Dubonos, and A. A. Firsov, *Two-dimensional gas of massless Dirac fermions in graphene.* Nature **438**, 197 (2005).

K. S. Novoselov, A. K. Geim, S. V. Morozov, D. Jiang, Y. Zhang, S. V. Dubonos, I. V. Grigorieva, and A. A. Firsov, *Electric field effect in atomically thin carbon films.* Science **306**, 666 (2004).

A. S. Núñez and R. A. Duine, *Effective temperature and Gilbert damping of a current-driven localized spin.* Phys. Rev. B **77**, 054401 (2008).

H. Park, J. Park, A. K. L. Lim, E. H. Anderson, A. P. Alivisatos, and P. L. McEuen, *Nanomechanical oscillations in a single-$C_{60}$ transistor.* Nature **407**, 57 (2000).

J. Park, A. Pasupathy, J. Goldsmith, C. Chang, Y. Yaish, J. Petta, M. Rinkoski, J. Sethna, H. Abruna, P. McEuen, and D. Ralph, *Coulomb blockade and the Kondo effect in single-atom transistors.* Nature **417**, 722 (2002).

J. J. Parks, A. R. Champagne, T. A. Costi, W. W. Shum, A. N. Pasupathy, E. Neuscamman, S. Flores-Torres, P. S. Cornaglia, A. A. Aligia, C. A. Balseiro, G. K.-L. Chan, H. D. Abruna, and D. C. Ralph, *Mechanical control of spin states in spin-1 molecules and the underscreened Kondo effect.* Science **328**, 1370 (2010).

A. N. Pasupathy, R. C. Bialczak, J. Martinek, J. E. Grose, L. A. K. Donev, P. L. McEuen, and D. C. Ralph, *The Kondo effect in the presence of ferromagnetism.* Science **306**, 86 (2004).

M. Piantek, G. Schulze, M. Koch, K. J. Franke, F. Leyssner, A. Krüger, C. Navio, J. Miguel, M. Bernien, M. Wolf, W. Kuch, P. Tegeder, and J. I. Pascual, *Reversing the thermal stability of a molecular switch on a gold surface: Ring-opening reaction of nitrospiropyran.* J. Am. Chem. Soc. **131**, 12729 (2009).

F. Pistolesi, *Cooling a vibrational mode coupled to a molecular single-electron transistor.* Jour. Low Temp. Phys. **154**, 199 (2009).

F. Pistolesi, Y. M. Blanter, and I. Martin, *Self-consistent theory of molecular switching.* Phys. Rev. B **78**, 085127 (2008).

J. R. Prance, C. G. Smith, J. P. Griffiths, S. J. Chorley, D. Anderson, G. A. C. Jones, I. Farrer, and D. A. Ritchie, *Electronic refrigeration of a two-dimensional electron gas.* Phys. Rev. Lett. **102**, 146602 (2009).

D. Ralph and M. Stiles, *Spin transfer torques.* J. Magn. Magn. Mater. **320**, 1190 (2008).

J. Rammer, *Quantum field theory of non-equilibrium states.* Cambridge University Press (2007).

A. R. Rocha, V. G. Suarez, S. W. Bailey, C. J. Lambert, J. Ferrer, and S. Sanvito, *Towards molecular spintronics.* Nature Mat. **4**, 335 (2005).

C. Romeike, M. R. Wegewijs, W. Hofstetter, and H. Schoeller, *Quantum-tunneling-induced Kondo effect in single molecular magnets.* Phys. Rev. Lett. **96**, 196601 (2006).

A. Rycerz, J. Tworzydlo, and C. W. Beenakker, *Anomalously large conductance fluctuations in weakly disordered graphene.* Europhys. Lett. **79**, 57003 (2007).

R. Saito, G. Dresselhaus, and M. Dresselhaus, *Physical Properties of Carbon Nanotubes.* Imperial College Press (1998).

S. Sanvito, *Molecular spintronics.* Chem. Soc. Rev. **40**, 3336 (2011).

F. Schedin, A. K. Geim, S. V. Morozov, D. Jiang, E. H. Hill, P. Blake, and K. S. Novoselov, *Detection of individual gas molecules absorbed on graphene.* Nature Mat. **6**, 652 (2007).

J. Schrieffer, *Theory of superconductivity.* W.A. Benjamin, Inc., Reading, Massachusetts (1964).

J. Schwinger, *Brownian motion of a quantum oscillator.* J. Math. Phys. **2**, 407 (1961).

J. Slonczewski, *Current-driven excitation of magnetic multilayers.* J. Magn. Magn. Mater. **159**, L1 (1996).

R. H. M. Smit, Y. Noat, C. Untiedt, N. D. Lang, M. C. van Hemert, and J. M. van Ruitenbeek, *Measurement of the conductance of a hydrogen molecule.* Nature **419**, 906 (2002).

G. A. Steele, A. K. Hüttel, B. Witkamp, M. Poot, H. B. Meerwaldt, L. P. Kouwenhoven, and H. S. J. van der Zant, *Strong coupling between single-electron tunneling and nanomechanical motion.* Science **325**, 1103 (2009).

J. Stettenheim, M. Thalakulam, F. Pan, M. Bal, Z. Ji, W. Xue, L. Pfeiffer, K. West, M. P. Blencowe, and A. J. Rimberg, *A macroscopic mechanical resonator driven by mesoscopic electrical back-action.* Nature **466**, 86 (2010).

H. L. Tierney, C. J. Murphy, A. D. Jewell, A. E. Baber, E. V. Iski, H. Y. Khodaverdian, A. F. McGuire, N. Klebanov, and E. C. H. Sykes, *Experimental demonstration of a single-molecule electric motor.* Nat. Nano. **6**, 625 (2011).

T. N. Todorov, D. Dundas, and E. J. McEniry, *Nonconservative generalized current-induced forces.* Phys. Rev. B **81**, 075416 (2010).

Y. Tserkovnyak, A. Brataas, and G. E. W. Bauer, *Enhanced Gilbert damping in thin ferromagnetic films.* Phys. Rev. Lett. **88**, 117601 (2002).

M. Urdampilleta, S. Klyatskaya, J. P. Cleziou, M. Ruben, and W. Wernsdorfer, *Supramolecular spin valves.* Nature Mat. **10**, 502 (2011).

B. J. van Wees, H. van Houten, C. W. J. Beenakker, J. G. Williamson, L. P. Kouwenhoven, D. van der Marel, and C. T. Foxon, *Quantized conductance of point contacts in a two-dimensional electron gas.* Phys. Rev. Lett. **60**, 848 (1988).

M. G. Vavilov, V. Ambegaokar, and I. L. Aleiner, *Charge pumping and photovoltaic effect in open quantum dots.* Phys. Rev. B **63**, 195313 (2001).

P. Wallace, *The band theory of graphite.* Phys. Rev. **71**, 622 (1947).

G. Weick, F. Pistolesi, E. Mariani, and F. von Oppen, *Discontinuous Euler instability in nanoelectromechanical systems.* Phys. Rev. B **81**, 121409 (2010).

D. Wharam, T. Thornton, and C. Foxon, *One-dimensional transport and the quantisation of the ballistic resistance.* J. Phys. C **21**, L209 (1988).

J. Whelan, D. Abdallah, J. Wojtyk, and E. Buncel, *Micro-environmental fine-tuning of electronic and kinetic properties of photochromic dyes.* J. Mater. Chem. **20**, 5727 (2010).

L. Yu, Z. Keane, J. Ciszek, L. Cheng, J. Tour, T. Baruah, M. Pederson, and D. Natelson, *Kondo resonances and anomalous gate dependence in the electrical conductivity of single-molecule transistors.* Phys. Rev. Lett. **95**, 256803 (2005).

L. H. Yu, Z. K. Keane, J. W. Ciszek, L. Cheng, M. P. Stewart, J. M. Tour, and D. Natelson, *Inelastic electron tunneling via molecular vibrations in single-molecule transistors.* Phys. Rev. Lett. **93**, 266802 (2004).

S. Zippilli, A. Bachtold, and G. Morigi, *Ground-state-cooling vibrations of suspended carbon nanotubes with constant electron current.* Phys. Rev. B **81**, 205408 (2010).

S. Zippilli, G. Morigi, and A. Bachtold, *Cooling carbon nanotubes to the phononic ground state with a constant electron current.* Phys. Rev. Lett. **102**, 096804 (2009).

D. Zueco and J. L. García-Palacios, *Longitudinal relaxation and thermoactivation of quantum superparamagnets.* Phys. Rev. B **73**, 104448 (2006).

R. Zwanzig, *Nonequilibrium statistical mechanics.* Oxford University Press (2001).